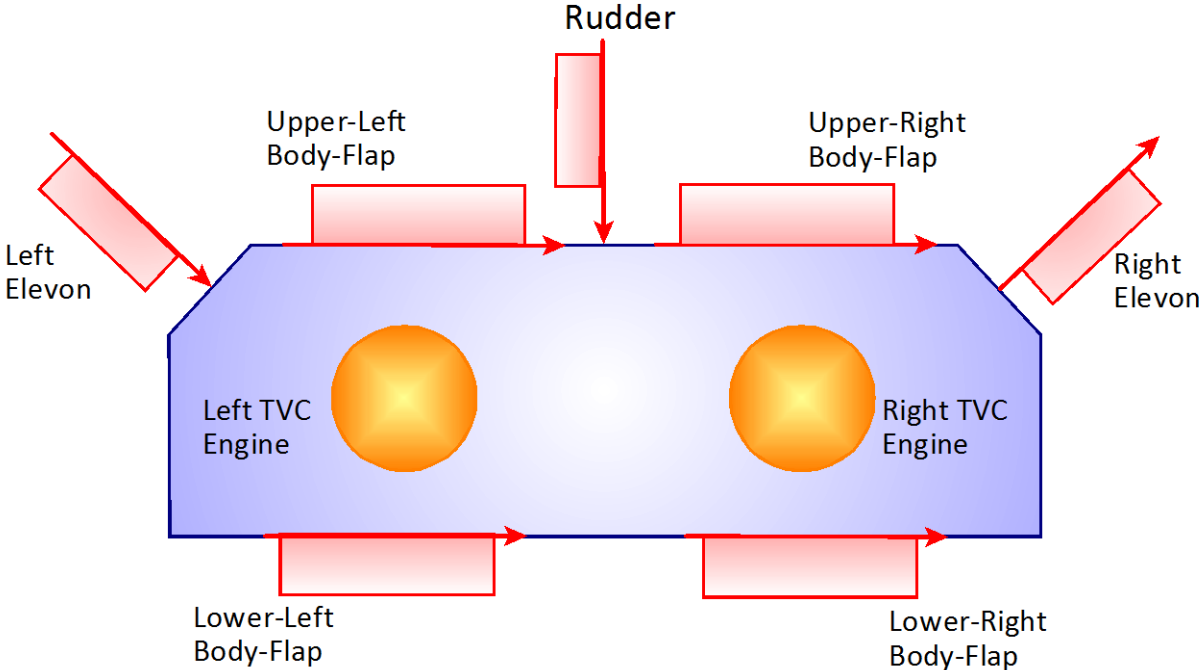


# Lifting-Body Space-Plane



In this example we will study a Lifting-Body aircraft that is used as a transportation vehicle from space. It is capable of returning from space by gliding and landing autonomously by using its aer-surfaces. It is also capable of taking-off vertically like a rocket by means of two TVC engines, reaching high altitudes and landing unpowered. The purpose of this example is to demonstrate a complete flight control design of a re-entry vehicle from de-orbit to landing, beginning with preliminary performance and controllability analysis, synthesizing control laws at selected Mach points, linear dynamic analysis and simulation. It also teaches the student how to create dynamic models for flight control design and linear analysis, how to design simple control laws in Matlab, and how to generate dynamic models for analyzing robustness to uncertain parameters. We will use the Flixan program to analyze this vehicle during both, boost and descent phases. We will finally show how to use Matlab/ Simulink to create a 6-dof non-linear re-entry simulation from de-orbit to landing. Information and details are included which are often missed out in textbooks, technical papers and presentations.

Figure (1) shows the vehicle effectors consisting of seven aero-surfaces and two TVC engines of 18,000 (lb) thrust each. The TVC engines are also capable of varying their thrusts. The vectors indicate the directions of positive aero-surface rotations. The multitude of aero-surfaces provide the capability to trim and to control the vehicle entirely by the 7 aero-surfaces during reentry. However, RCS is available but it is only used to maneuver and to control attitude at low dynamic pressures and also as a back-up system during re-entry. The elevons and rudder primary function is to provide roll, pitch, and yaw control torques. The four body-flaps are mainly used for trimming and for speed control. However, they are also providing some rotation control assistance to the elevons.



**Figure 1 Control Effectors are Shown from the Rear End of the Vehicle, Consisting of: Seven Aero-Surfaces and Two Throttling TVC Engines**

## 1.0 Reentry Analysis

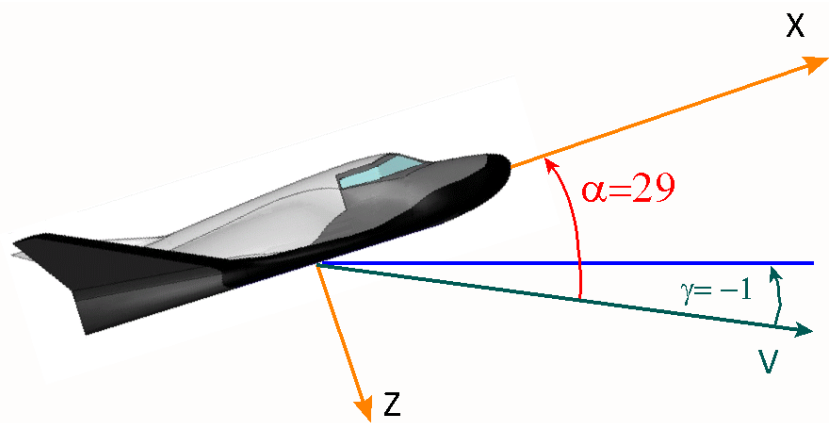
The reentry trajectory begins when the dynamic pressure is sufficient for the vehicle to trim and to be controlled by the seven aero-surfaces alone without RCS assistance. The control requirements are not the same in different phases of the reentry flight and each phase requires a different control mode of operation and, therefore, the analysis that follows is separated in four sections describing the four control modes in detail, which are:

1. The hypersonic phase where the Mach number varies between 28 and 20, and the flight path angle ( $\gamma$ ) is at a very shallow dive of  $-1^\circ$  to avoid overheating due to friction. The angle of attack is controlled at  $30^\circ$  to increase heat protection provided by shielding. In the lateral directions the control system can perform roll maneuvers about the velocity vector  $V_0$ .
2. Normal acceleration ( $N_z$ ) control phase during which the vehicle is tracking an almost steady ( $N_z$ ) acceleration command from guidance. Then it transitions to flight-path angle  $\gamma$ -control mode.
3. Flight path angle  $\gamma$ -control phase during which the flight control system tracks a  $\gamma$ -command angle provided by a closed-loop guidance. It also performs a heading alignment maneuver to point its direction towards runway.
4. The approach and landing phase during which longitudinal guidance attempts to control altitude and speed. The speed-brake is partially deployed and velocity is controlled by modulating its opening. In lateral heading guidance controls the flight direction against crosswinds by banking.

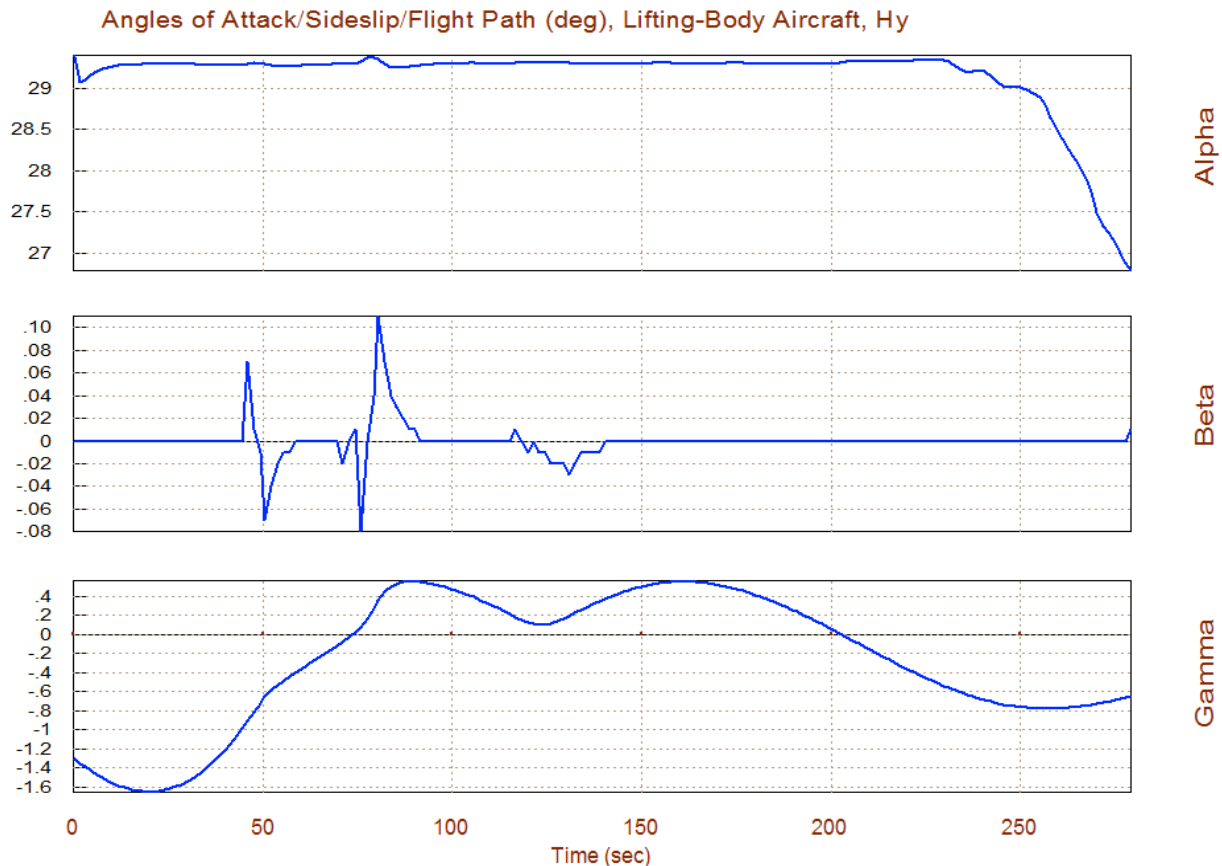
A preliminary reentry trajectory is used in this analysis. The trajectory is separated in four segments corresponding to the four control phases and it is analyzed in separate folders. We will analyze each of these phases separately by trimming the effectors and analyzing static performance along the trajectory. We will use contour plots and vector diagrams to analyze performance and maneuverability. We will use Flixan to generate dynamic models at selected flight conditions along the trajectory, perform flight control designs, and analyze stability and robustness to uncertainties at selected trajectory points. A separate control analysis and detail documentation will be presented at each of the four control modes, including simulations. We will finally demonstrate the design by creating a 6-dof non-linear simulation of the entire reentry flight from de-orbit to landing in Simuling using the control laws derived from the analysis.

## 1.1 Early Re-Entry Phase Using Alpha Control

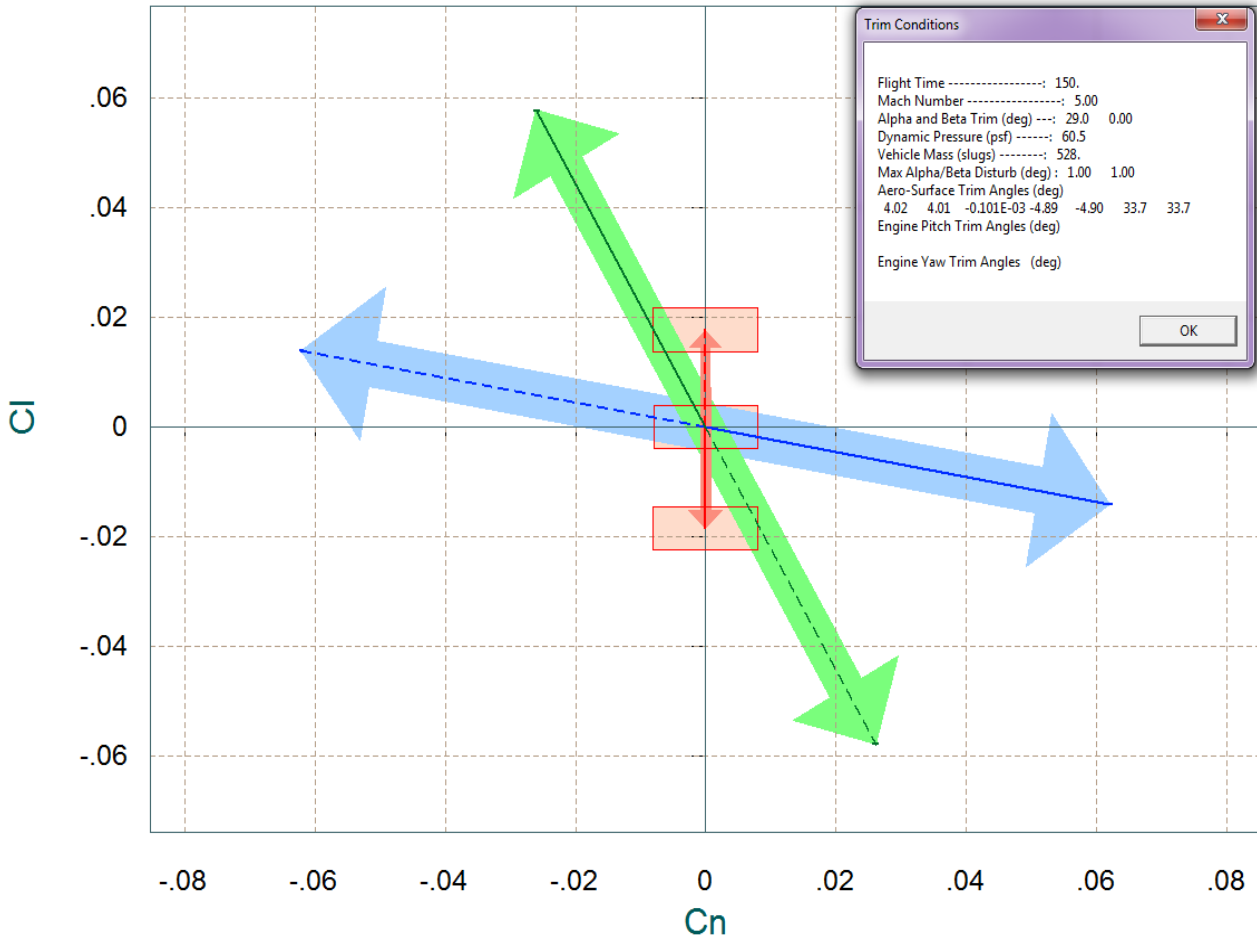
After de-orbiting and during the early phase of reentry (first 300 sec) the vehicle uses the RCS jets to maintain a  $29.5^\circ$  constant angle of attack which optimizes aero heating. The flight-path angle ( $\gamma$ ) is at a shallow dive of  $-1^\circ$  approx. As the dynamic pressure increases the aero-surfaces are used to trim and to control the angle of attack at  $29.5^\circ$ .



Atmospheric reentry begins at an altitude of 250,000 (ft) and at Mach 28. The vehicle banks by rolling about its velocity vector  $V$  to maintain a mostly negative ( $\gamma$ ) and to avoid from bouncing back off into space. The flight control system uses estimated ( $\alpha$ ) to control the angle of attack. The angle ( $\alpha$ ) is gradually reduced and the control system eventually switches to normal acceleration ( $N_z$ ) control. The following figures show some of the trajectory parameters in the hypersonic region between Mach (28 to 19).

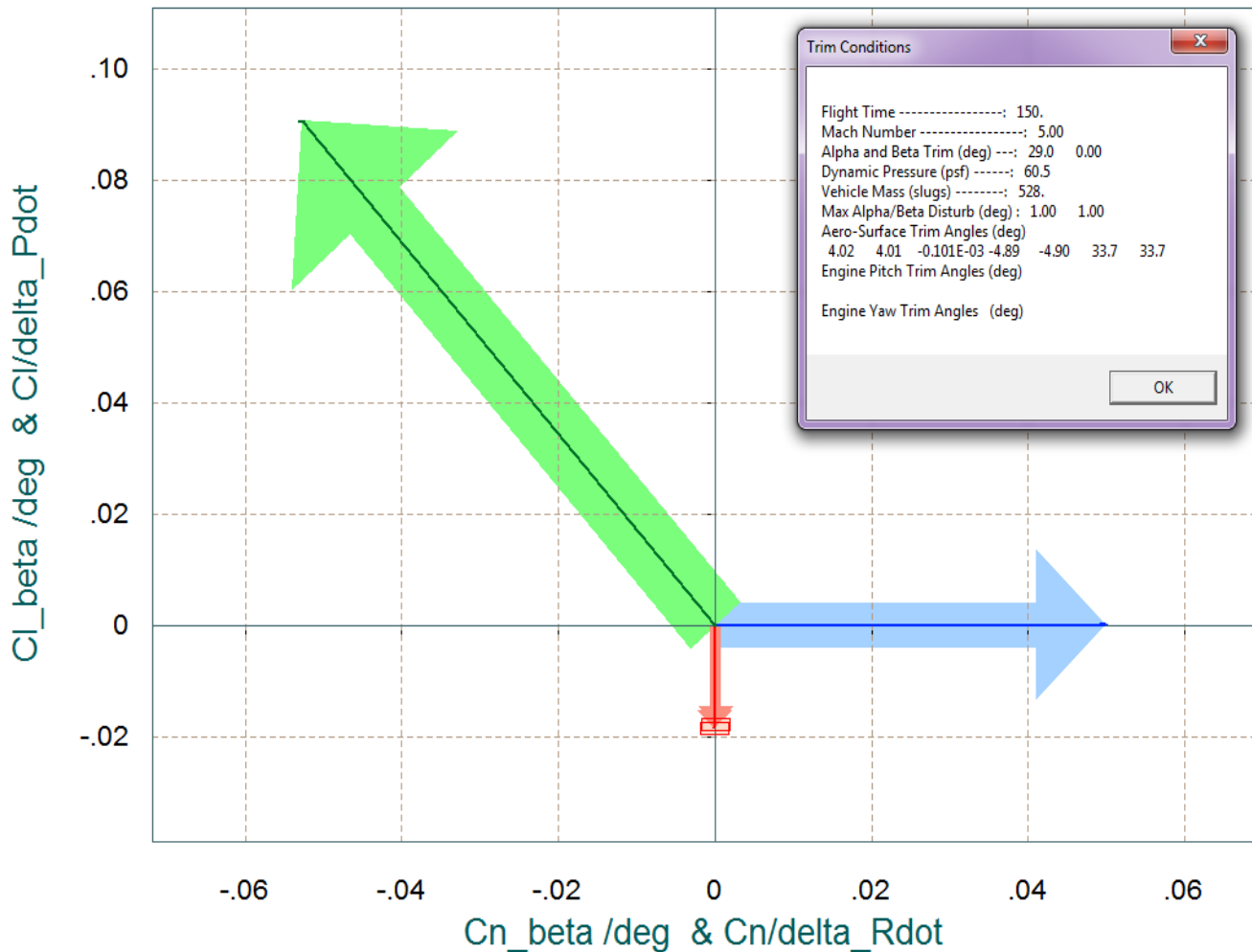


Comparison Between Maximum Control Moments Against Maximum Disturb Moments (red)  
 Roll & Yaw Control Moments (non-dimension) vers Disturb Moment due to Max Beta/Alpha



The above vector diagram shows the roll and yaw moments (non-dimensional) produced when the roll and yaw FCS demands are maximized (before saturating the aero-surfaces). The solid blue vector corresponds to max positive yaw FCS demand ( $+\delta R_{FCS\_Max}$ ), and the dashed blue vector to max negative yaw demand ( $-\delta R_{FCS\_Max}$ ). Similarly, the green vectors correspond to the roll FCS demands ( $\pm \delta P_{FCS\_Max}$ ). The two red vectors show the disturbance moments generated due to variations of the angles of attack and sideslip ( $\pm \alpha_{max}$  and  $\pm \beta_{max}$ ) from their trim positions. The disturbance is mainly in roll due to  $\beta$  variations, +ve  $\beta_{max}$  generates a -ve rolling moment because the vehicle has significant amount of dihedral effect. The red rectangles at the tips of the arrows show the amount of estimated uncertainty in  $C_l$  and in  $C_n$  at this flight condition. The aero-uncertainties are obtained from file "*LiftBody.Unce*".

Comparison Between Control Moment Partial Versus Aero-Disturb Moment Partial (red)  
 Yaw & Roll Control Partial  $C_n/\delta_R$  and  $C_l/\delta_P$  versus  $C_n/\beta$  &  $C_l/\beta$



The above moment partials vector diagram shows the variation in roll and yaw moments per acceleration demands in roll and yaw in  $(\text{rad}/\text{sec}^2)$ . The blue vector is  $\{C_n\delta_R, C_l\delta_R\}$  which is almost in the yaw direction, and the green vector is  $\{C_n\delta_P, C_l\delta_P\}$  which is mostly in the roll direction but it also couples into yaw. The red vectors at the bottom are the  $\{C_n\beta, C_l\beta\}$  partials. Notice that  $C_l\beta$  is negative due to the dihedral and it is much bigger in magnitude than  $C_n\beta$ . The red rectangle centered at the tip of the  $\{C_n\beta, C_l\beta\}$  vector is due to the uncertainties in the two partials from file "*LiftBody.Unce*".

## LQR Control Design

The file "init.m", shown below, loads the simulation and design systems and the surface mixing matrix into Matlab and it performs the pitch and lateral LQR designs.

```
d2r=pi/180; r2d=180/pi;
[Aps, Bps, Cps, Dps] = pitch_des;           % Load Pitch aero-surf Design Model
[Als, Bls, Cls, Dls] = later_des;          % Load Lateral aero-surf Design Model
[Ave, Bve, Cve, Dve] = vehicle_sim;       % Simulation Model 6-dof
load KmixM27.mat -ascii; Kmix=KmixM27;     % Load Surfaces Mix Logic (7 x 3)

alfa0=29.274; VO=24675.1; Thet0=27.69; ge=32.174;% Additional Vehicle Parameters
calfa=cos(alfa0*d2r); salfa=sin(alfa0*d2r); % for Body to Stability Transform

% Convert Lateral State Vector from Body to Stability Axes, Outputs=States
[A14,B14,C14,D14]= linmod('Ldes5x');      % 5-state model {ps,rs,bet,pint,betint}
A15= C14*A14*inv(C14); B15= C14*B14;    % Stability axis System
C15= C14*inv(C14); D15= D14;

% Lateral LQR Design Using Only the RCS Jets % States: {ps,rs,bet,psint,betint}
R=[1,1]*5; R=diag(R);                   % Cntrl LQR Weights R=[1,1]*5
Q=[1 0.4 0.5 0.2 0.005]*3; Q=diag(Q);    % State LQR Weights Q=[1 0.4 0.5 0.2 0.005]
[Kpr,s,e]=lqr(A15,B15,Q,R)              % Lateral LQR design
save Kpr_M27_0.mat Kpr -ascii

% Pitch LQR Design Using the 7 Aero-Surfaces % States: {gami,gama,q,alfa,alfint}
[Ap4,Bp4,Cp4,Dp4]= linmod('Pdes4xb');    % 4-state des model {gami,gama,q,alfa,alfint}
R=4; Q=[0.001 0.1 20.0 100]; Q=diag(Q);  % LQR Weights {gama,q,alfa,alf_int}
[Kq,s,e]=lqr(Ap4,Bp4,Q,R)               % Perform LQR design on Surf
save Kq_M27_0.mat Kq -ascii
```

## Pitch Design

The pitch design model "*Lifting-Body Aircraft Hypersonic Pitch Design Model*" from file "*pitch\_des.m*" consisting of states:  $\{\theta, q, \text{ and } \alpha\}$  is augmented (using Simulink file *Pdes4x.Mdl*) to include also  $\alpha$ -integral in the state-vector. The phugoid states ( $\delta h$  and  $\delta V$ ) are not included in this model. The state-feedback matrix generated from the LQR algorithm using Matlab is a (1 x 4) gain matrix "*Kq\_M27\_0.mat*".

The following Simulink model "*Sim\_Pitch\_Simple.Mdl*" is used for evaluating the pitch LQR design. It includes the state-feedback matrix *Kq* and the mixing-logic matrix *KmixM27*. It shows the system's response to 1° change command in  $\alpha$ . The surface deflections are mainly in the two elevons, but the four body-flaps are also participating by a smaller amount.

## Stability Analysis

Figure (1.5) shows the Simulink model "Stab\_Anal.mdl" used for analyzing the stability margins in the frequency domain. This model is similar to the simulation "Simul\_6dof.Mdl" but it is configured for open-loop analysis. One loop is opened and the other two loops are closed (in the case shown below the pitch loop is opened). The Matlab file "Frequ.m" uses this model to calculate the frequency response across the opened loop. The next two figures show the Nichols plots in the pitch and roll directions and the red lines show the phase and gain margins for the Mach # 27 case.

### Stability Analysis Model

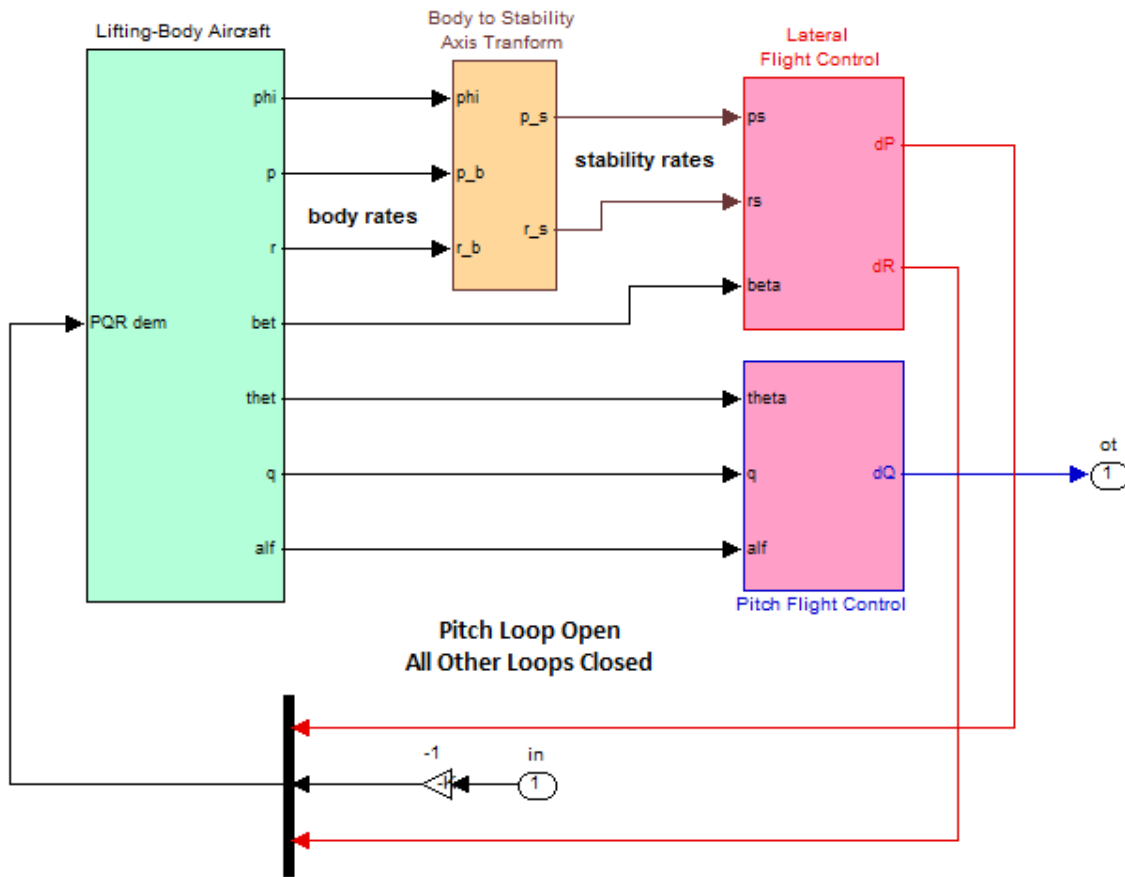
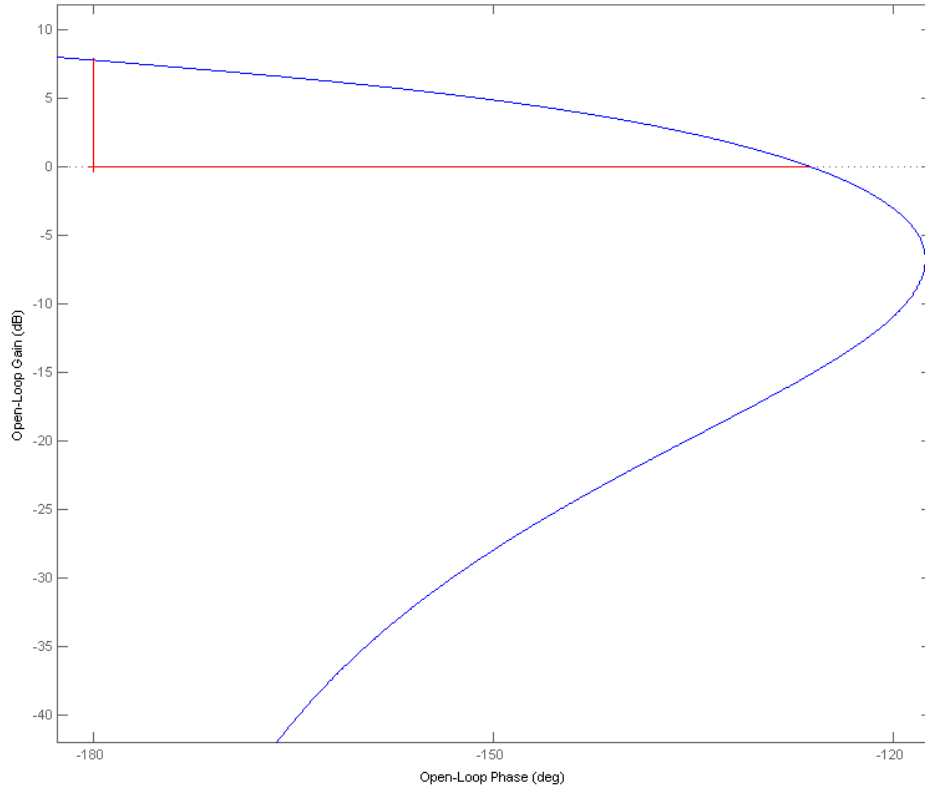


Figure 1.5 Stability Analysis Model "Stab\_Anal.mdl" used for frequency response analysis

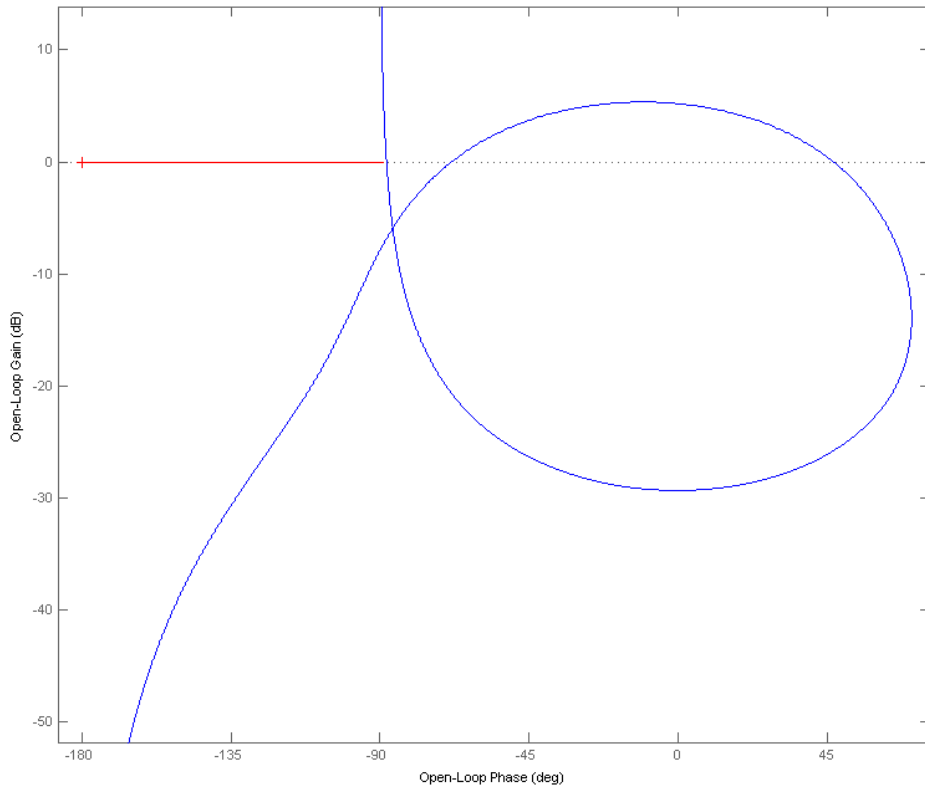
### Stability Margins in the Pitch Loop

Pitch Axis Loop Opened, Roll & Yaw Loops Are Closed



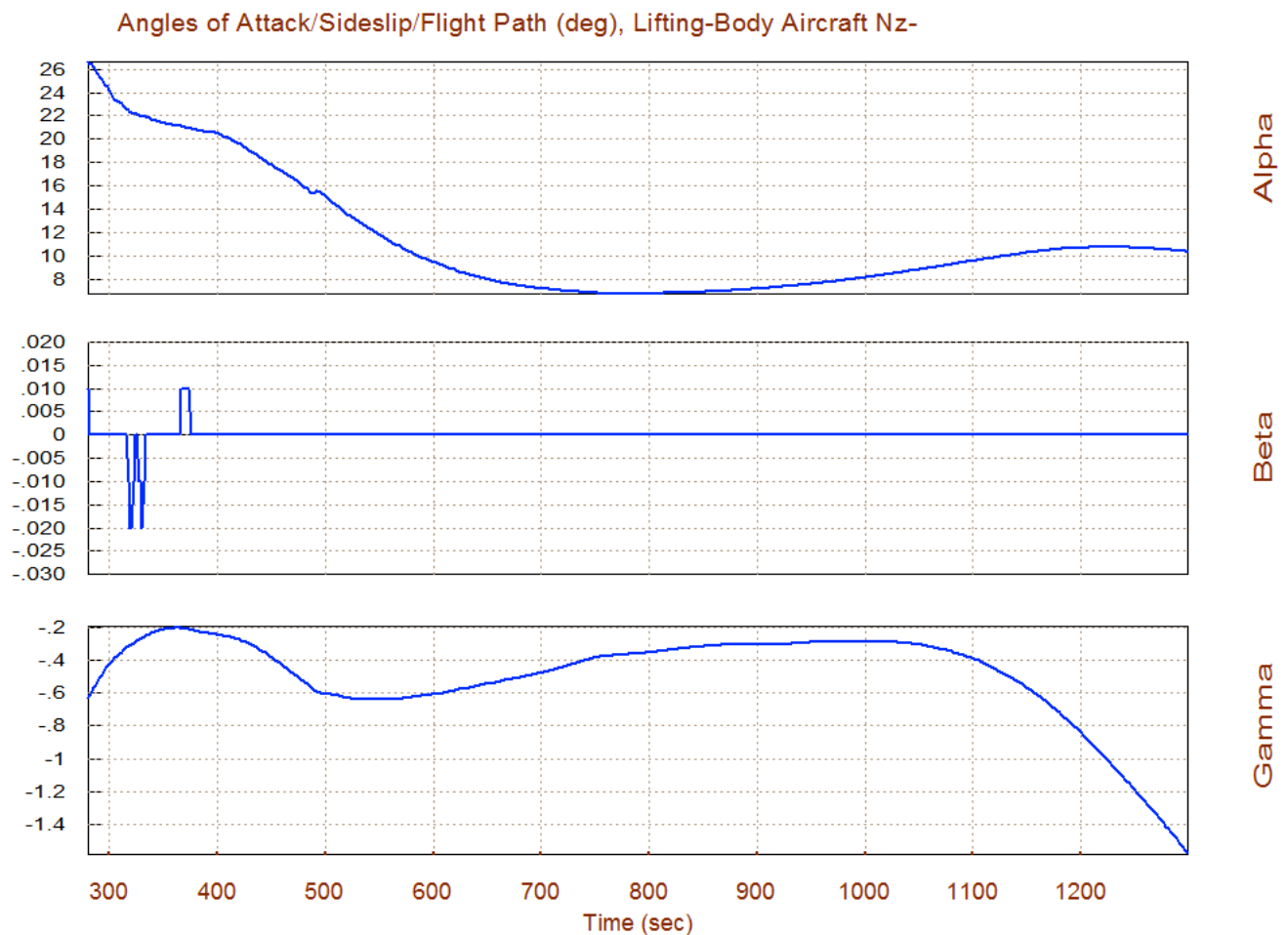
### Stability Margins in the Roll Loop

Roll Axis Loop Opened, Pitch & Yaw Loops Are Closed



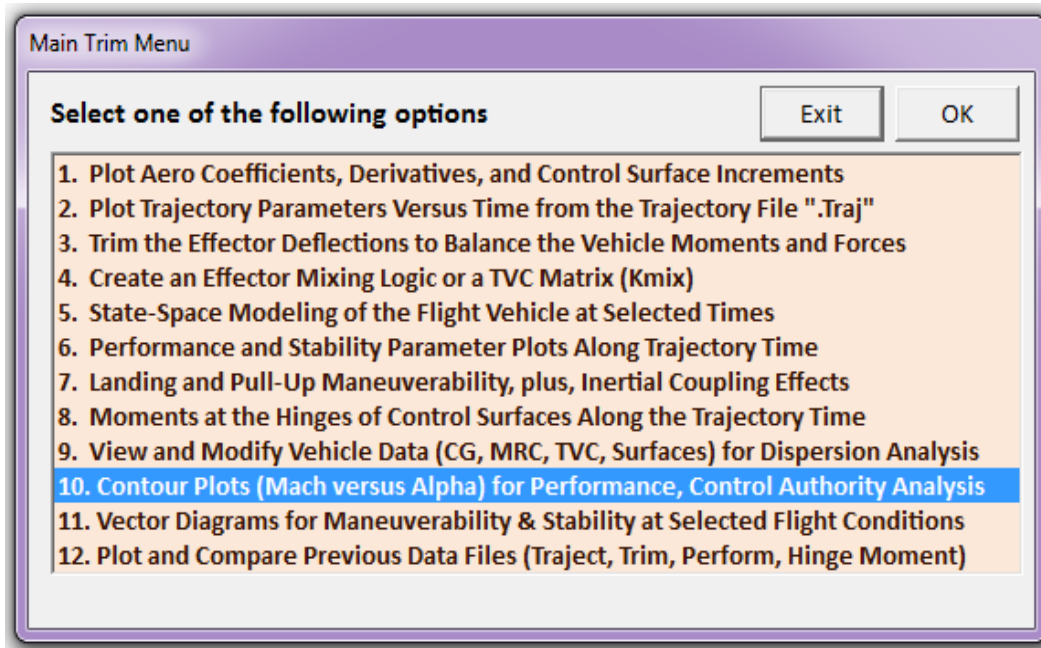
## 1.2 Normal Acceleration Control Mode

As the  $\alpha$ -command begins to come down from  $29^\circ$ , at  $t=270$  sec the flight control system begins to transition from the alpha-control mode to the Nz-control mode by using feedback from the normal accelerometer. Initially it attempts to maintain a steady Nz of  $-33.5$  (ft/sec<sup>2</sup>) and the command is gradually reduced to a smaller value. This section of the trajectory is analyzed in folder "C:\Flixan\Trim\Examples\Lifting-Body Aircraft\ Reentry from Space\ Trim\_Anal\ Nz\_Control". The Nz-controlled section of the trajectory is in file "Nz\_Control.Traj". The surface mixing matrix "KmixM10" has already been calculated and saved in file "Kmix.Qdr". The remaining files are the same as in the alpha-control section. The following figures show some of the trajectory parameters in the Nz-control region between Mach (19 to 5).



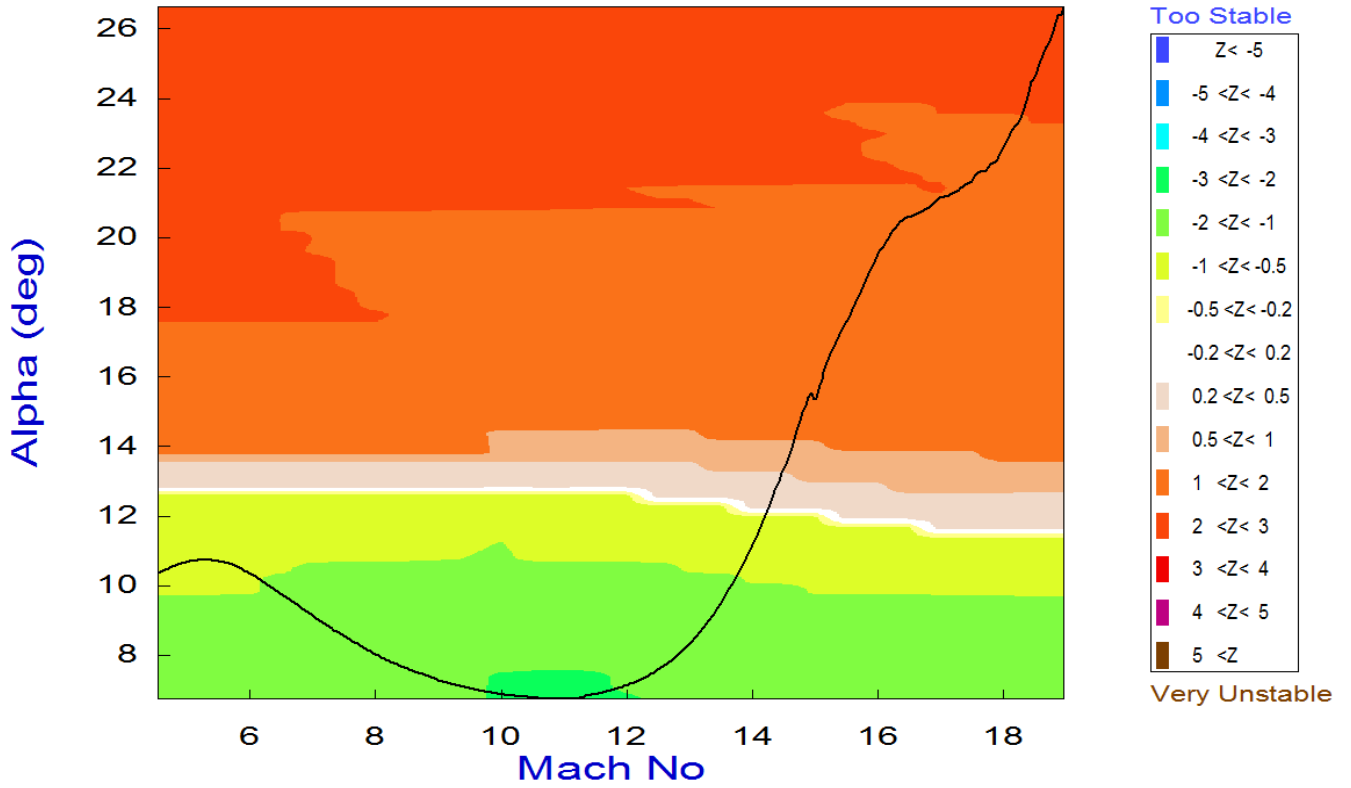
## Contour Plots Analysis

We may now present some of the critical performance parameters in contour plots. Contour plots allow us to view vehicle performance over the entire Mach versus Alpha range. Performance parameters are function of the effector mixing matrix so we must select again matrix KmixM10 from file "Kmix.Qdr". Contour plots is the 10<sup>th</sup> option selected from the Trim main menu, as shown.

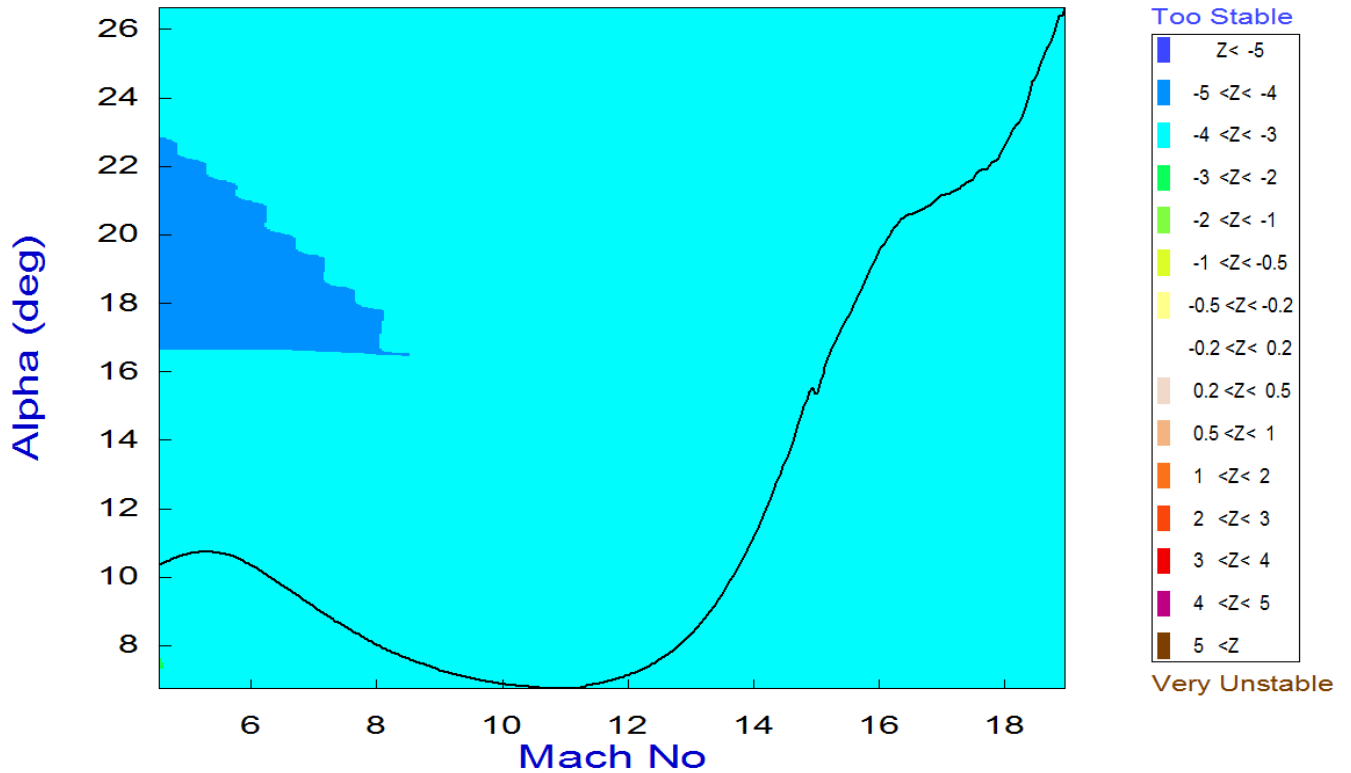


The first two plots show the pitch and lateral stability parameter in the entire Mach versus alpha range. The trajectory is shown by the dark line beginning in the upper right-hand corner and ending in the lower left-hand side. In the pitch axis, although the vehicle can be trimmed over a wide range of alphas, it is statically unstable at angles of attack greater than 13°. Neutral stability is at approximately  $\alpha=12.5^\circ$  visible as a horizontal white band across the pitch stability contour plot. In the lateral direction the vehicle is always statically stable and the stability parameter is almost constant. The LCDP ratio which is a measure of dynamic roll controllability is good for angles of attack below 14°. A different control-surface mixing logic matrix is required at high angles of attack. The following contour plots were calculated using a constant mixing-logic matrix but in actual flight or simulations the mixing-logic is not constant but it is also scheduled similar to the control gains as a function of Mach and alpha. The roll control authority for  $\beta_{\max}= 1^\circ$  disturbances is marginally acceptable for angles of attack below 11°. The pitch and yaw control authority against 1° of ( $\alpha_{\max}$  and  $\beta_{\max}$ ) disturbances is good.

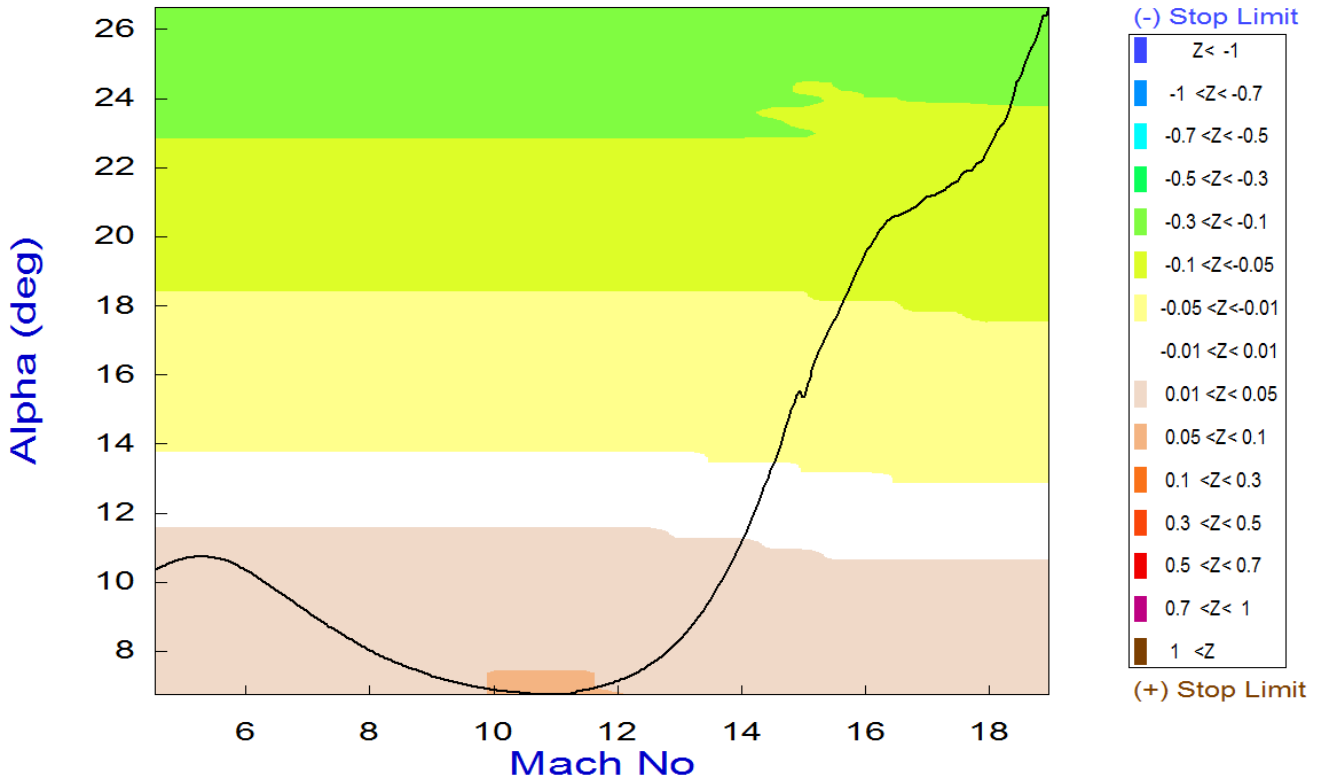
### Pitch Stability Contour Plot (Mach vs Alpha)



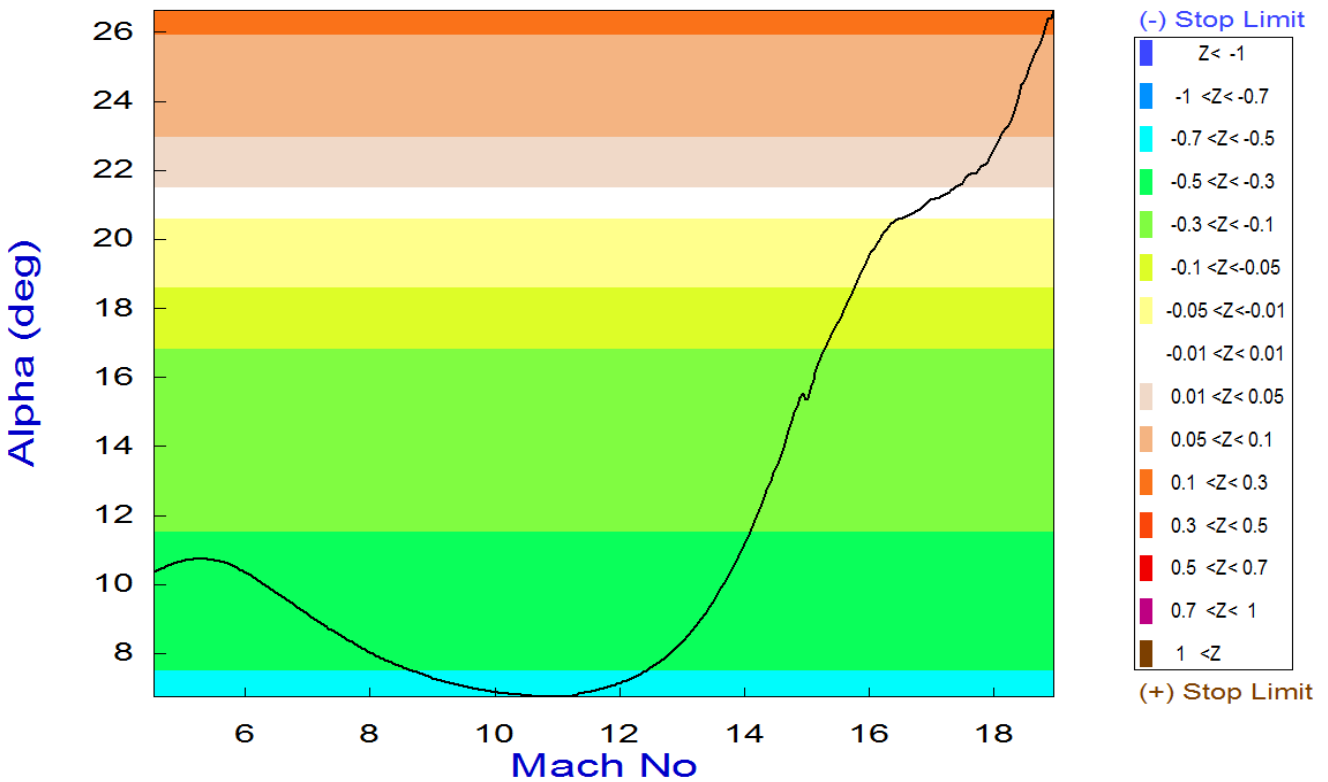
### Lateral Stability Contour Plot (Mach vs Alpha)



Pitch Control Effort Contour Plot (Mach vs Alpha)

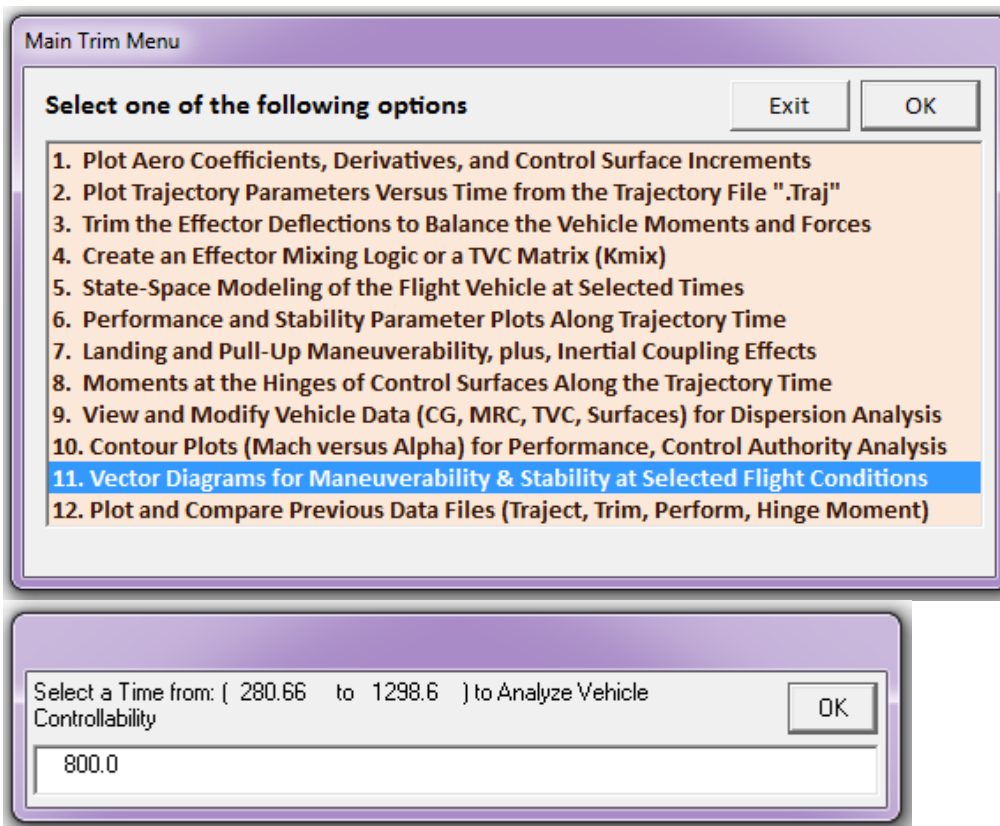


Yaw Control Effort Contour Plot (Mach vs Alpha)



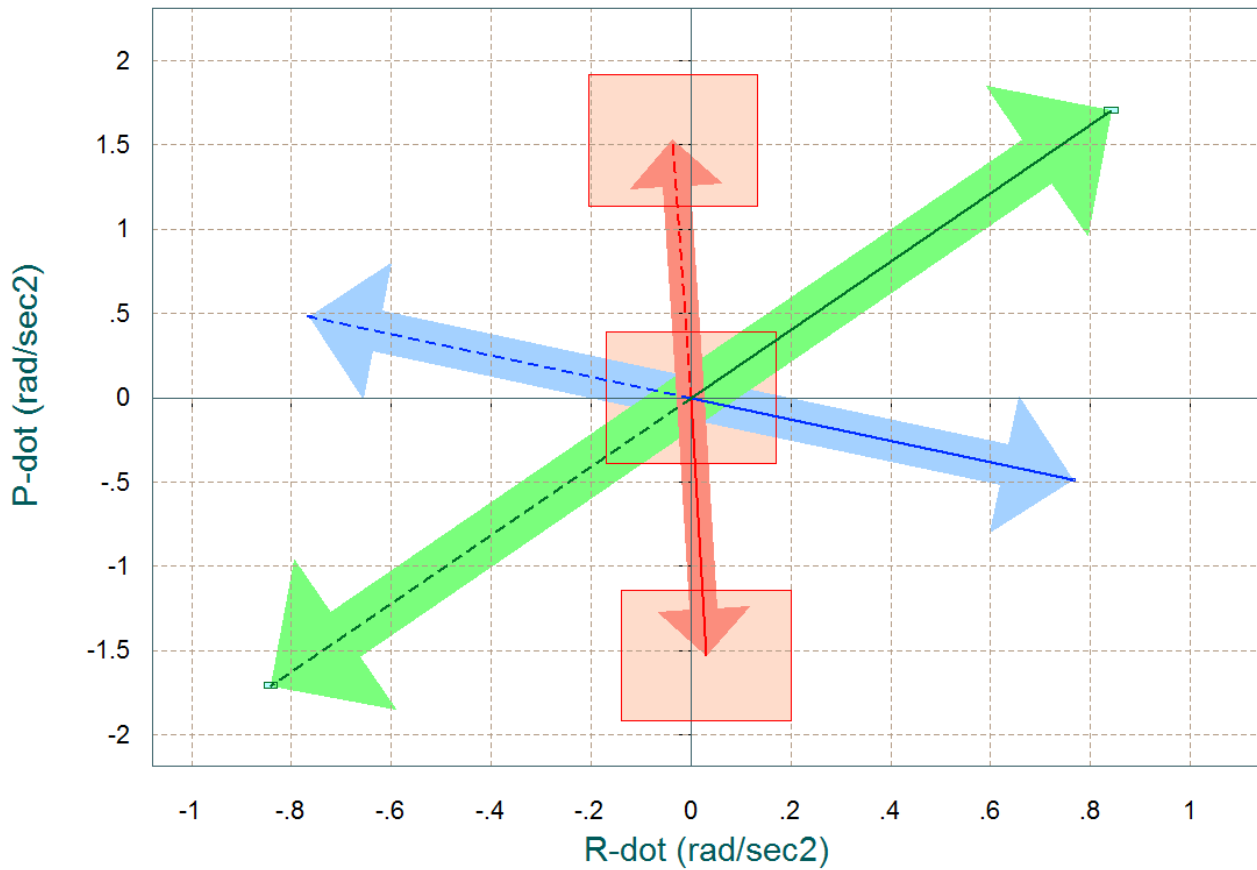
## Controllability Analysis by Using Vector Diagrams

Vector diagrams are 2-dimensional diagrams used for analyzing the vehicle controllability at a specified flight condition. We visually compare the control capability of the aero-surfaces in two directions (mainly roll and yaw in this case) against the effect of wind-shear disturbance on the vehicle due to beta in the same two directions and determine if the vehicle has sufficient control authority to counteract against the disturbance moments. It is not just a magnitude comparison but it also allows the analyst to examine the directions of the controls versus the disturbance directions. This helps to evaluate the orthogonality of the control system, compare the accelerations magnitudes due to controls and winds, and to determine if the controls are more powerful and their corresponding directions capable of counteracting the disturbance moments along the roll, pitch and yaw directions in this case. From the Trim menu select option (11), and then an arbitrary flight condition at t=800 sec, in the middle of the Nz-controlled trajectory, corresponding to Mach 10.



The following dialog consists of menus used for selecting the vehicle mass, Mach number, alpha, and beta. The default values correspond to the selected flight time. You may keep those parameters or change them into something different. In this case we select the default values and click "Select". Notice that we do not have aero data for Mach 10. The nearest one is Mach 5. The disturbances are caused by wind-shear defined by the maximum alpha and beta produced. In the following dialog enter the maximum disturbance angles ( $\alpha_{\max}$  and  $\beta_{\max}$ )=1°, and then select the (7x3) control surface combination matrix "KmixM10" from file Kmix.Qdr, as shown.

Comparison Between Maximum Control Accelerations and Max Accels due to Beta (red)  
 Roll & Yaw Accelerations due to Maximum Roll/ Yaw Control and due to Max Beta



The above vector diagram shows the roll and yaw accelerations produced when the roll and yaw FCS demands are maximized (before saturating the aero-surfaces). The solid blue vector corresponds to max positive yaw FCS demand ( $+\delta R_{FCS\_Max}$ ) and the dashed blue vector to max negative yaw demand. Similarly, the green vectors correspond to the roll FCS demands ( $\pm\delta P_{FCS\_Max}$ ). The two red vectors show the angular acceleration effects generated due to the variations in the angles of attack and sideslip ( $\pm\alpha_{max}$  and  $\pm\beta_{max}$ ) from their trim positions. The disturbance is mainly in roll due to  $\beta$  variations, +ve  $\beta_{max}$  generates a -ve rolling moment because the vehicle has significant amount of dihedral effect. The red rectangles at the tips of the arrows show the amount of uncertainty in roll and yaw accelerations at this flight condition. The uncertainties are read from file "*LiftBody.Unce*".

## Linear Simulation Model

The Matlab simulation model for the Mach 10 case is in file "*Simul\_6dof.mdl*", shown in figure (1.2.2). It is similar to the  $\alpha$ -control case but instead of  $\alpha$ -feedback it uses  $N_z$ -feedback instead. It is used for evaluating the coupled system's response to roll and  $N_z$  commands and to wind disturbances. The output rates in this model are body rates since the rate-gyro measurements are in body axes. The controller, however, was design based on the stability axis model and it expects to see roll and yaw rates about the velocity vector  $V_0$ . A body to stability axis transformation block is, therefore, included in the simulation to convert the ( $p$  &  $r$ ) body rates to stability rates ( $p_{stab}$  &  $r_{stab}$ ) which are required in the lateral LQR state-vector feedback. The linearized turn-coordination terms are also included in this block.

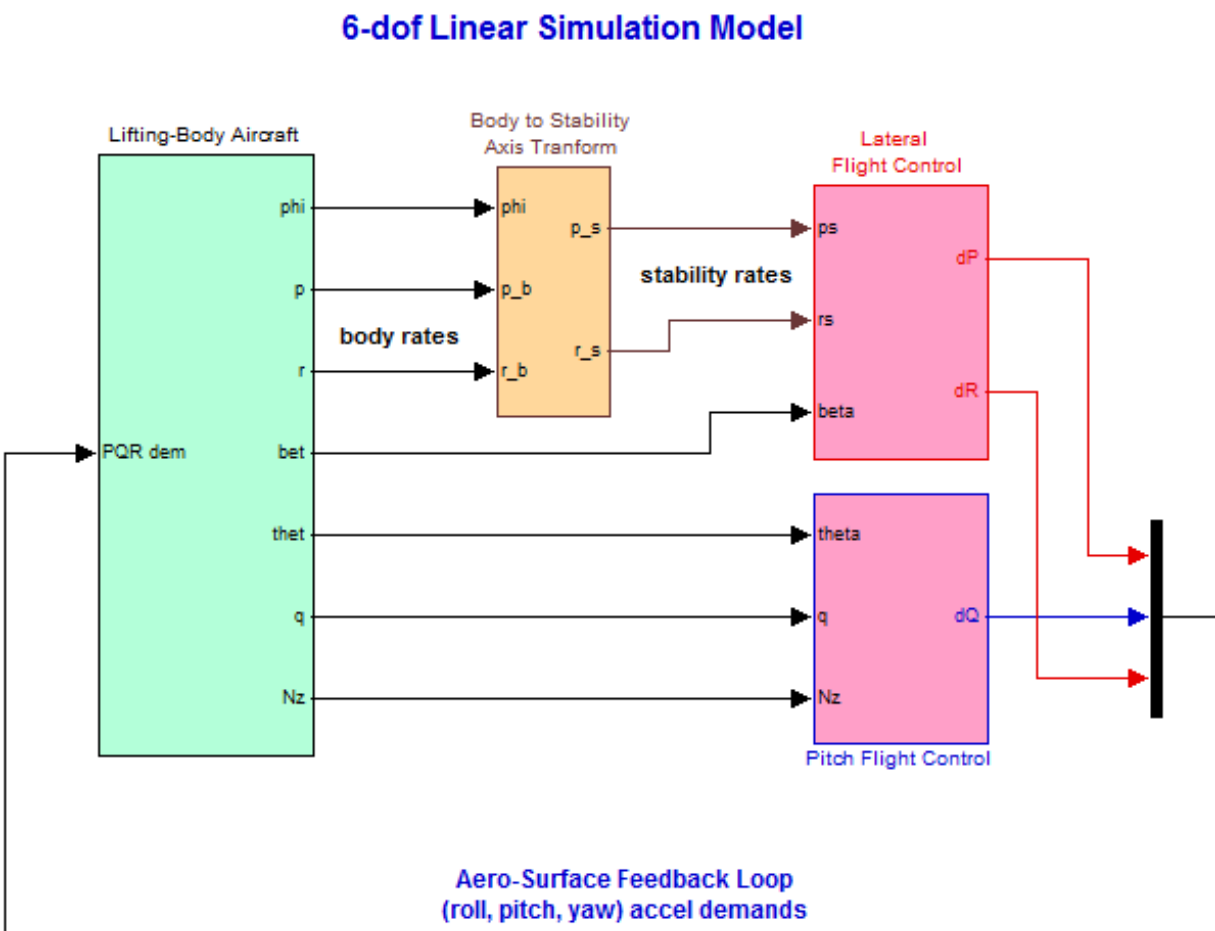
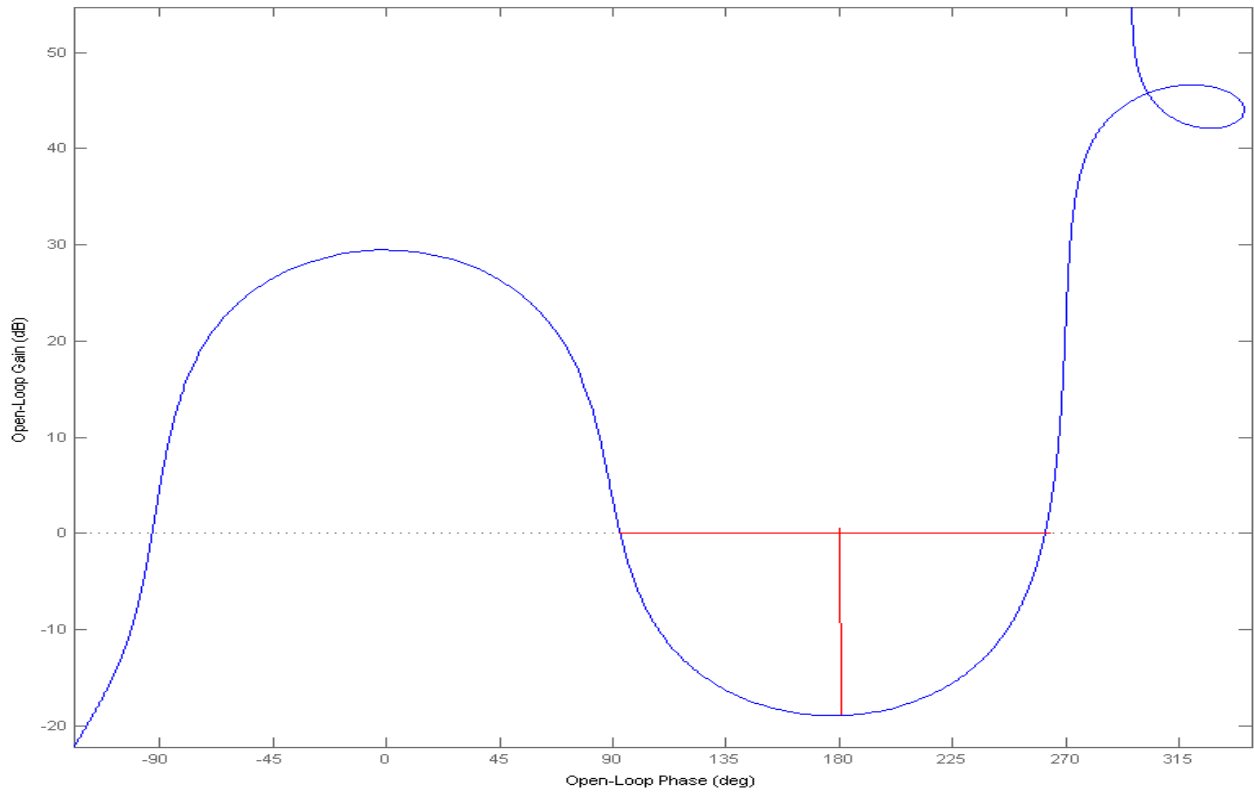


Figure 1.2.2a Simulation Model in File "*Simul\_6dof.Mdl*"

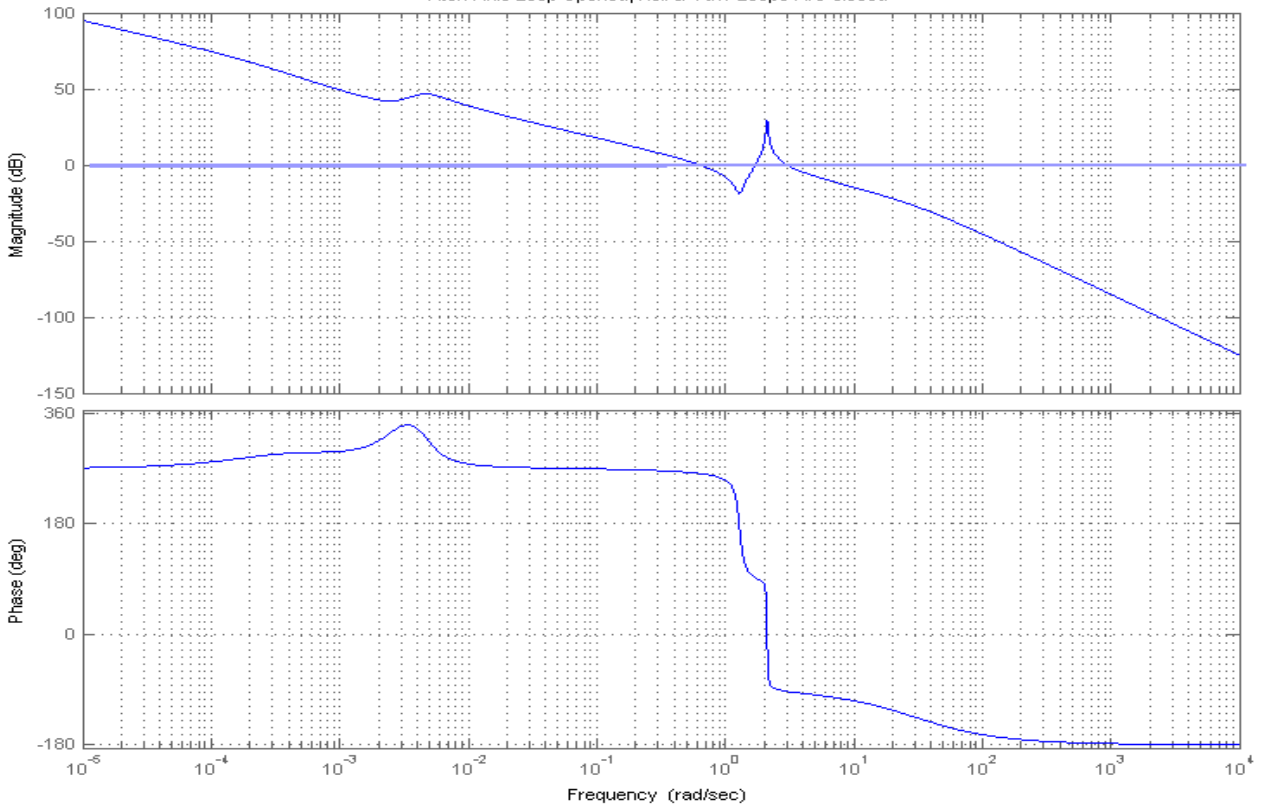
### Pitch Axis Stability Margins

Pitch Axis Loop Opened, Roll & Yaw Loops Are Closed



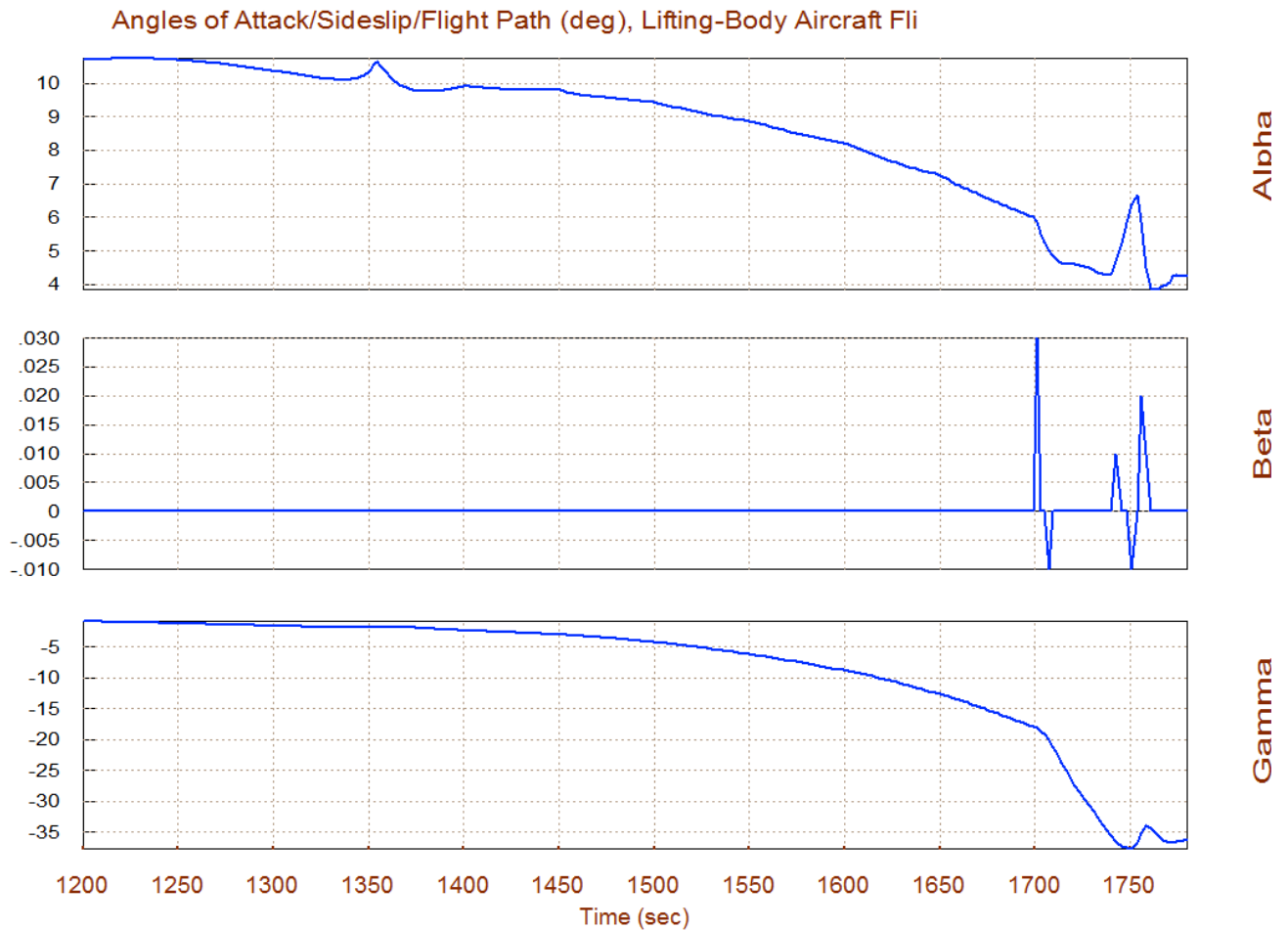
### Pitch Axis Bode Plot

Pitch Axis Loop Opened, Roll & Yaw Loops Are Closed

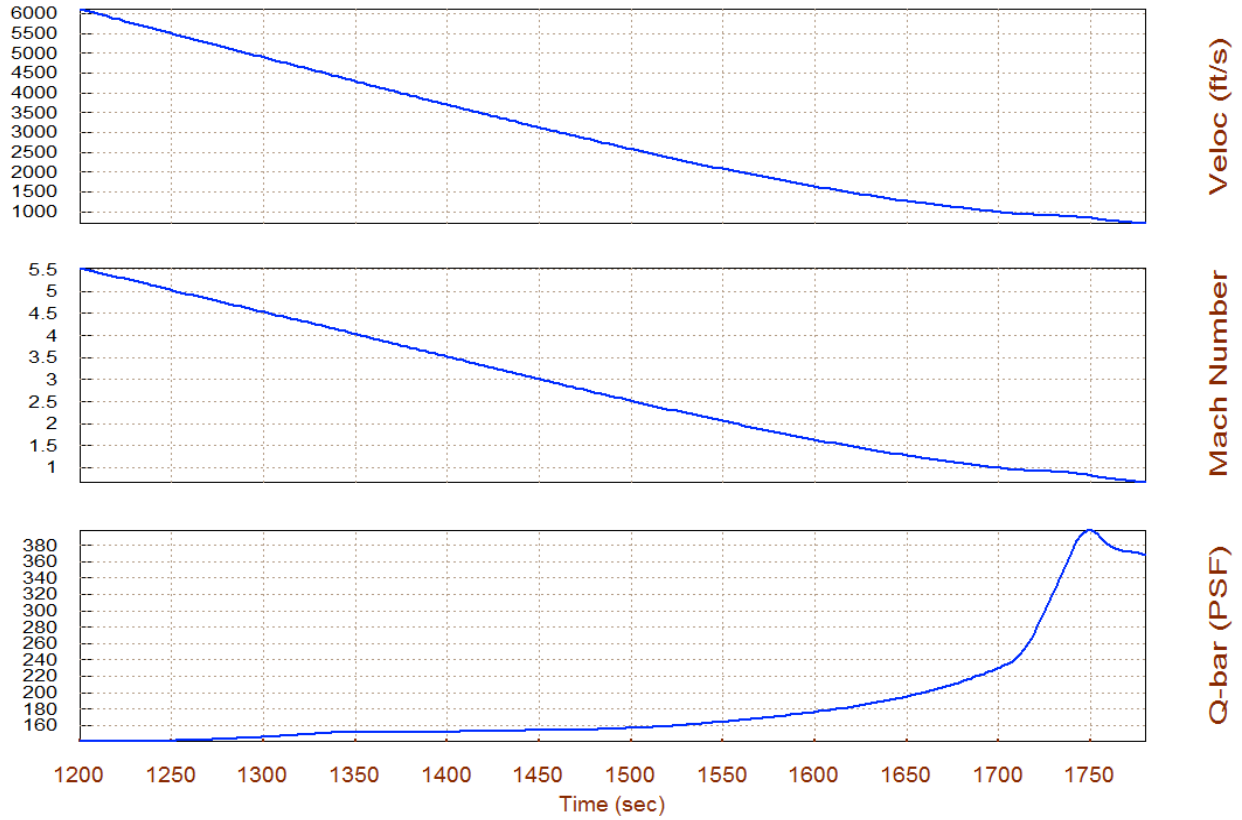


### 1.3 Flight-Path Angle Control Mode

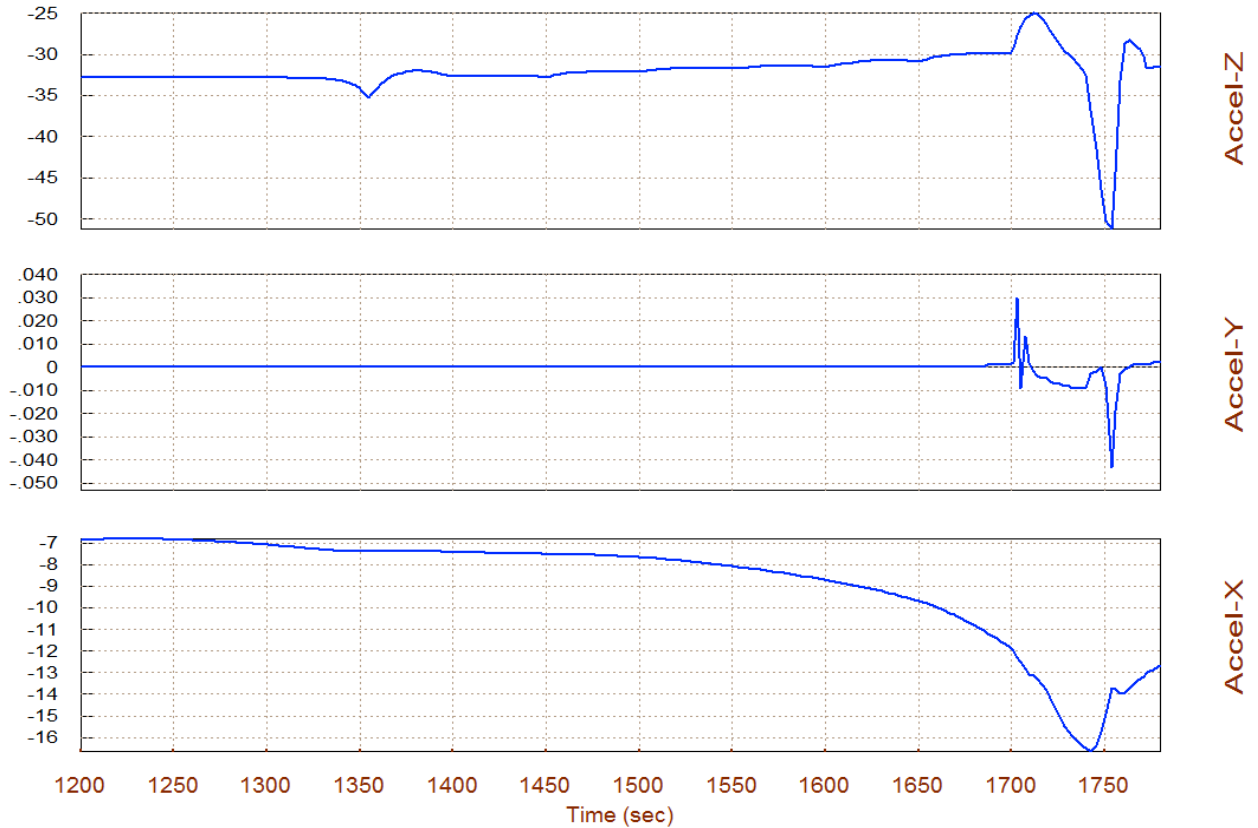
Flight-path ( $\gamma$ ) control is phased-in (to avoid transients) while  $N_z$ -control is phased-out. It provides a more direct control of the vehicle direction by a closed-loop guidance system which calculates the flight-path angle command as a function of range, altitude, and speed. Guidance, however, is beyond the scope of this example. This section of the trajectory is analyzed using Trim in folder "C:\Flixan\Trim\Examples\Lifting-Body Aircraft\Reentry from Space\Trim\_Anal\ Gamma\_Control". The Gamma-controlled section of the trajectory is in file "Gamma\_Cntl.Traj". The surface mixing matrix "KmixM2" has already been calculated and saved in file "Kmix.Qdr". The remaining files are the same as in the  $\alpha$ -control section. The following figures show some of the trajectory parameters in the  $\gamma$ -control region between Mach (5 to 0.9). The flight-path angle drops significantly towards the end of this section, at  $t=1700$ , after the vehicle performs a  $30^\circ$  bank maneuver to align its direction with the runway and in order to gain speed before it performs its landing flare. Also the dynamic pressure increases significantly in this final period as it approaches for landing at 30,000 (ft) altitude.



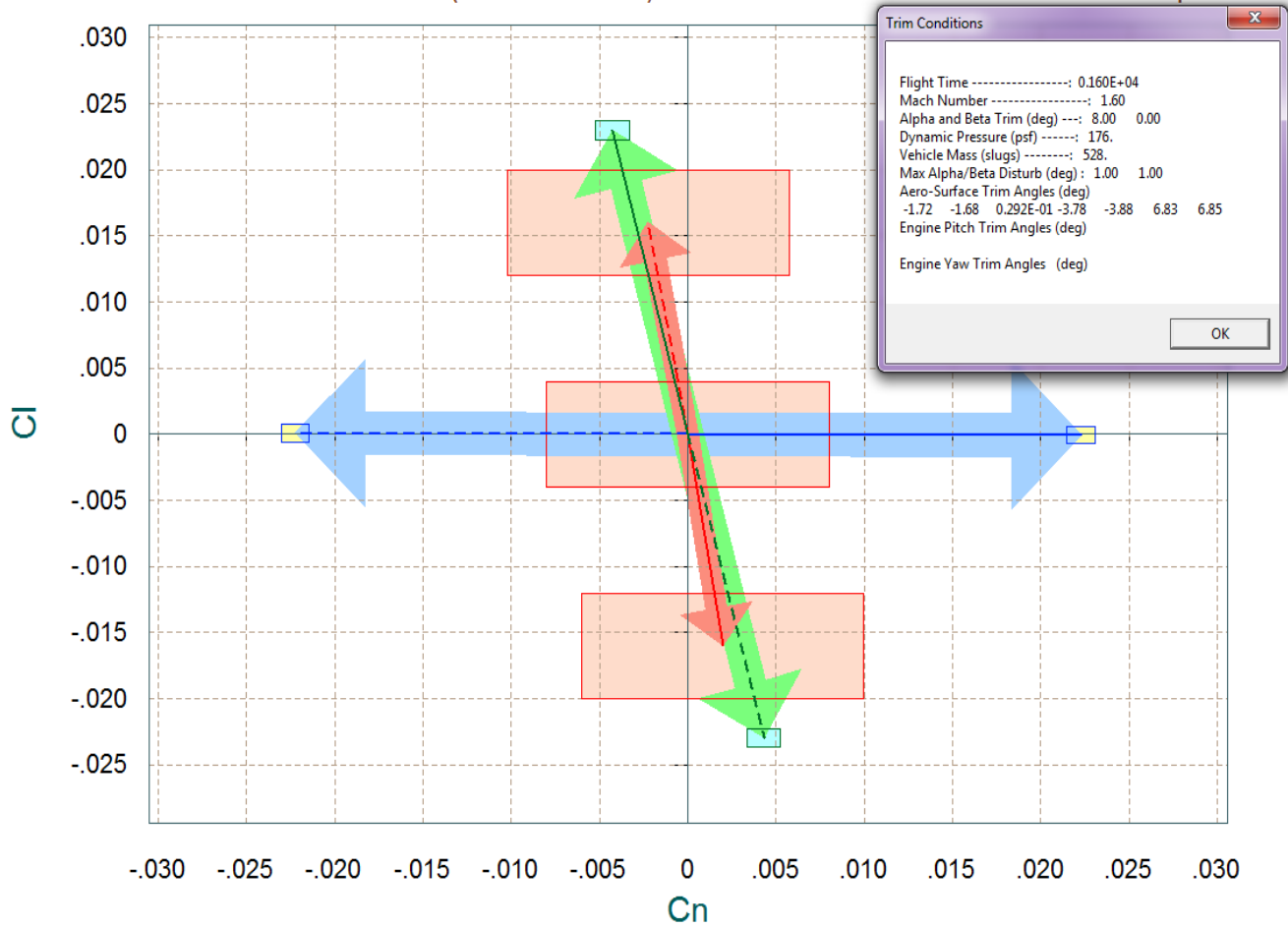
### Velocity, Dynamic Pressure, Lifting-Body Aircraft Flight-Path Control



### Sensed Acceleration in (ft/sec<sup>2</sup>), Lifting-Body Aircraft Flight-Path Control

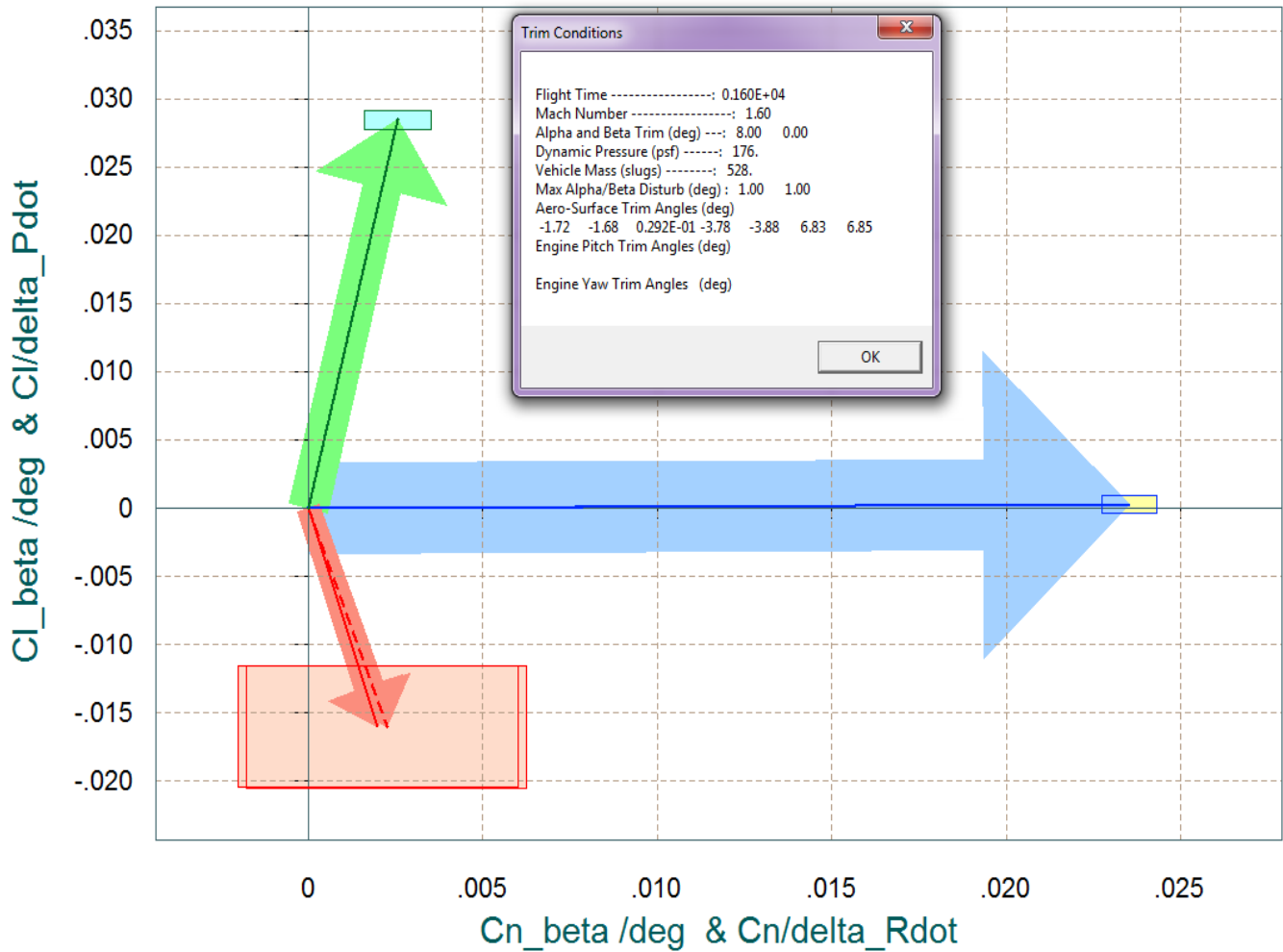


## Comparison Between Maximum Control Moments Against Maximum Disturb Moments (red) Roll & Yaw Control Moments (non-dimension) vers Disturb Moment due to Max Beta/Alpha



The above vector diagram shows the roll and yaw moments, non-dimensional ( $C_l$  &  $C_n$ ), produced when the roll and yaw FCS demands are maximized (before saturating the aero-surfaces). The solid blue vector corresponds to max positive yaw FCS demand ( $+\delta R_{FCS\_Max}$ ) and the dashed blue vector to max negative yaw demand ( $-\delta R_{FCS\_Max}$ ). Similarly, the green vectors correspond to the roll FCS demands ( $\pm \delta P_{FCS\_Max}$ ). The two red vectors show the roll and yaw moments generated by the variations in the angles of attack and sideslip ( $\pm \alpha_{max}$  and  $\pm \beta_{max}$ ) from their trim positions. The disturbance in this case is mainly in roll due to  $\beta$  variations, +ve  $\beta_{max}$  generates a -ve rolling moment because the vehicle has significant amount of dihedral effect. The red rectangles at the tips of the arrows show the roll and yaw moments uncertainty in this flight condition. The rectangles at the tips of the control vectors represent the control uncertainties in moments. The uncertainties are obtained from file "*LiftBody.Unce*".

## Comparison Between Control Moment Partial Versus Aero-Disturb Moment Partial (red) Yaw & Roll Control Partial $C_n/\delta_R$ and $C_l/\delta_P$ versus $C_n/\beta$ & $C_l/\beta$



The above figure is moment partials vector diagram showing the variation in roll and yaw moments per acceleration demands in roll and yaw in  $(\text{rad}/\text{sec}^2)$ . The blue vector is  $\{C_n/\delta_R, C_l/\delta_R\}$  which is mainly in the yaw direction, and the green vector is  $\{C_n/\delta_P, C_l/\delta_P\}$  which affects both roll and yaw directions. The red vectors pointing downward are the  $\{C_n/\beta, C_l/\beta\}$  partials. Notice that  $C_l/\beta$  is negative due to the dihedral and it is bigger in magnitude than  $C_n/\beta$ . The red rectangle centered at the tip of the  $\{C_n/\beta, C_l/\beta\}$  vector is due to the uncertainties in the two partials. Similarly the yellow rectangle at the tip of the yaw control partial is due to the uncertainties in  $\{C_n/\delta_R, C_l/\delta_R\}$ , and the cyan rectangle at the tip of the roll control partial is due to the uncertainties in  $\{C_n/\delta_P, C_l/\delta_P\}$ . The uncertainties are obtained from file "*LiftBody.Unce*".

## Stability Analysis

Figure (3.8) shows the Simulink model "Stab\_Anal.mdl" used for analyzing the stability margins for the Mach 2 case. This model is similar to the simulation "Simul\_6dof.Mdl" but it is configured for open-loop analysis. One loop is opened and the other two loops are closed (in the case shown below the roll loop is opened). The Matlab file "Freque.m" uses this model to calculate the frequency response across the opened loop. The next two figures show the Nichols plots in the pitch and roll directions and the red lines are highlighting the phase margins for the Mach 2 case.

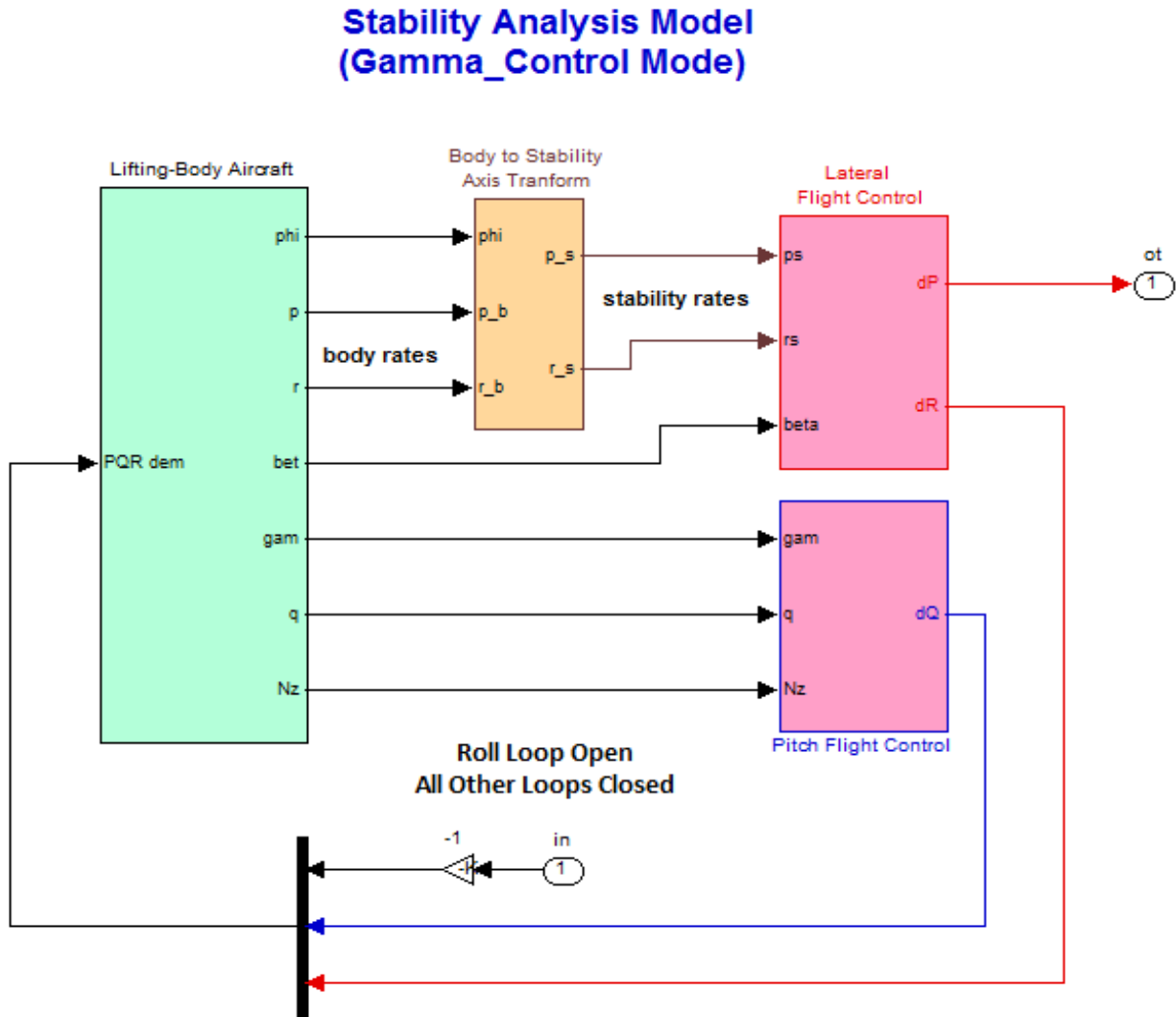
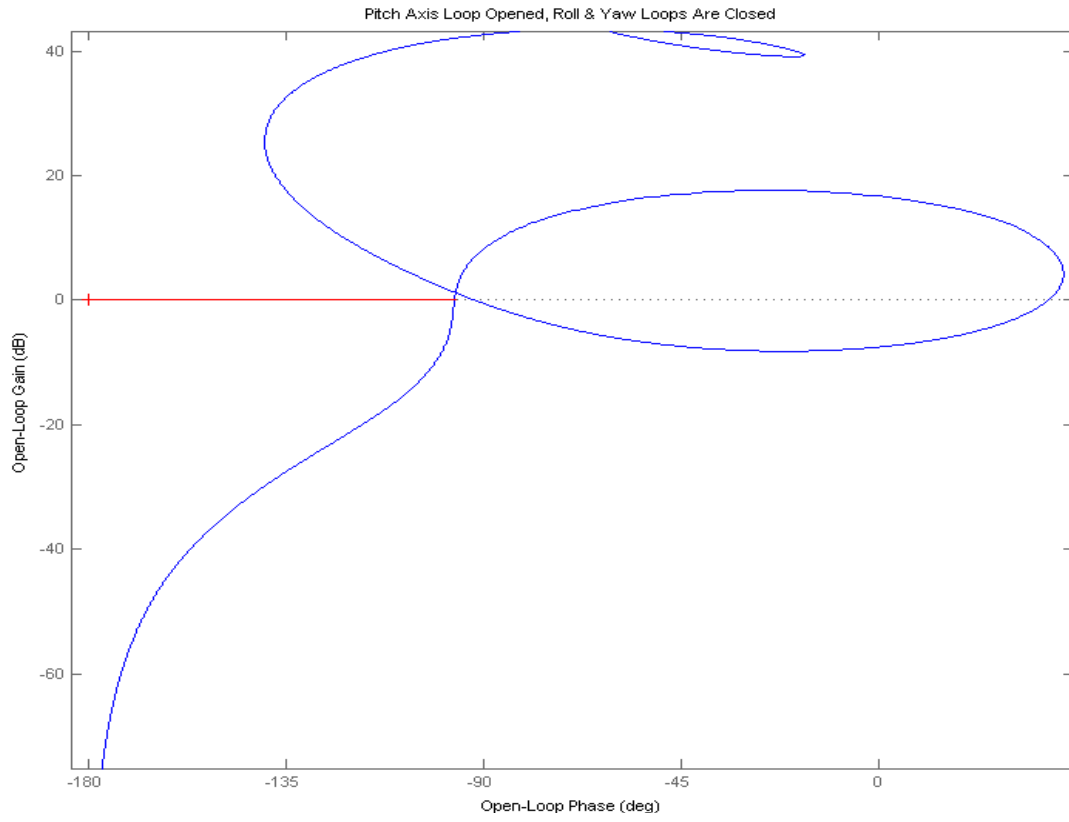
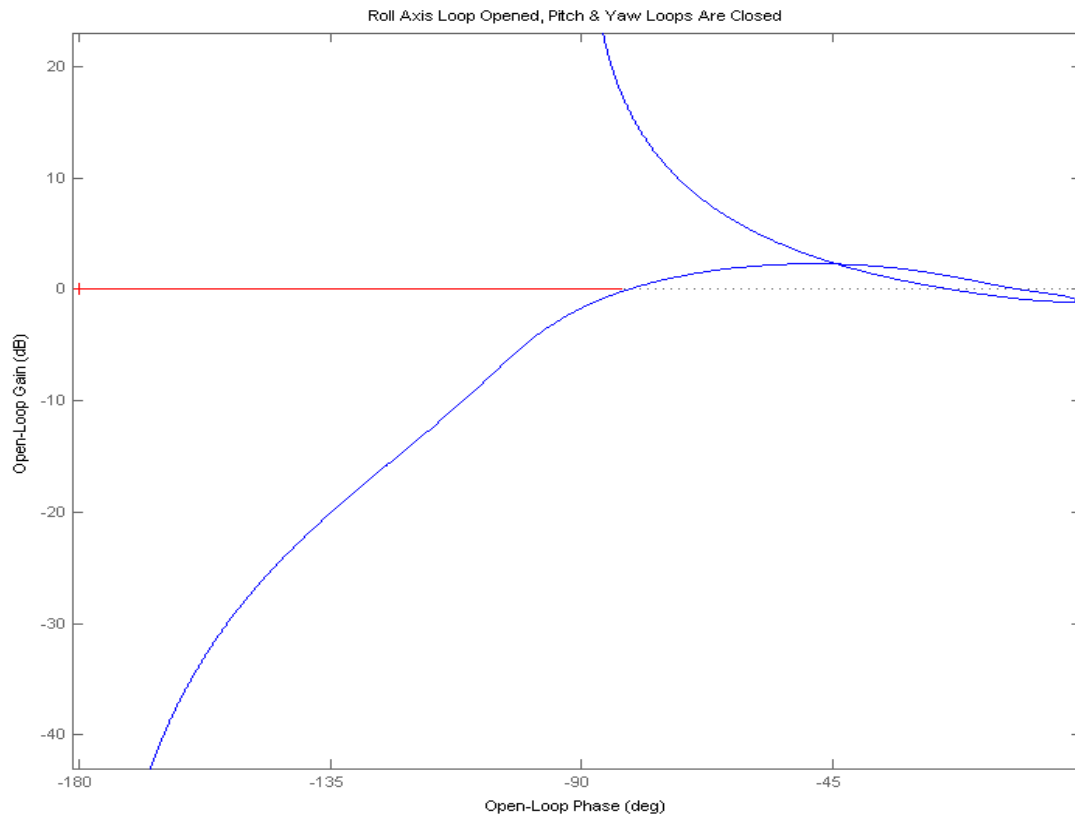


Figure 3.8 Stability analysis model "Stab\_Anal.mdl" used for frequency response analysis

### Pitch Axis Stability



### Roll Axis Stability



## 1.4 Approach and Landing Mode

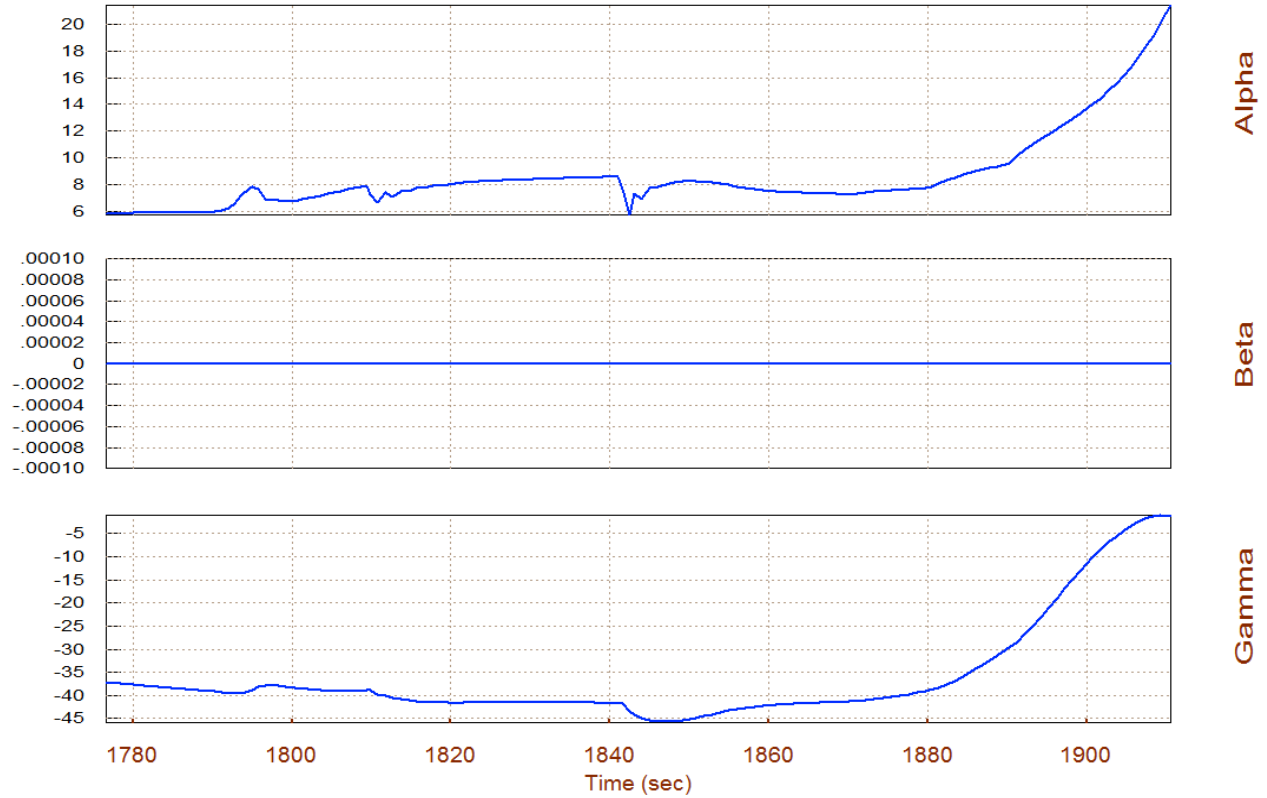
The approach and landing phase is different and more complex in comparison with the previous three phases and we will analyze it in more detail. It begins at an altitude of approximately 20,000 (ft) and the vehicle dives by increasing its ( $\gamma$ ) to  $-50^\circ$  in order to gain sufficient speed and to be able to perform its final pitch-up flare without stalling, where  $\gamma$  is reduced to zero. There is a closed-loop guidance system that controls altitude and velocity. The flight control system receives changes in altitude and velocity commands from guidance and it translates them to surface



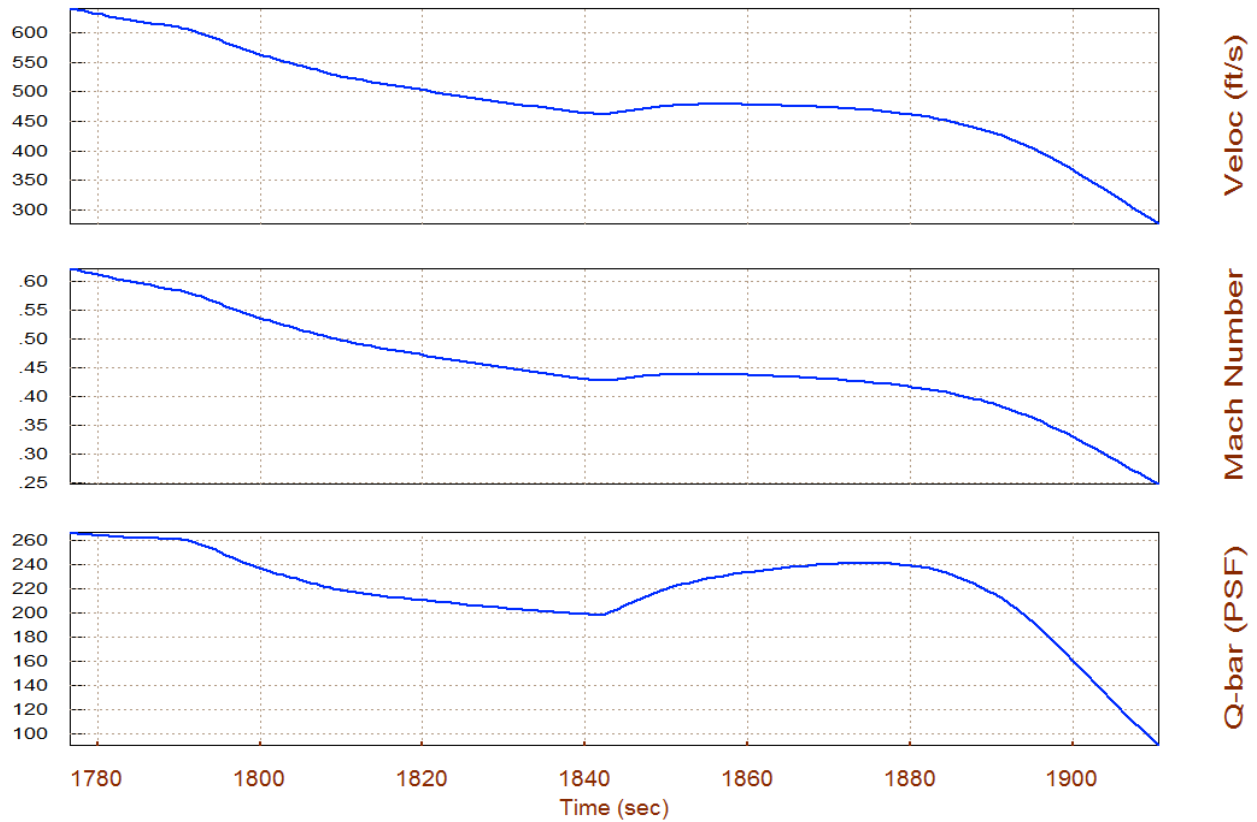
deflections. In the lateral direction there are no major roll maneuvers to be performed because the vehicle is already aligned with the runway. Directional feedback from radar become small changes in direction commands to the heading control system and they are converted to small roll adjustments that take out any misalignment errors due to cross-winds. This approach and landing section of the trajectory is analyzed in folder "*C:\Flixan\Trim\ Examples\ Lifting-Body Aircraft\Reentry from Space\Trim\_Anal\Approach\_Land*". The trajectory is in file "*Apprch\_Land.Traj*". The surface mixing logic will be scheduled in the simulation as a function of Mach#, but in this analysis we will use a fixed matrix "*KmixM0p4b*" that is already prepared and saved in file "*Kmix.Qdr*". The remaining files are the same as in the previous sections. The following figures show some of the trajectory parameters during the approach and landing phase between Mach (0.7 to 0.3). We will repeat a similar trim and performance analysis for this section of the trajectory, design and analyze the landing flight-control system which is significantly different here because in the longitudinal axis we now have two separate control loops for altitude and velocity control. In addition to the classical stability analysis we will also use the Flixan program to generate uncertainty models and analyze the flight control system robustness to structured parameter variations by using  $\mu$ -analysis.

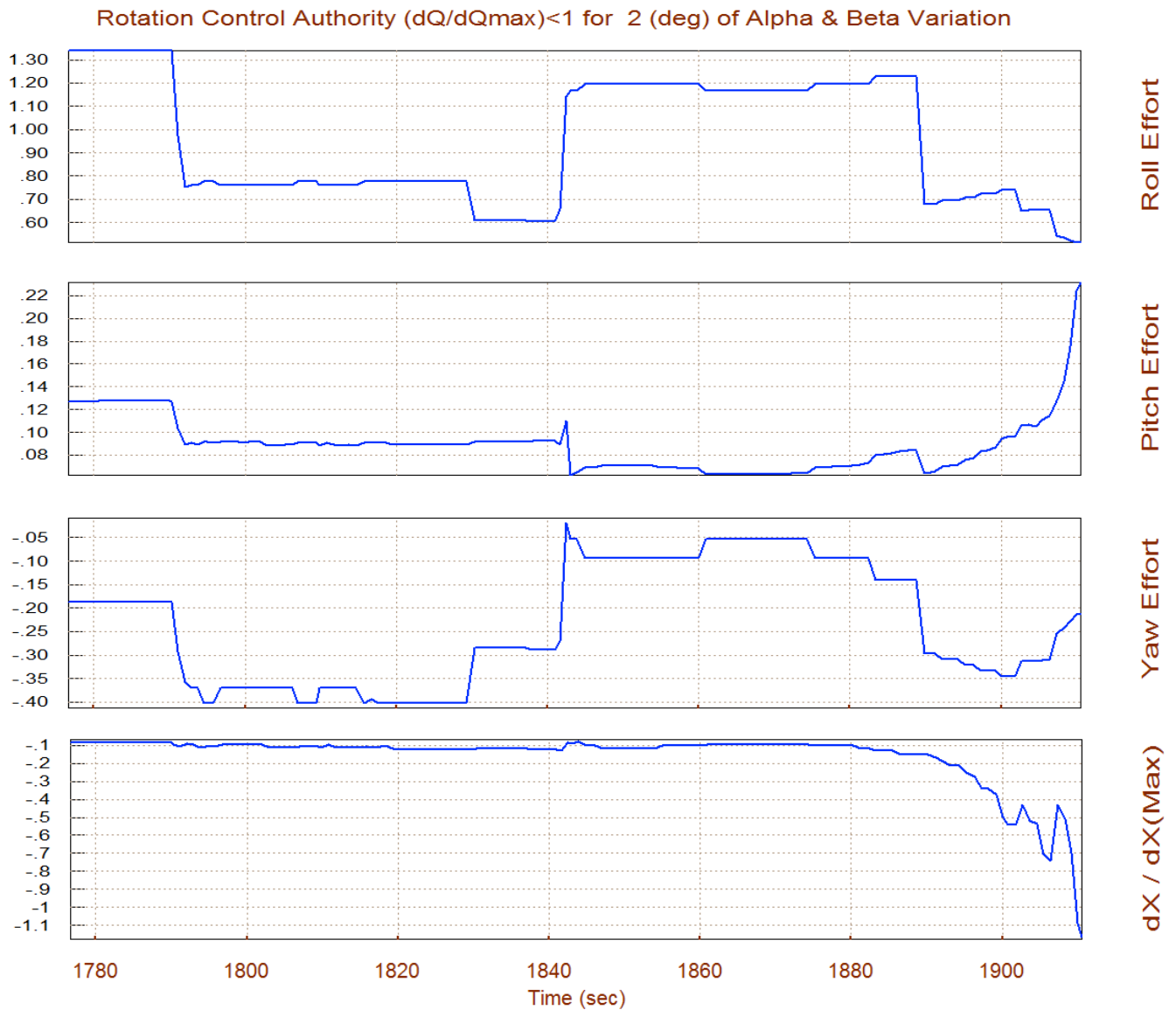
Let us begin by first taking a look at the trajectory. Notice that the speed-brake is partially deployed for a 55 sec period before landing, between  $t=1790$  to  $t=1845$  sec. The speed-brake is mechanized by differential body-flap deflections controlled by the 4th column of the mixing-logic matrix. By partially deploying the speed-brake it enables the velocity control system to modulate the vehicle drag and thus control speed against wind variations. The speed-brake, however, is re-deployed about a minute before touch-down to enable better pitch/altitude control which is more critical for the final flare. Notice how the speed increases before the pitch-up flare when the speed-brake is re-deployed.

Angles of Attack/Sideslip/Flight Path (deg), Lifting-Body Aircraft App



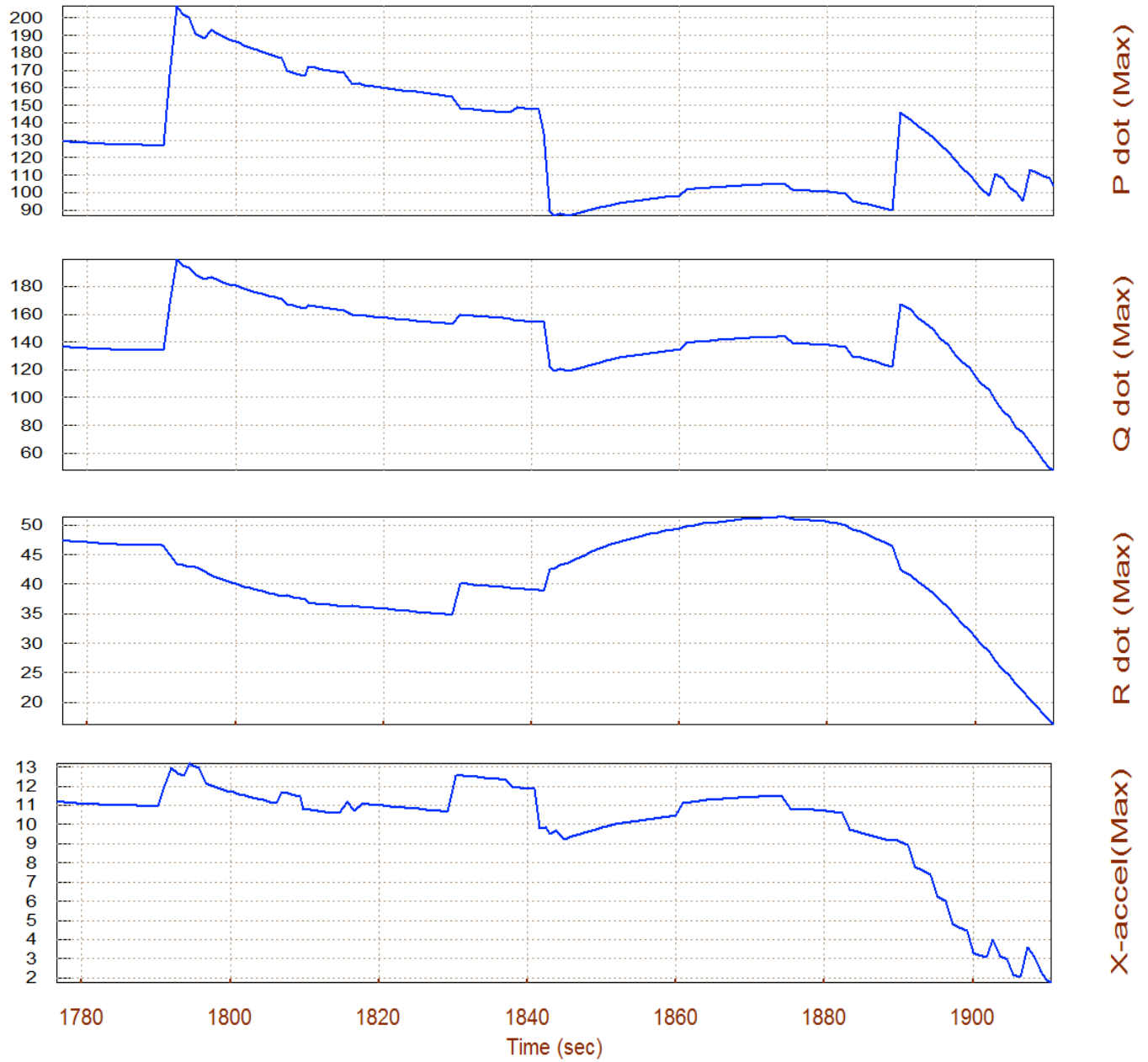
Velocity, Dynamic Pressure, Lifting-Body Aircraft Approach and Land, with SB





The performance results show that during this phase the vehicle is statically stable both in pitch and lateral. The short-period resonance varies between 1.8 to 3 (rad/sec) and the static margin varies between 4.5% to 9%. In the lateral direction the Dutch-roll resonance varies between 2.8 to 3.8 (rad/sec). The Q-alpha, Q-beta loading is acceptable with a maximum of 2200 (psf-deg). Remember, that this is due to the 2° of ( $\alpha_{max}$  and  $\beta_{max}$ ) excursions caused by wind-shear. The control effort against those wind excursions are sufficiently small in pitch and yaw. In roll, however, the control authority exceeds the acceptable limit. Roll authority was compromised in order to increase the LCDP magnitude and to avoid roll-reversals. It means that in the presence of a strong gust the RCS jets will be energized. The RCS control is always available as an outer loop. The  $Cn\beta$ -dynamic is positive which means that the vehicle is directionally stable. The bank angle parameter ( $\phi$ ) is the bank angle due to a cross-wind causing a  $\beta_{max}=2^\circ$ . It is less than 3° near landing, which is acceptable.

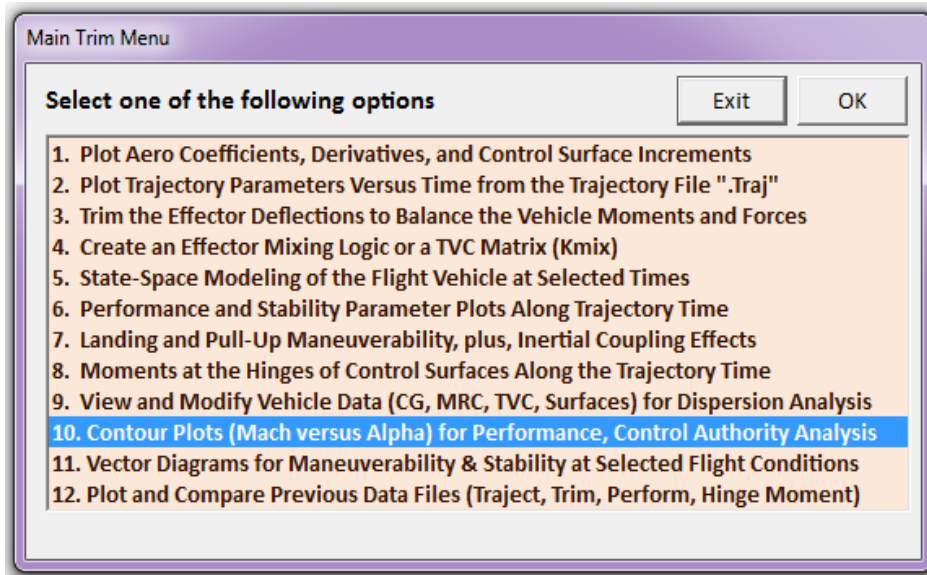
Max Angular Accelerat (deg/sec<sup>2</sup>), at Max Control Demand Lifting-Body Aircraft A



Maximum accelerations in (deg/sec<sup>2</sup>) and (ft/sec<sup>2</sup>) at full control demands in the corresponding directions.

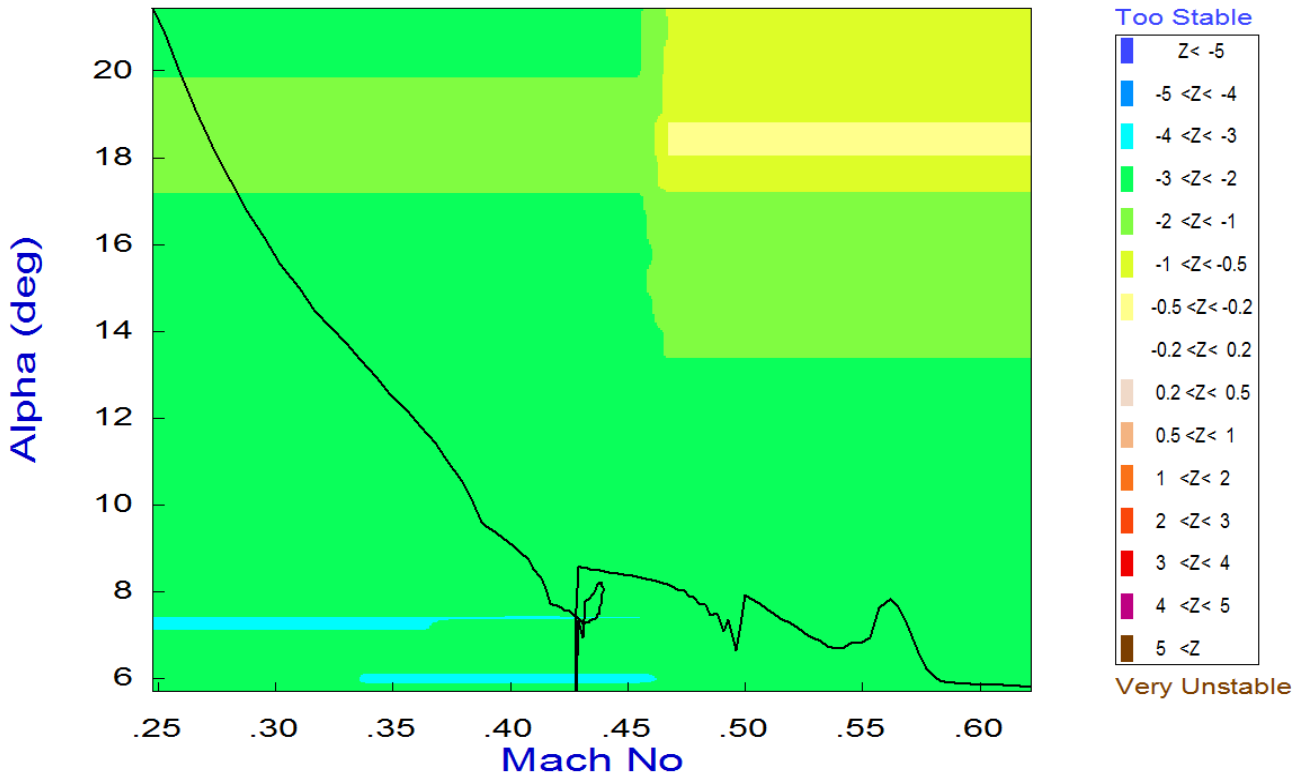
## Contour Plots Analysis

We will now show some important performance parameters by using contour plots. Contour plots allow us to visualize vehicle performance over the entire Mach versus Alpha range. It is selected from the main menu. The surface mixing matrix KmixM0p4b is also selected from file "Kmix.Qdr".

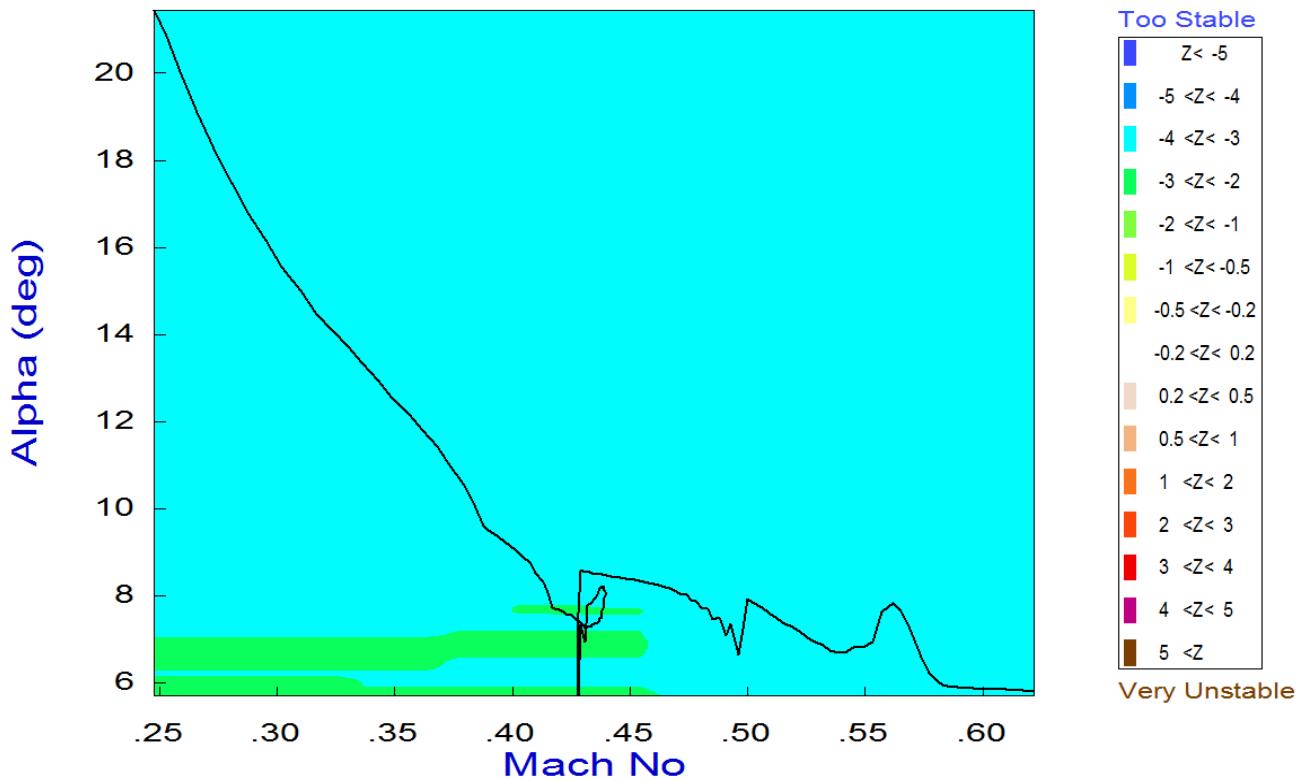


The first two plots show the pitch and lateral stability parameter in the entire Mach versus alpha range. The trajectory travel is shown by the dark line starting from the lower right-hand corner (Mach 0.65) and ending in the upper left-hand side (Mach 0.25). The stability parameters show that the vehicle is statically stable in both directions. In the lateral direction the stability parameter is almost constant. The next two plots show the pitch and yaw control authority which is good in both directions against  $2^\circ$  of ( $\alpha_{\max}$  and  $\beta_{\max}$ ) disturbances. The roll control authority, however, is not sufficient in some regions shown in brown color and it is barely marginal in the purple regions. The LCDP ratio which measures dynamic controllability in roll is good. The surface mixing logic matrix was adjusted to improve the LCDP at the expense of reducing roll control authority, as already discussed. Notice that these contour plots were calculated using a constant mixing-logic matrix but in actual flight or simulations the mixing-logic is not constant but it is also scheduled similar to the control gains as a function of Mach and alpha.

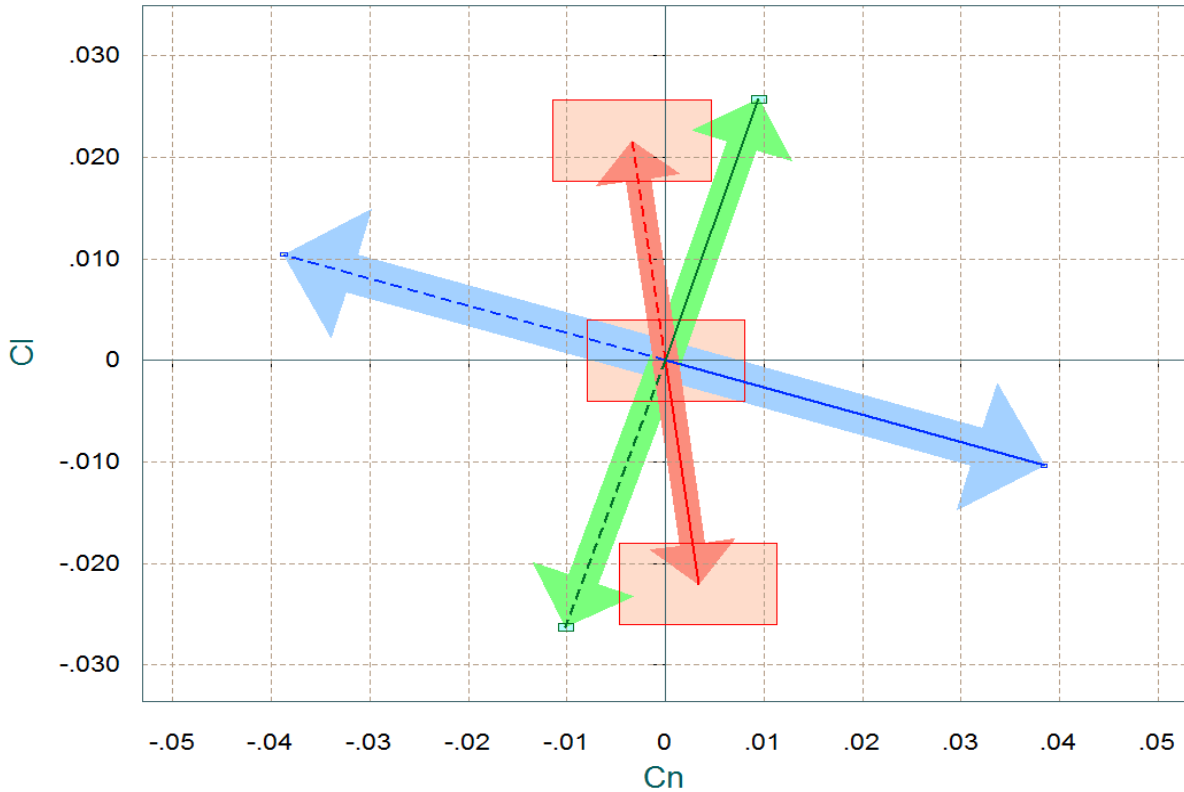
### Pitch Stability Contour Plot (Mach vs Alpha)



### Lateral Stability Contour Plot (Mach vs Alpha)



Comparison Between Maximum Control Moments Against Maximum Disturb Moments (red)  
Roll & Yaw Control Moments (non-dimension) vers Disturb Moment due to Max Beta/Alpha



Comparison Between Lateral Maxim Moment & Forces, Control Versus Beta Forces (red)  
Control Yaw Moment & Side-Force against Moment and Force due to Max Beta Variation

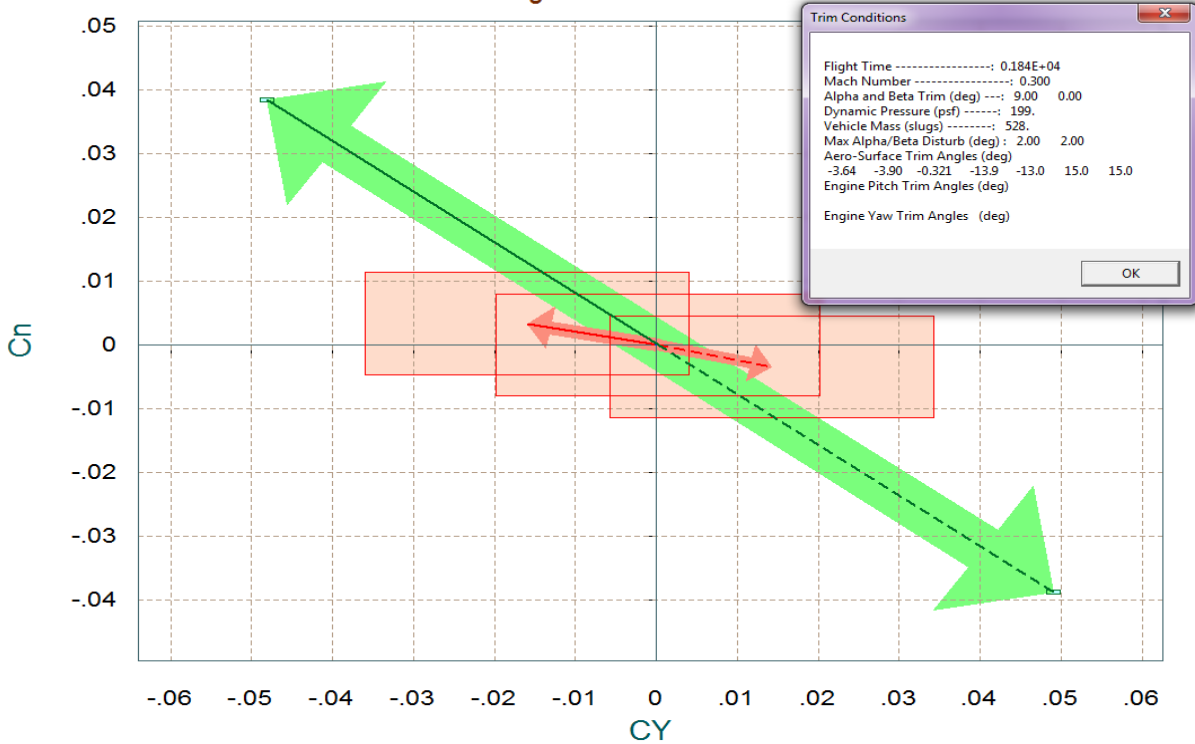


Figure 1.4.1 Lateral Moments and Side-Force produced due to  $\pm\beta_{max}$  and Controls

## Linear Simulation Model

The Matlab simulation model for the approach and landing mode is in file "*Landing\_Sim.Mdl*", shown in figure (1.4.5). The longitudinal axis is different from the previous control modes because now the FCS uses altitude and velocity feedback affecting pitch and speed-brake controls respectively. In the lateral axis directional errors are converted to roll commands. Control in the 4 axes is implemented by combinations of surface deflections as defined in the surface mixing matrix. The simulation model is used for evaluating the system's response to  $\phi$ ,  $\delta h$ , and  $\delta V$  commands and also to wind-gust disturbances. Notice, the  $\alpha$ -feedback is replaced with  $N_z$  feedback in this model. The output rates are body rates since the rate-gyro measurements are in body axes. The controller, however, was designed based on the stability axis model and it expects to see roll and yaw rates about the velocity vector  $V_0$ . A body to stability axis transformation block is, therefore, included in the simulation to convert the ( $p$  &  $r$ ) body rates to stability rates ( $p_{stab}$  &  $r_{stab}$ ) which are required in the lateral LQR state-vector feedback. The linearized turn-coordination terms are also included in this block.

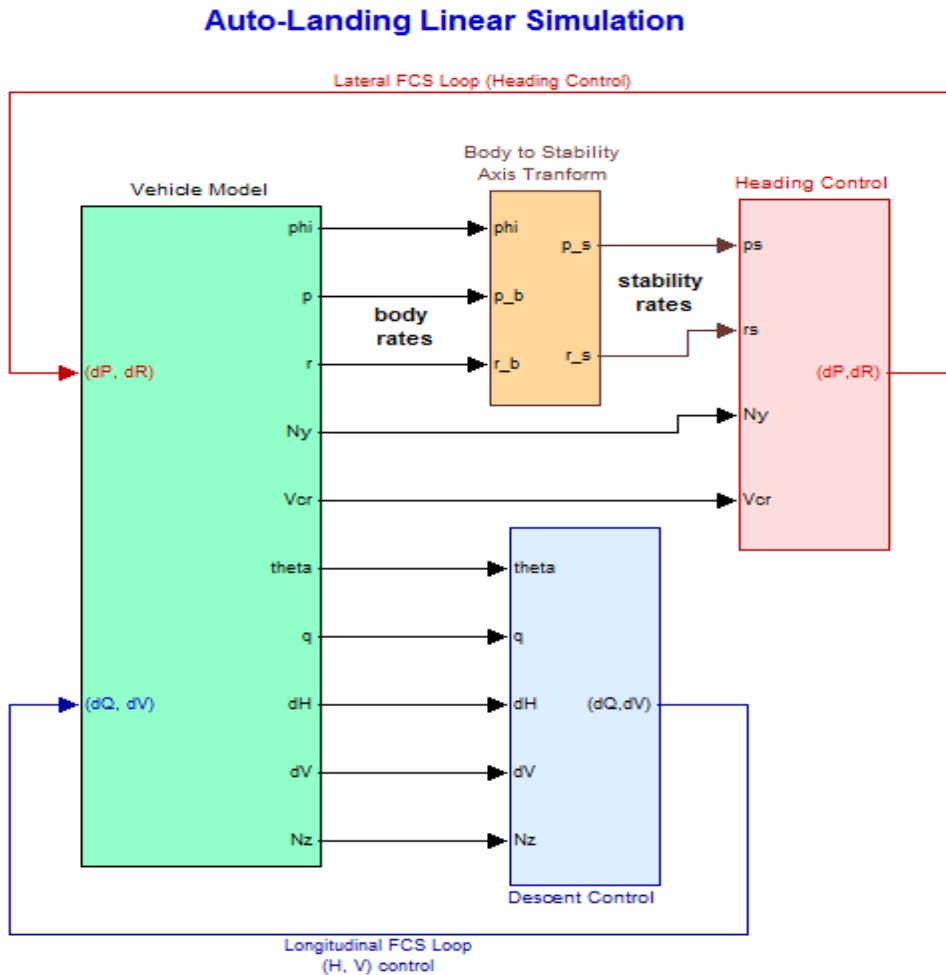


Figure 1.4.5a Simulation Model in File "*Landing\_Sim.Mdl*". The pitch controller now uses altitude and velocity feedback.

Figure (1.4.5b) shows the vehicle dynamics (green) block expanded. It uses the body-axis vehicle model "Lifting-Body Aircraft Near Landing, Simulation Model" that was generated by Flixan and has the additional  $\delta V$  output #15. It is loaded in Matlab from file "vehicle\_sim.m". The lateral inputs to this block from flight control are: roll, and yaw acceleration demands (red), and the longitudinal inputs are: pitch and axial accelerations (blue). The 4 control demands are converted to surface deflections by the surface mixing logic  $K_{mix}M0p4$ . Actuator dynamics are included in the yellow block. The gust input is a low-pass shaped gust impulse of 30 (ft/sec) velocity. The direction of gust is defined relative to the vehicle in the input data file "Land\_M0,4\_0.Inp", and it excites both pitch and yaw, perpendicular to the X-body and at 45° between +Y and +Z axes (typical).

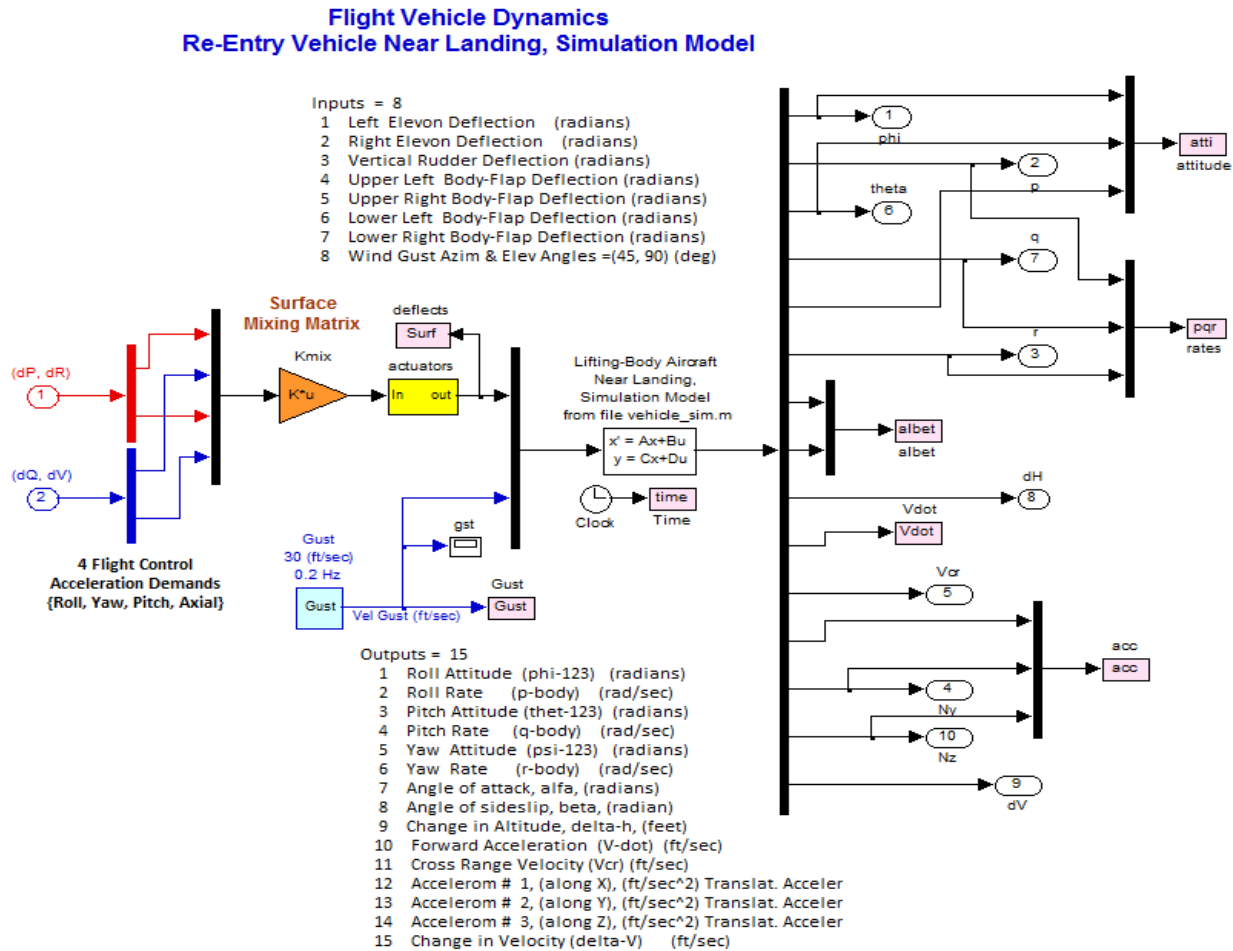


Figure 1.4.5b Vehicle Dynamics Block including the aero-surface Mixing Logic, Gust disturbance and Actuators

The following figure shows the pitch and lateral control laws which are state-feedback gains as already described. In the longitudinal axis the controller consists of a  $(2 \times 5)$ ,  $\{\theta, q, N_z, \delta h, \text{ and } \delta V\}$  state-feedback gain  $K_q$ , ( $\alpha$  was replaced with  $N_z$  by a gain relationship  $N_z2a$ ). An  $N_z$ -filter is also included. The guidance command inputs are time histories of altitude and velocity, see Figure (1.4.6b). The two inputs are not for maneuvering since the aircraft is unpowered but they are coordinated from guidance as a function of energy. The control loops also compensate against wind disturbances. In the lateral direction the controller is a  $(2 \times 5)$ ,  $(p_s, r_s, \beta, p_s\text{-integr}, \beta\text{-integr})$  state-

## Simulation Results

Let us now use the linear simulation model for the Mach 0.4 case "*Landing\_Sim.Mdl*" and command it to track the coordinated altitude and velocity time histories of Figure (1.4.6). The lateral directions are also excited at the same time by commanding a  $10^\circ$  change in the heading direction. At the same time the model is also excited with a wind disturbance noise shown in Figure (1.4.8). This linear model is used for a preliminary evaluation of the flight control system performance. A better evaluation of the design will be obtained from the 6-dof non-linear simulation. Figure (1.4.7a) shows the altitude and velocity response to the longitudinal commands. Figure (1.4.8) shows the heading direction response to the  $10^\circ$  command.

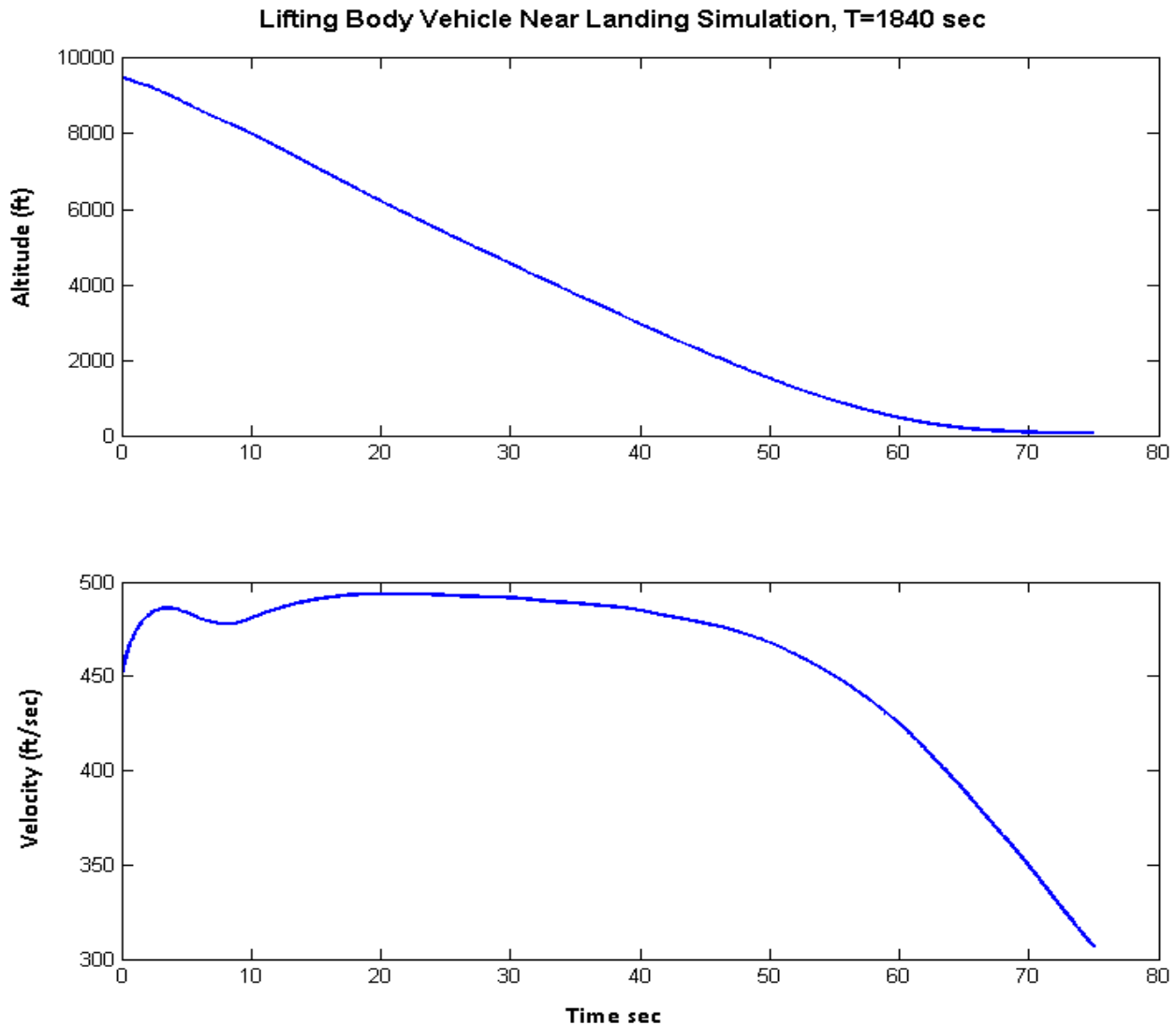
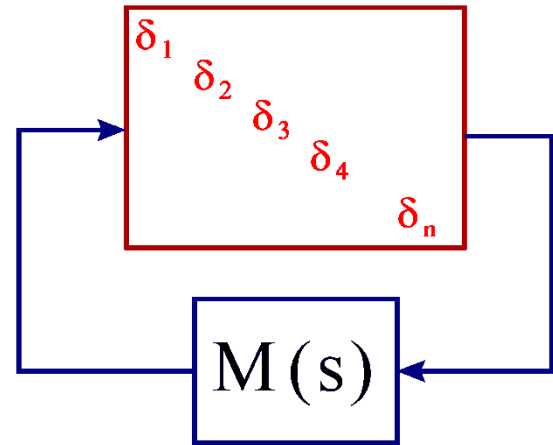


Figure 1.4.7a Response of the Simulation model "*Landing\_Sim.Mdl*" to the Altitude and Velocity Commands

## Robustness Analysis to Parameter Uncertainties

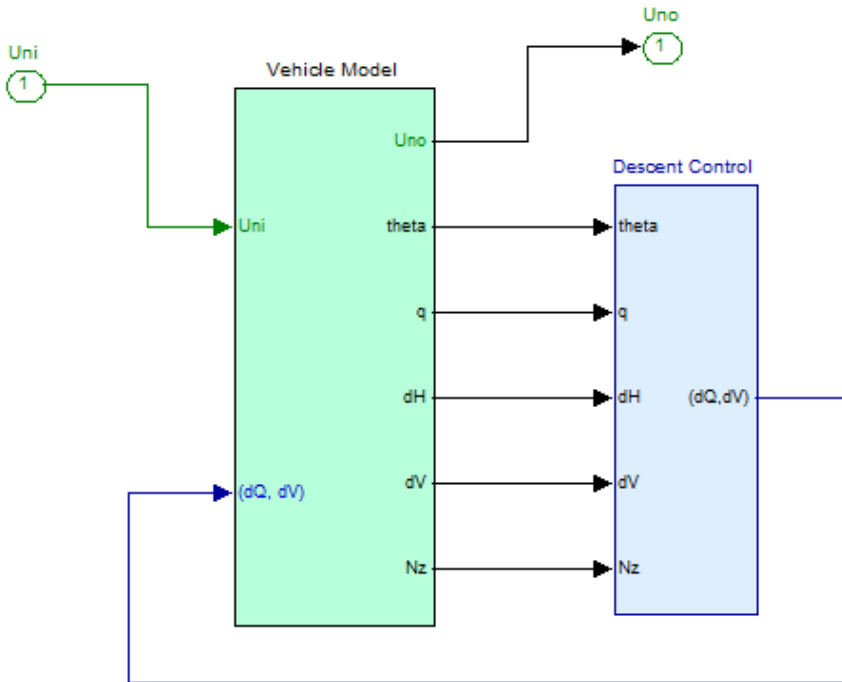
We will now use structured singular value (SSV) or  $\mu$ -analysis to evaluate the aircraft robustness to structured parameter uncertainties. In the vehicle input data file "Land\_MO,4\_0.Inp" we have created a system with 60 structured uncertainties. Its title is "Lifting-Body Aircraft Landing Phase (Robust Analysis with 60 Uncert)". Each uncertainty is defined by an input/output pair in addition to the ordinary vehicle model inputs and outputs. The amount of uncertainty of each parameter is defined in a separate data-set which is also located in "Land\_MO,4\_0.Inp". The data-set title is "Uncertainties at Mach=0.43, Alpha=10" and it is processed by Flixan together with the vehicle data to generate the multi-input-output uncertainties state-space model. The uncertainties model dynamically is the same as the simulation model with the exception that it has a lot of additional inputs and output pairs, each pair representing one of the uncertainties, thus allowing the uncertainties to be pulled out of the model in a separate  $\Delta$  block, see figure. The remaining block  $M(s)$  now represents the stabilized vehicle model with its control loops closed (not shown). It is not uncertain because its uncertainties were pulled out and placed in the diagonal  $\Delta$  block. It is only connected to the uncertainties  $\Delta$  block by the input and output vectors. We should also mention that the closed-loop vehicle model  $M(s)$  should be stable and that it is also properly scaled so that its diagonal  $\Delta$  block now has elements that can only vary between  $\pm 1$ . Robustness is measured by calculating the SSV across the  $M(s)$  block and the closed-loop system cannot be destabilized by any combination of the uncertainties, as long as  $\mu[M(j\omega)] < 1$ , at all frequencies.



Separate  $\mu$ -analysis will be performed for the longitudinal and lateral directions. The dynamic model with the 60 uncertainties is separated in two subsystems. The uncertainties were also separated into longitudinal and lateral uncertainties. The longitudinal model has 28 uncertainties and its title is "Lifting-Body Aircraft Near Landing, Pitch Robust Analysis (28 Uncs)". The lateral model has 32 uncertainties and its title is "Lifting-Body Aircraft Near Landing, Lateral Robust Analysis (32 Uncs)". They are saved in files "pitch\_unc.m" and "later\_unc.m" respectively and used in the  $\mu$ -analysis. The model separation is defined in "Land\_MO,4\_0.Inp" and it is automatically executed when running the batch set. Most of the uncertainties are rank-1, meaning that they create a single input/output pair. The X-cg, however, affects both longitudinal and lateral models and it creates 3 input/output pairs. The input/output pairs must be separated carefully by observing the states with which they are coupling. It seems that two X-cg uncertainty pairs are affecting the longitudinal states and one X-cg pair affects the lateral states. The Y-cg is only affecting the lateral directions. The following two models in Figure (1.4.10) are used to calculate the SSV of the longitudinal and lateral systems with the

control loops closed, and the next two figures show the longitudinal and lateral (green) vehicle blocks in detail.

### Auto-Landing Pitch Robustness Analysis



### Auto-Landing Lateral Robustness Analysis

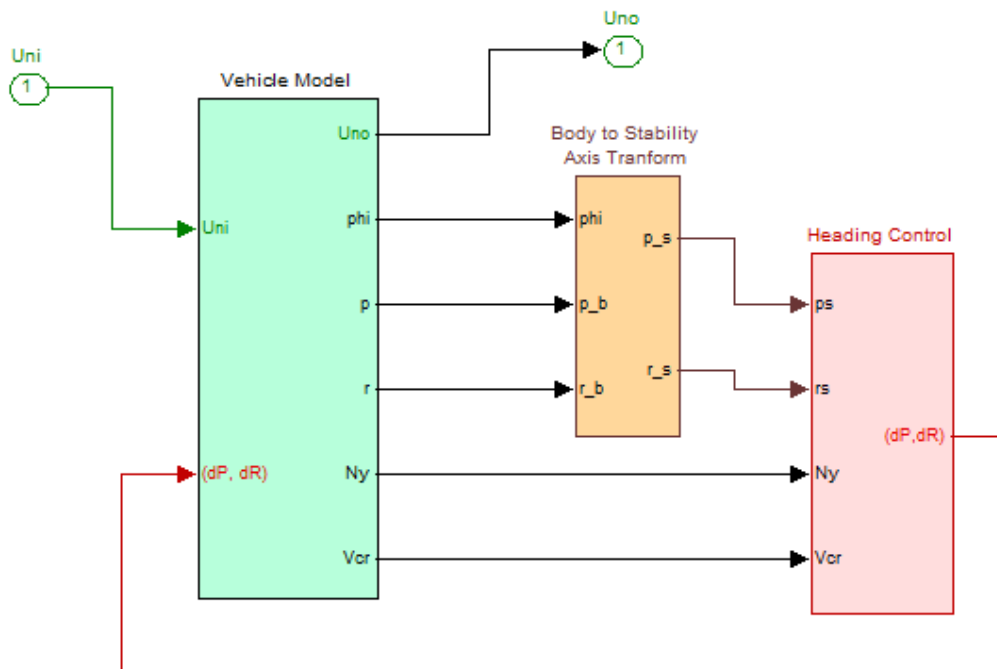
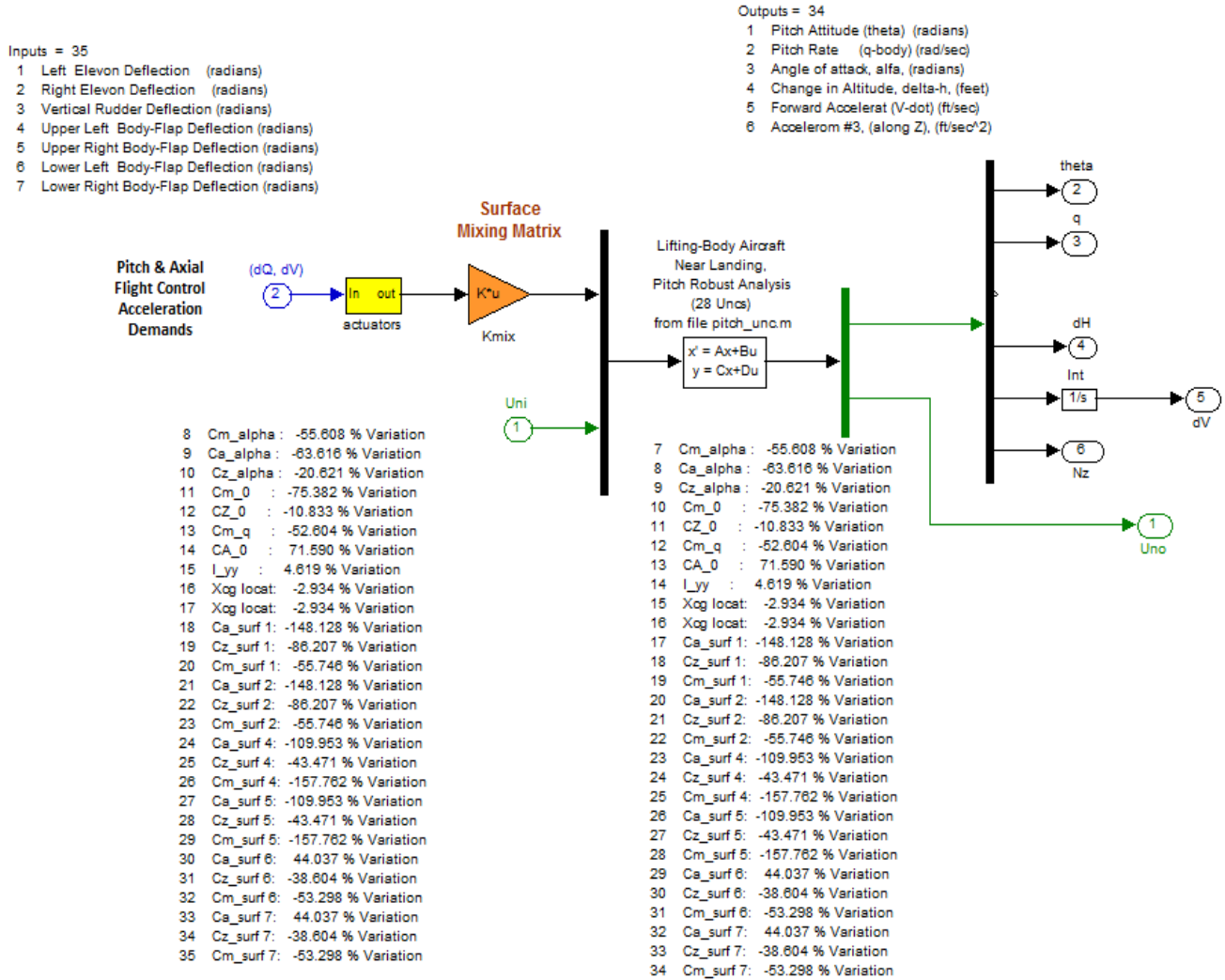


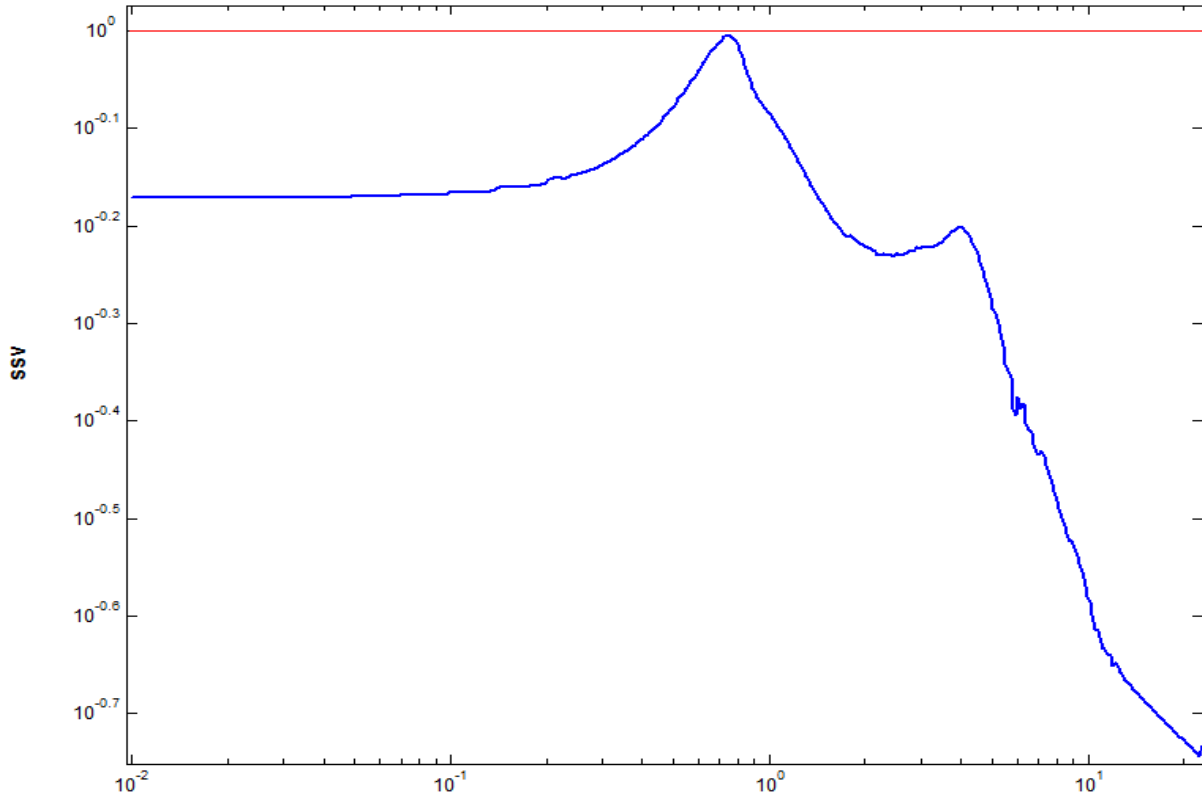
Figure 1.4.10 Simulink Models "Pitch\_Robust\_Anal.Mdl" and "Lateral\_Robust\_Anal.Mdl" used in the  $\mu$ -analysis

## Re-Entry Vehicle Near Landing, Pitch Robustness Analysis

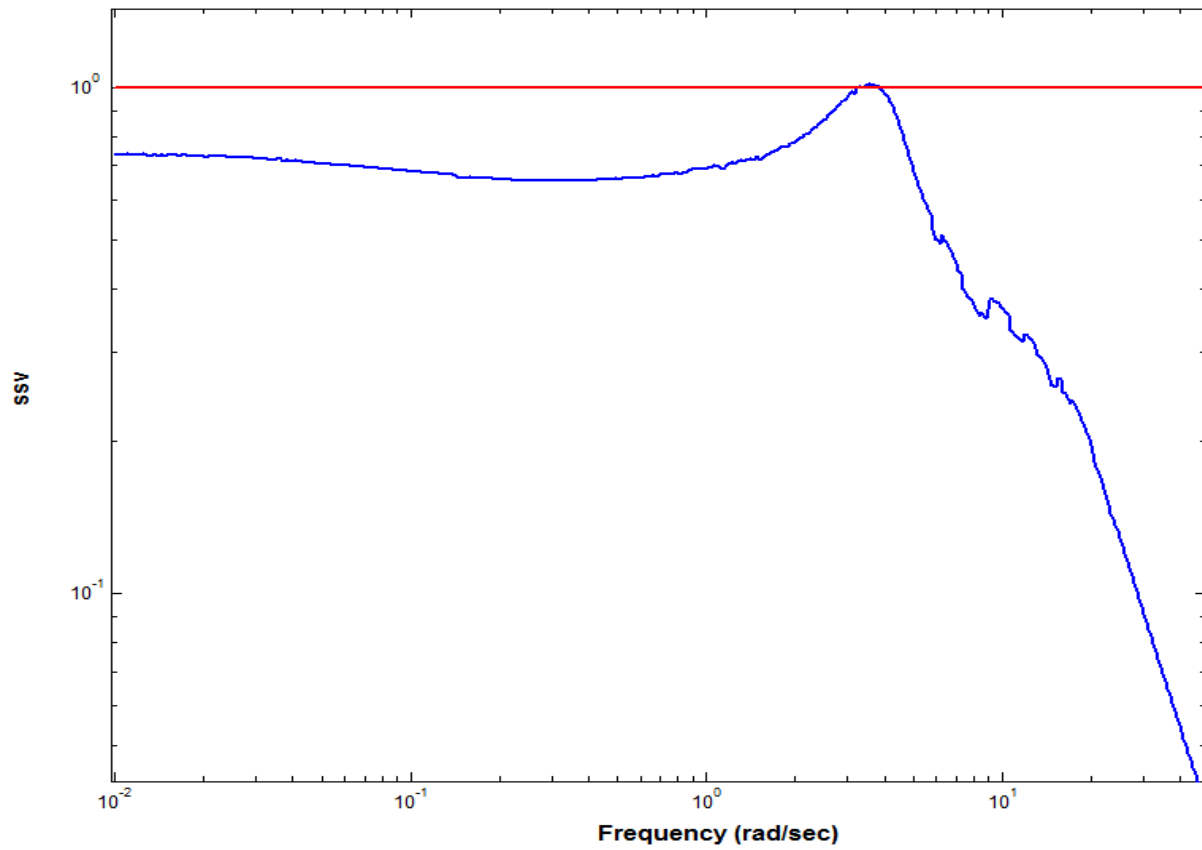


This figure shows the longitudinal vehicle block in the Simulink model "Pitch\_Robust\_Anal.Mdl" used for calculating the SSV in the longitudinal directions. It includes the longitudinal vehicle model with the 28 uncertainties from file "pitch\_unc.m". It includes also the effectors mixing matrix and actuators. The pitch and axial acceleration controls are converted to 7 aero-surface deflections. The inputs (Uni) and outputs (Uno) are theoretically connecting with the normalized uncertainty block  $\Delta$ . The SSV is calculated across those input and output vectors. They are labeled to show which uncertainty they represent and also the percentage of each variation.

Pitch Mu Analysis



Lateral Mu Analysis



## 1.5 Six-Dof Non-Linear Simulation

The entire re-entry design will now be demonstrated by means of a six-degrees-of-freedom (6-dof) simulation in Matlab/ Simulink. The simulation begins some time after the de-orbit maneuver and when the vehicle is oriented at an  $\alpha=30^\circ$ , and it completes 1900 seconds later when the vehicle successfully lands on the runway. The guidance and control system maneuver the aircraft through various phases by employing four types of control modes that achieve different performance goals during each phase. The simulation is located in folder "*C:\Flixan\ Trim\Examples\ Lifting-Body Aircraft\Reentry from Space\ Simulations 6-dof\Re-Entry Simulation (6-dof) -HV Track*" and the Simulink model is "*Reentry-6dof-Sim.Mdl*", shown in Figure (1.5.1). The environment subsystem block is shown in detail in Figure (1.5.2). The block in Figure (1.5.3) calculates the angles of attack, sideslip, dynamic pressure, and Mach number from the velocity vector (x, y, z). The blocks in Figure (1.5.4 through 1.5.7) calculate the aerodynamic forces and moments on the vehicle as a function of the aerodynamic coefficients, Mach number, the angles of attack and sideslip, and the aero-surface deflections.

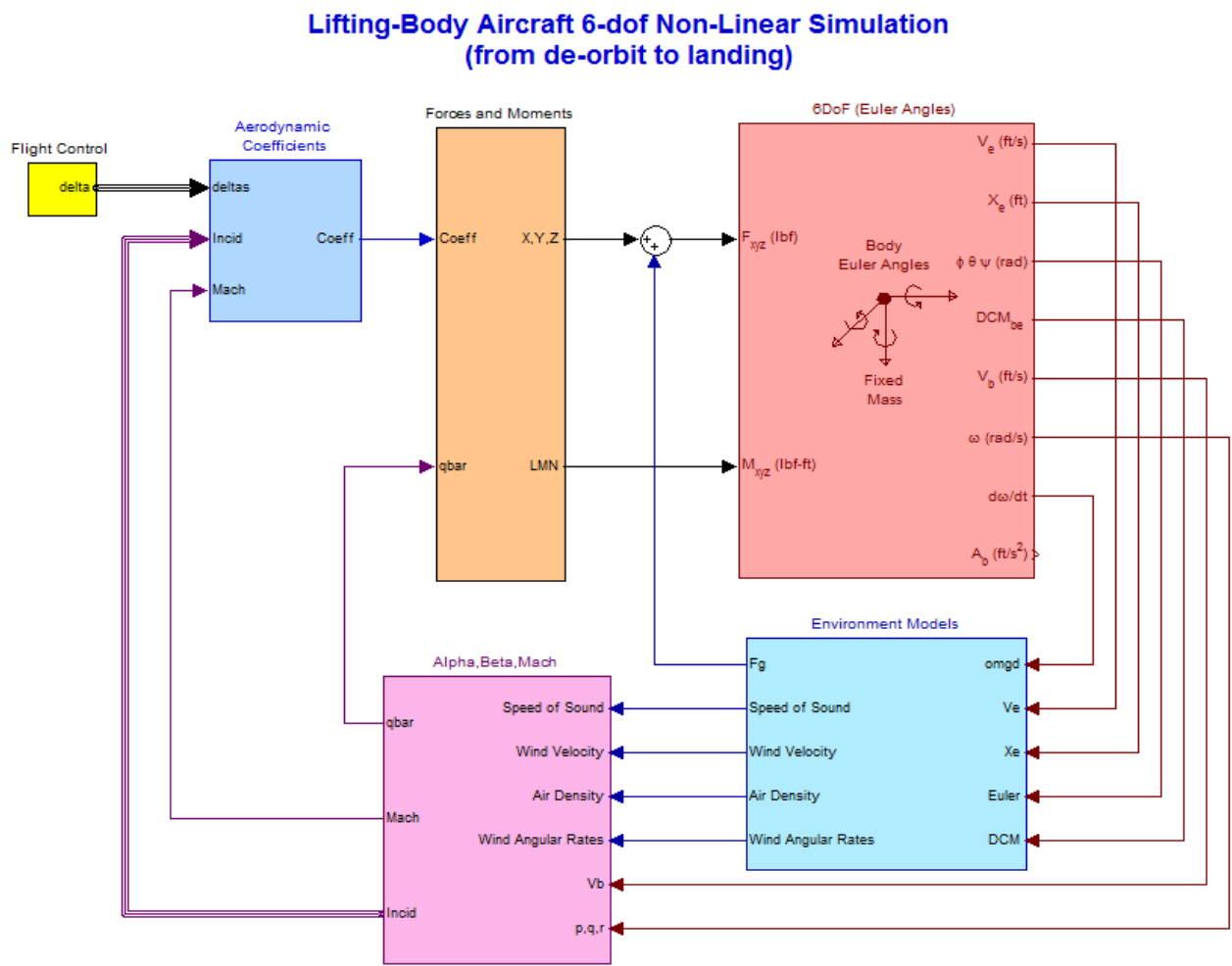


Figure 4.5.1 Simulation Model "*Reentry\_6dof\_Sim.Mdl*"

## Environment

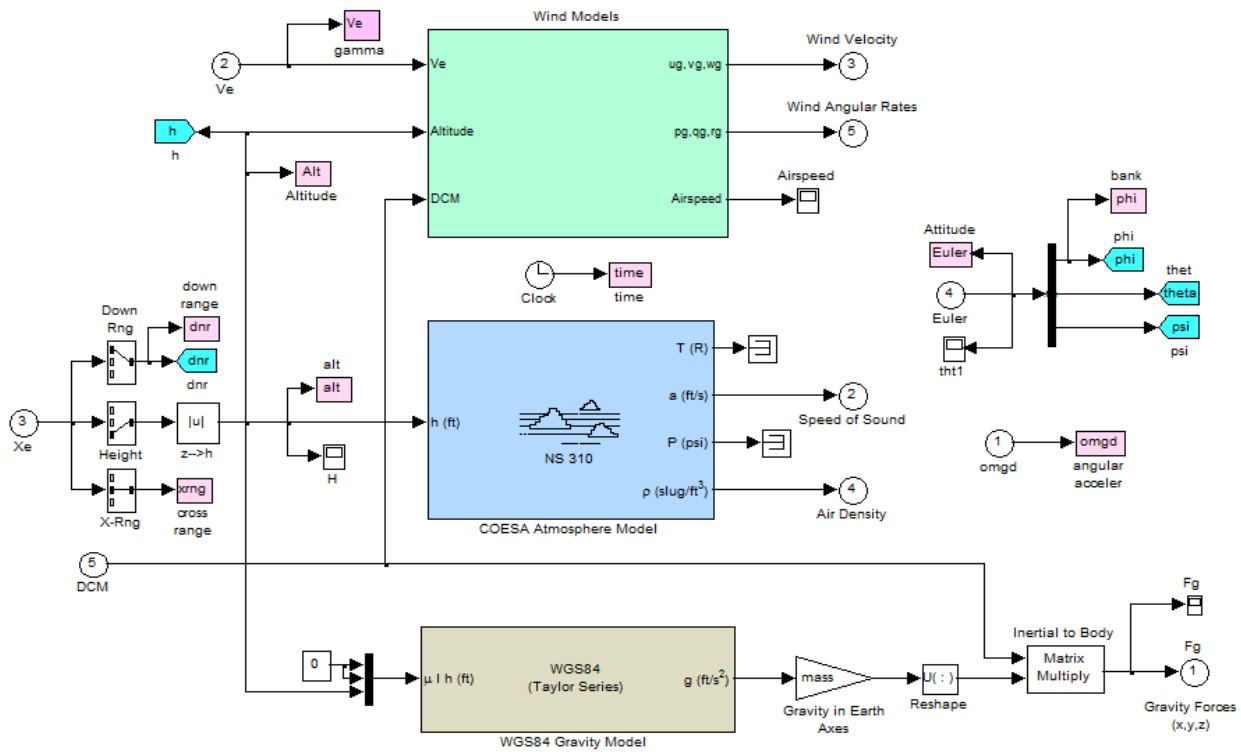


Figure 1.5.2 Environment Subsystem

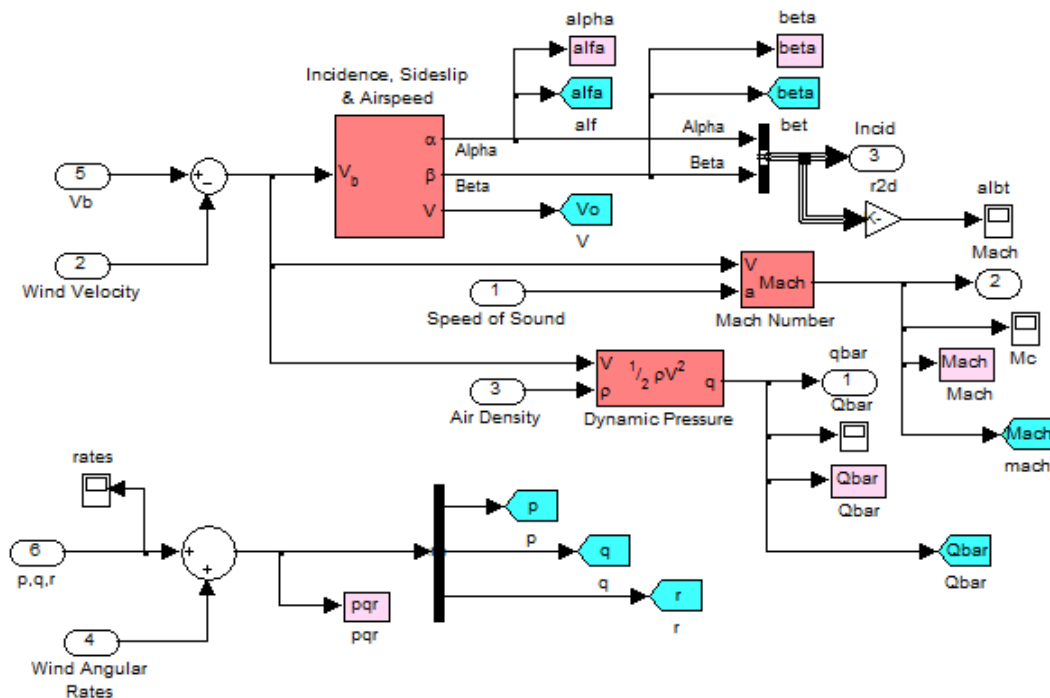


Figure 1.5.3 Angles of Attack, Sideslip and Mach Number calculations

## Moments and Forces due to the Aerodynamics

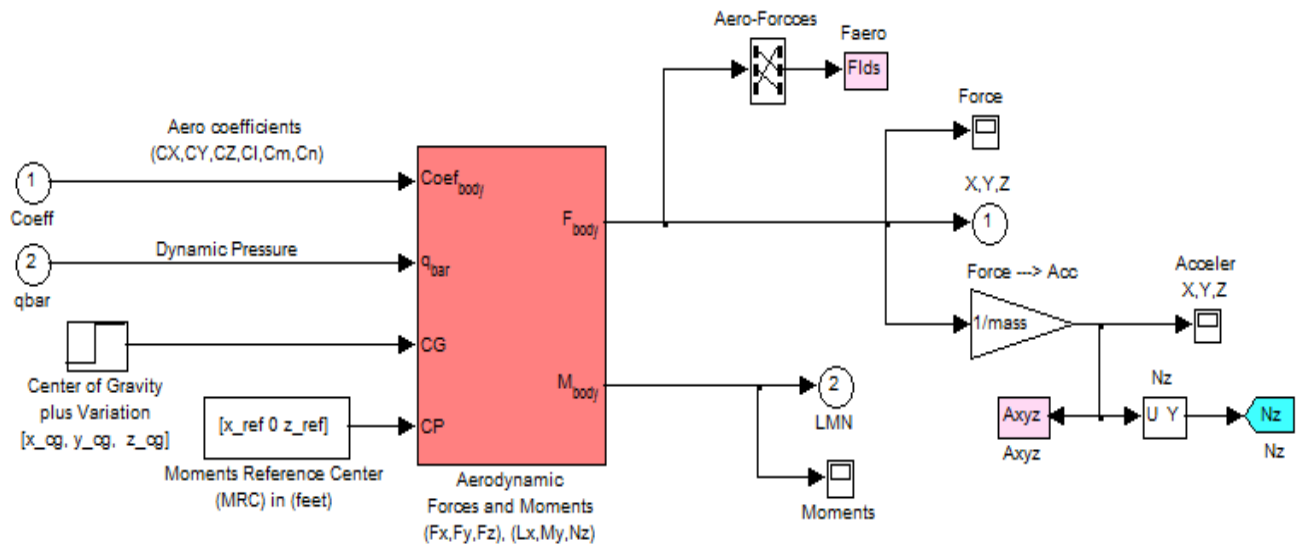


Figure 1.5.4 The Aerodynamic Forces and Moments are functions of the Dynamic Pressure, the Aero-Coefficients, and the CG location relative to the Moments Reference Center.

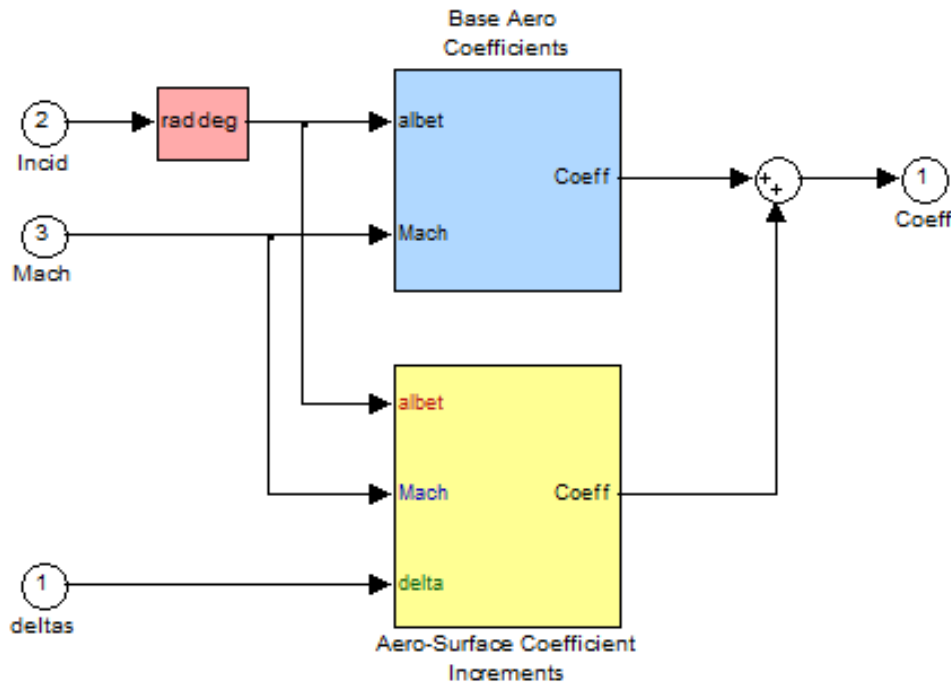


Figure 1.5.5 The Aerodynamic Coefficients consist of Base Body coefficients plus Increments due to Surface Deflections, and they are functions of the Angles of Attack and Sideslip (deg), Mach number, and Surface Deflections (deg).

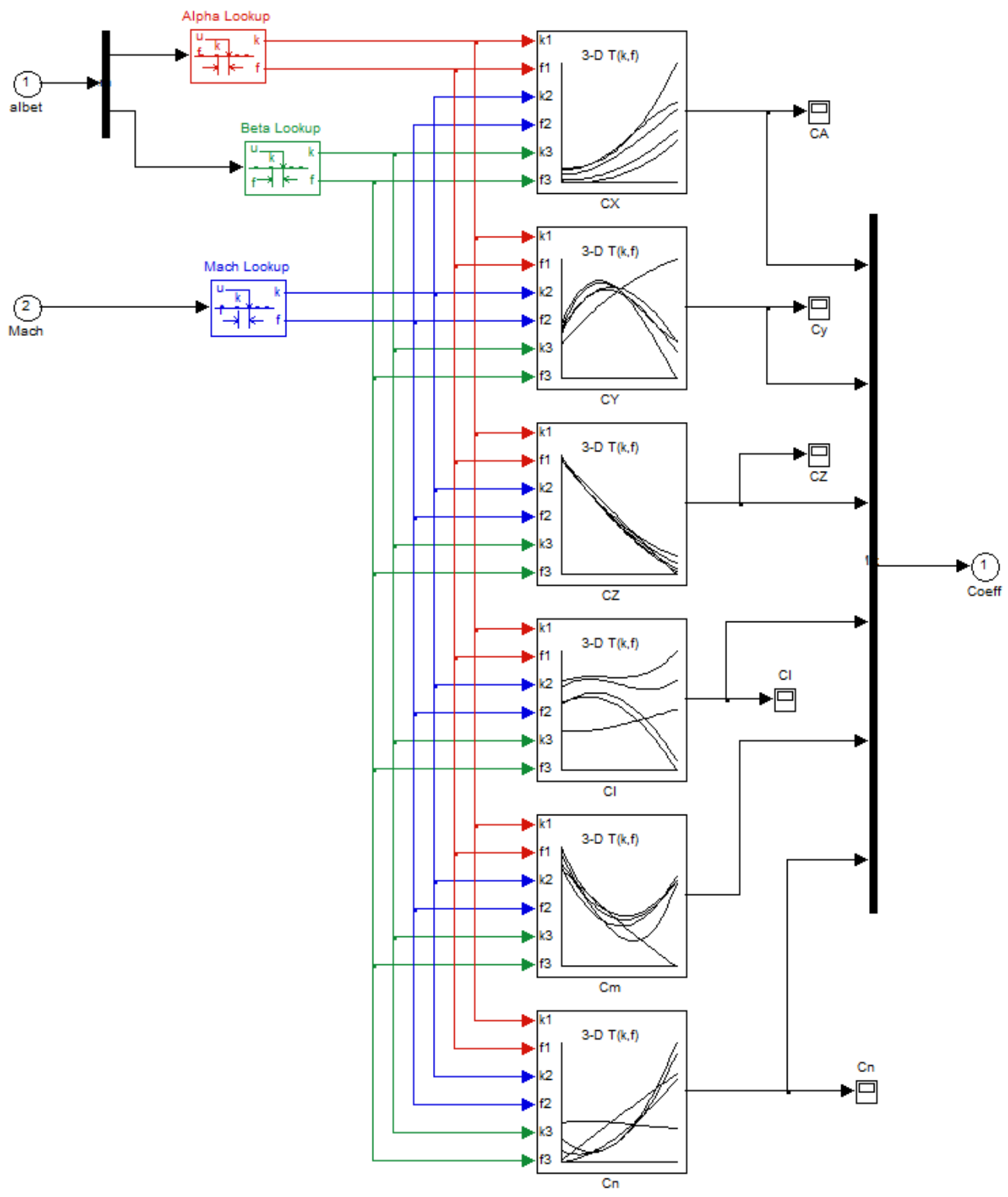


Figure 1.5.6 Base Aero Coefficients {CA, CY, CZ, CI, Cm, Cn} are functions of: Alpha, Beta, and Mach Number

## Flight Control System

Figure (1.5.8) highlights the flight control system in top-level form. It consists of two blocks consisting of the longitudinal and the lateral control laws which are basically state-feedback designs operating in different modes, as already described in the control design sections. Control designs and linear analysis were performed at specific Mach numbers and they are located in separate folders under "C:\Flixan\Trim\Examples\ Lifting-Body Aircraft\Reentry from Space\Mat\_Anal", as shown below. The 7 aero-surfaces are shared by both controllers and the deflection command signals from the two blocks are, therefore, superimposed before being applied to the surface actuators. Note that the sensor feedback signals are not shown in the simulation blocks to avoid messy block-diagrams.

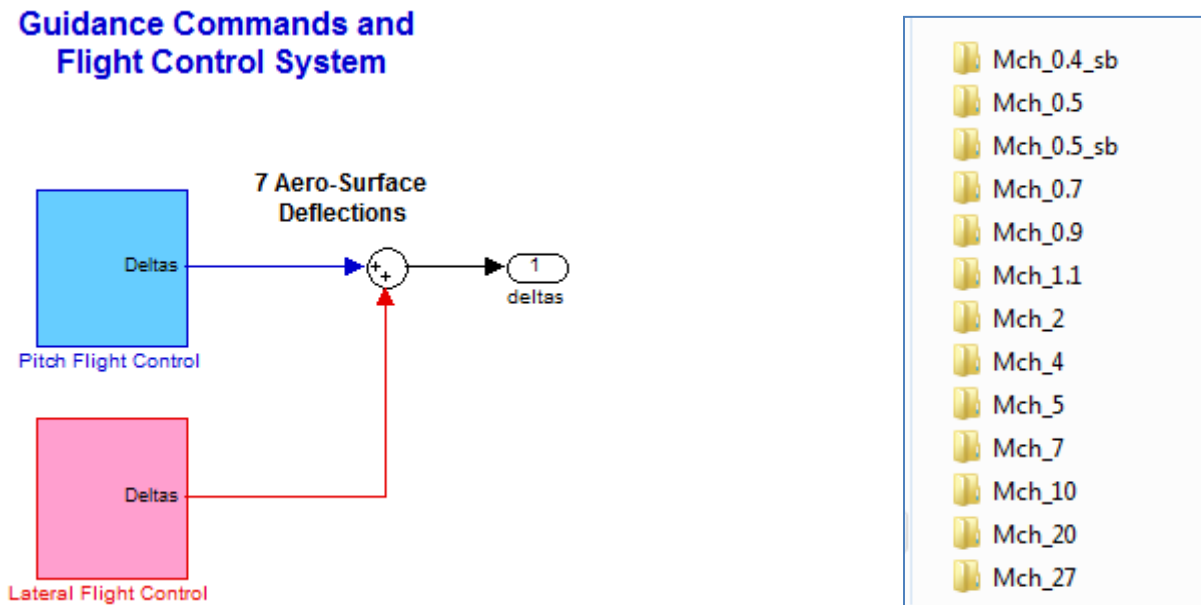


Figure 1.5.8 Flight Control System

## Pitch Flight Control System

The longitudinal control law is shown in more detail in Figure (1.5.9). It consists of a state-feedback gain matrix  $K_q$  converting  $\{\gamma, \gamma\text{-integral}, q, \alpha, \alpha\text{-integral}, N_z, \text{ and } N_z\text{-integral}\}$  error signals to pitch commands. The pitch flight control law is implemented in Matlab function "*Pitch\_FCS.m*", see Figure (1.5.10), which converts the pitch state-feedback to surface deflections and also interpolates the gains between the design cases which are at different Mach numbers. It includes also and interpolates the mixing-logic matrix  $K_{mix}$  that is also calculated at different Mach numbers. Notice that not all of the state variables are feeding-back simultaneously but some of the gains in the state-feedback matrix  $K_q$  are set to zero depending on which mode the pitch flight control system is operating. This type of implementation allows an easier transitioning between the four control modes, which are:  $\alpha$ -control,  $N_z$ -control,  $\gamma$ -control, and altitude/ velocity control.

The aero-surface actuators do not only receive deflection commands from the flight control system but the surface positions are pre-scheduled open-loop as shown in Figure (1.5.15). The aero-surface trim positions were obtained from the trim analysis performed earlier along the preliminary trajectory as already described in previous sections.

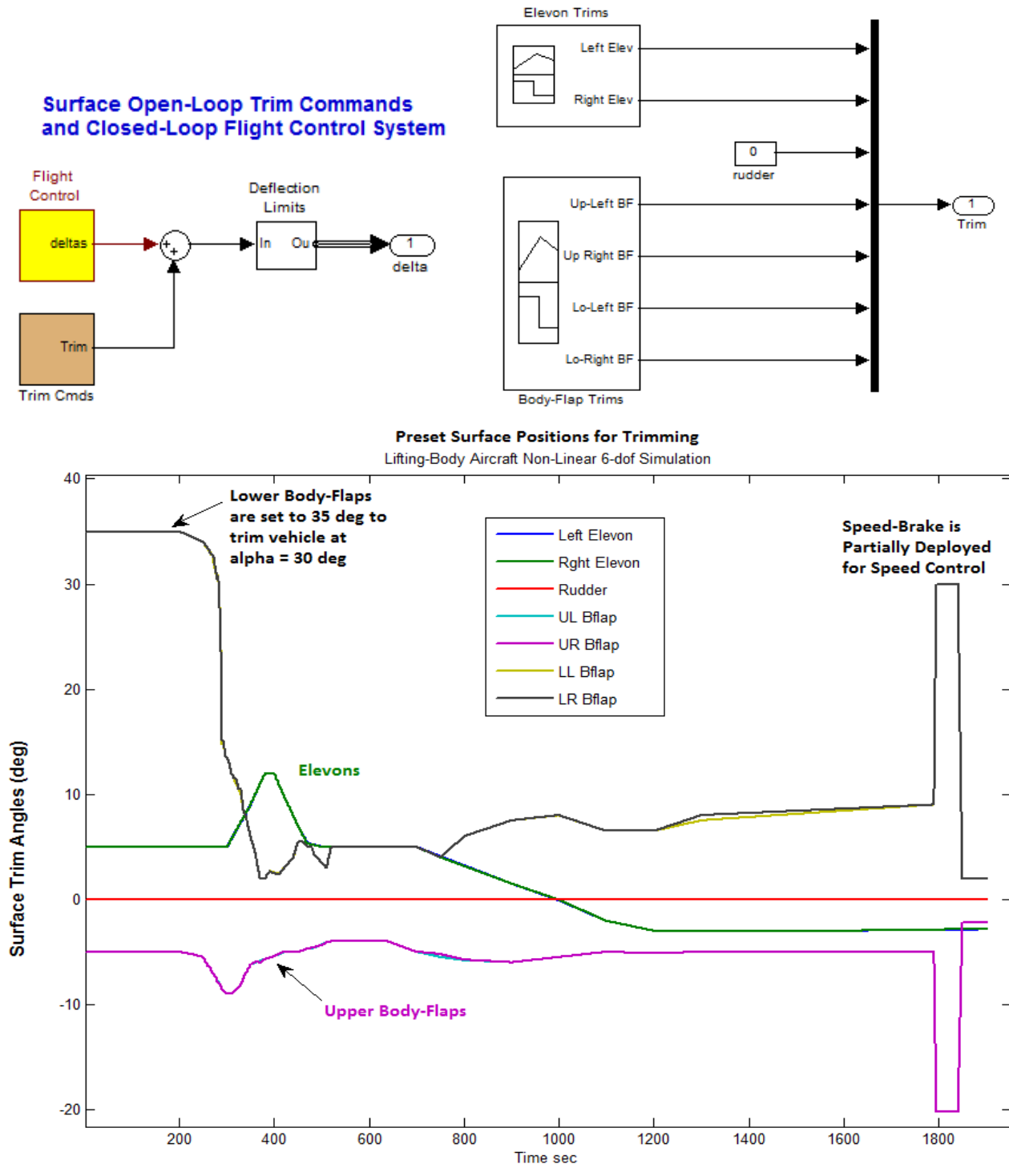
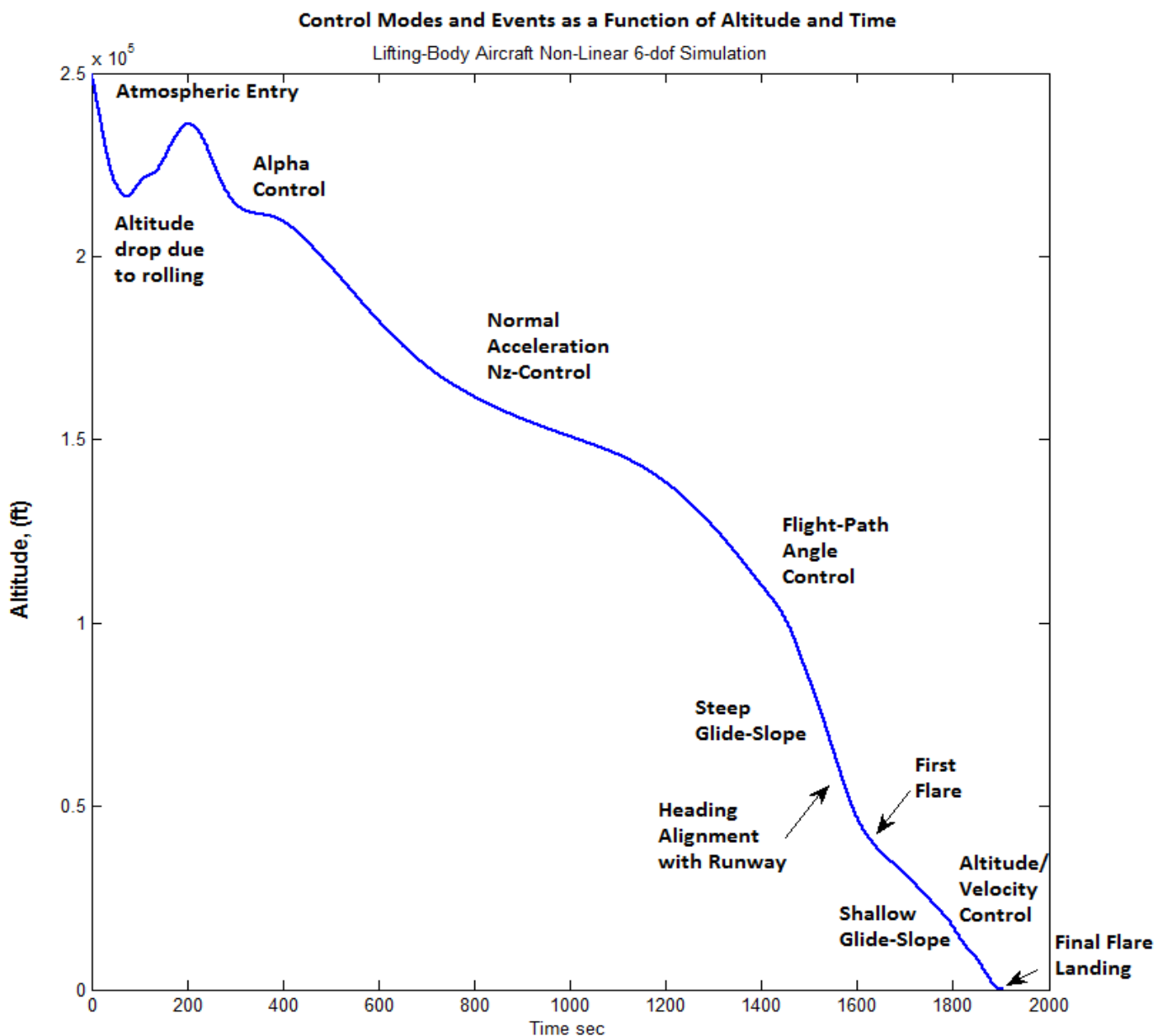


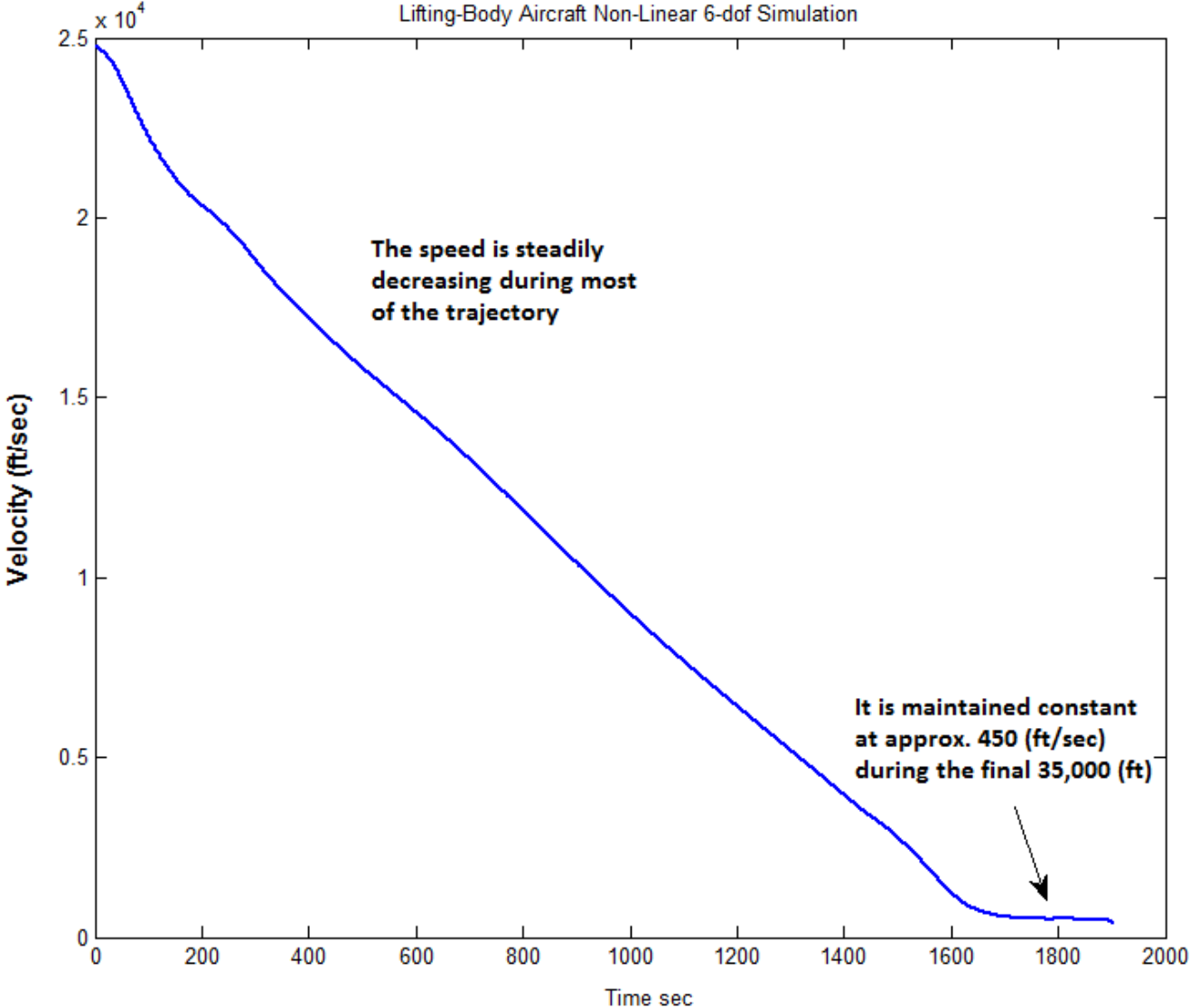
Figure 1.5.15 Aero-Surface Scheduling is based on previous Trim Analysis

## Simulation Analysis

The following figure shows the altitude variation versus time and highlights the control modes and major events. The simulation begins at an altitude of 250,000 (ft) above ground where it enters the atmosphere with a low negative ( $\gamma$ ) and it rolls a couple of times to drop altitude and to avoid skipping back up. The flight control system operation begins in the alpha-control mode where the aircraft is trimmed to maintain a  $29.5^\circ$  angle of attack which optimizes heat protection during this period. Further down the angle of attack is reduced and the control mode is transitioned to normal acceleration control where it maintains a comfortable and almost constant  $N_z$  acceleration for a long period. Then guidance is turned on to guide the vehicle towards the landing site by controlling its flight-path angle ( $\gamma$ ). In our simulation guidance is implemented with an open-loop  $\gamma$ -command.

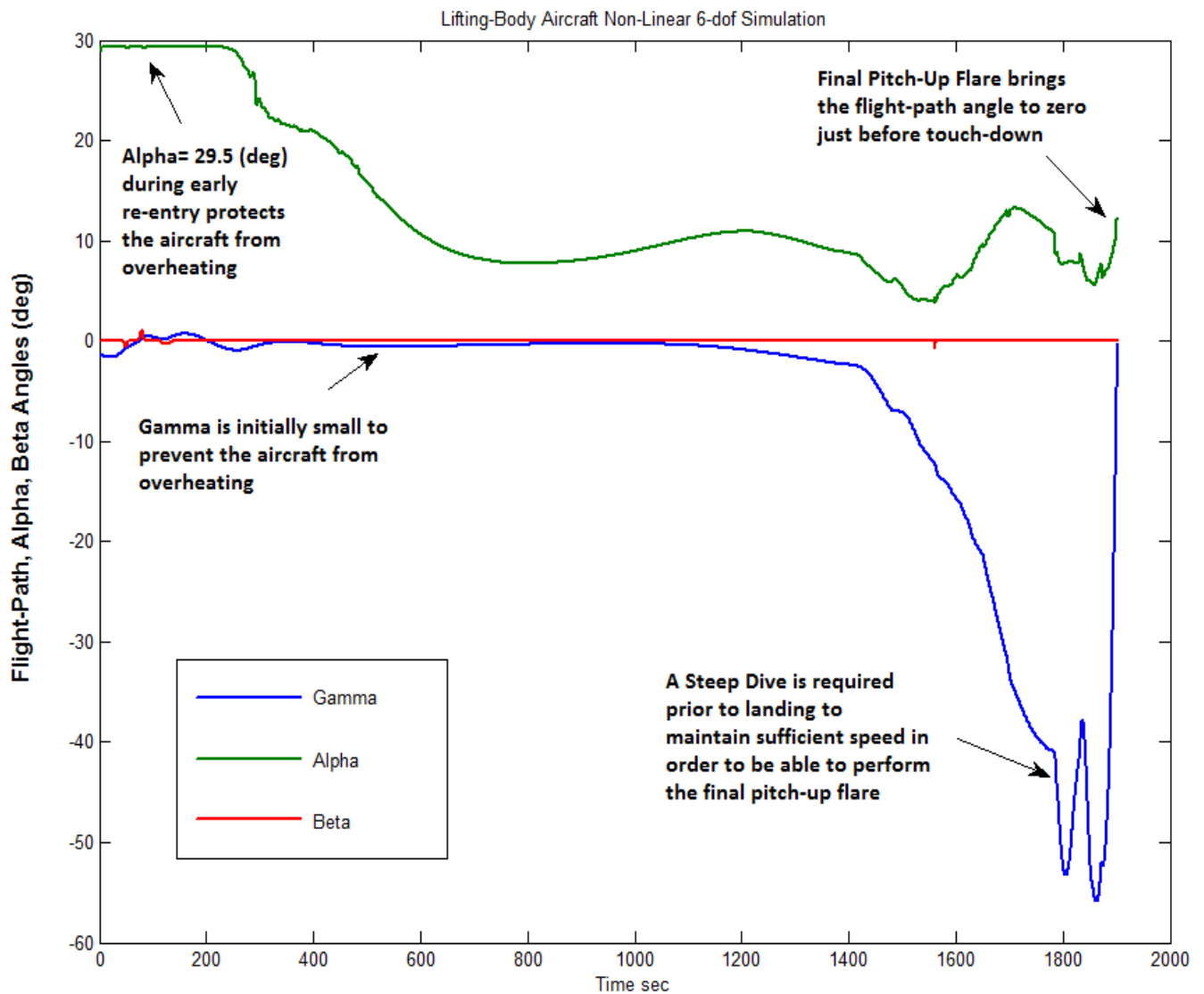


The  $\gamma$  angle is then further reduced in order to maintain sufficient speed for landing. At approximately 50,000 (ft) it rolls again in order to perform a heading correction and to align its direction with the runway. The glide-slope is reduced and the speed is maintained at around 450 (ft/sec) during the final 35,000 (ft) of altitude. In the final 1000 (ft) of altitude the glide-slope is gradually further reduced and at approximately 50 (ft) altitude it performs the final-flare and lands with an  $\alpha=13^\circ$ .



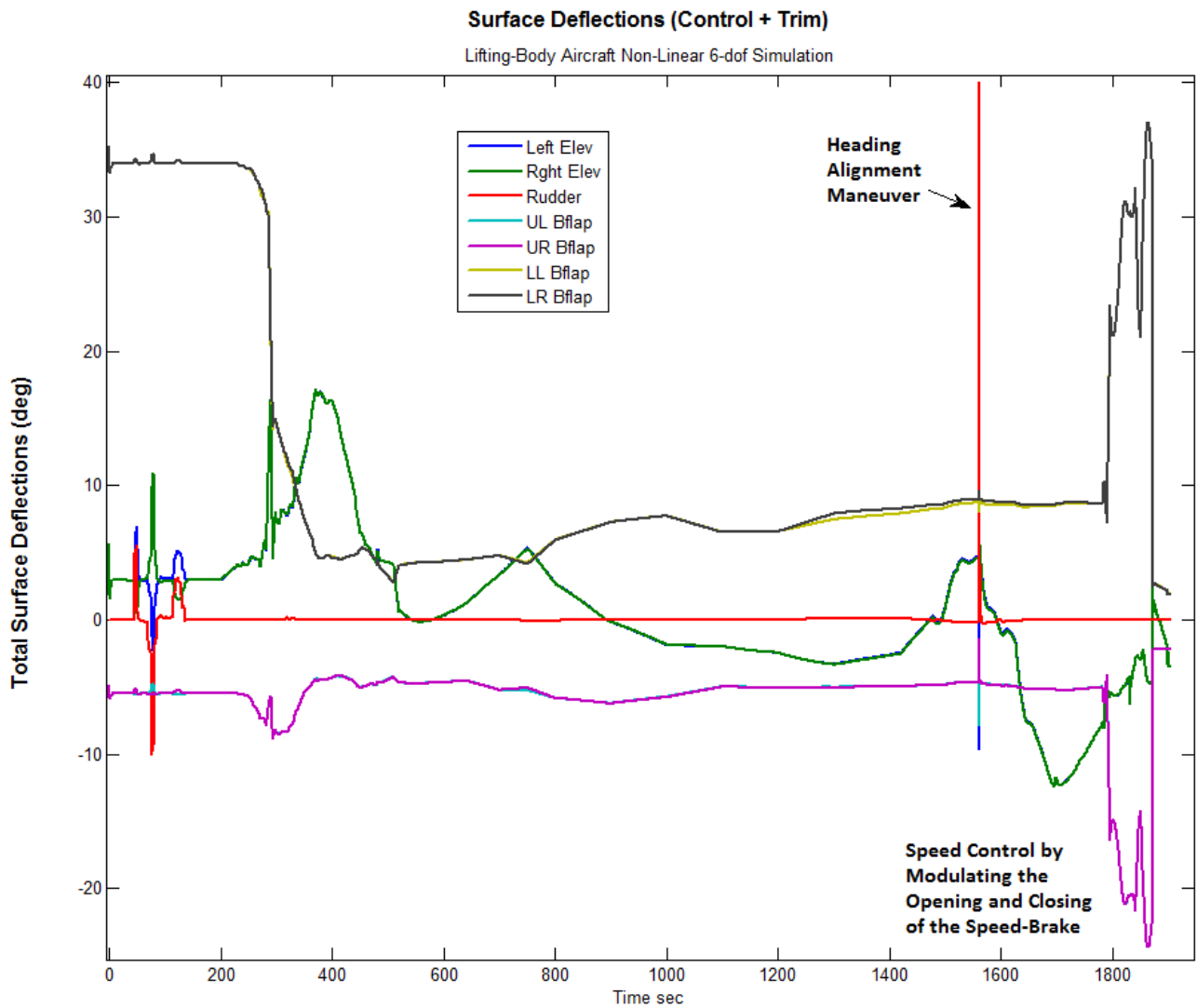
## Angles of Attack, Sideslip, and Flight-Path

This figure shows the angles of attack, sideslip, and flight-path as a function of time. The angle of attack begins at 29.5 (deg) in the alpha-control mode and it is gradually reduced to smaller values during the Nz-control period and further. It ends at approximately 13° after the final flare, where gamma ends up at zero (horizontal speed). The flight-path angle ( $\gamma$ ) is initially very shallow negative to minimize the atmospheric friction and vehicle heating. Then it is reduced to a steep dive of over -50° required to maintain high velocity for the landing flares. The final flare brings gamma to zero just before landing. There is a low frequency phugoid oscillation of 1 minute period during the steep glide which is attenuated later and it does not affect landing. The sideslip angle is mostly zero. The small transients occur during the roll maneuvers.



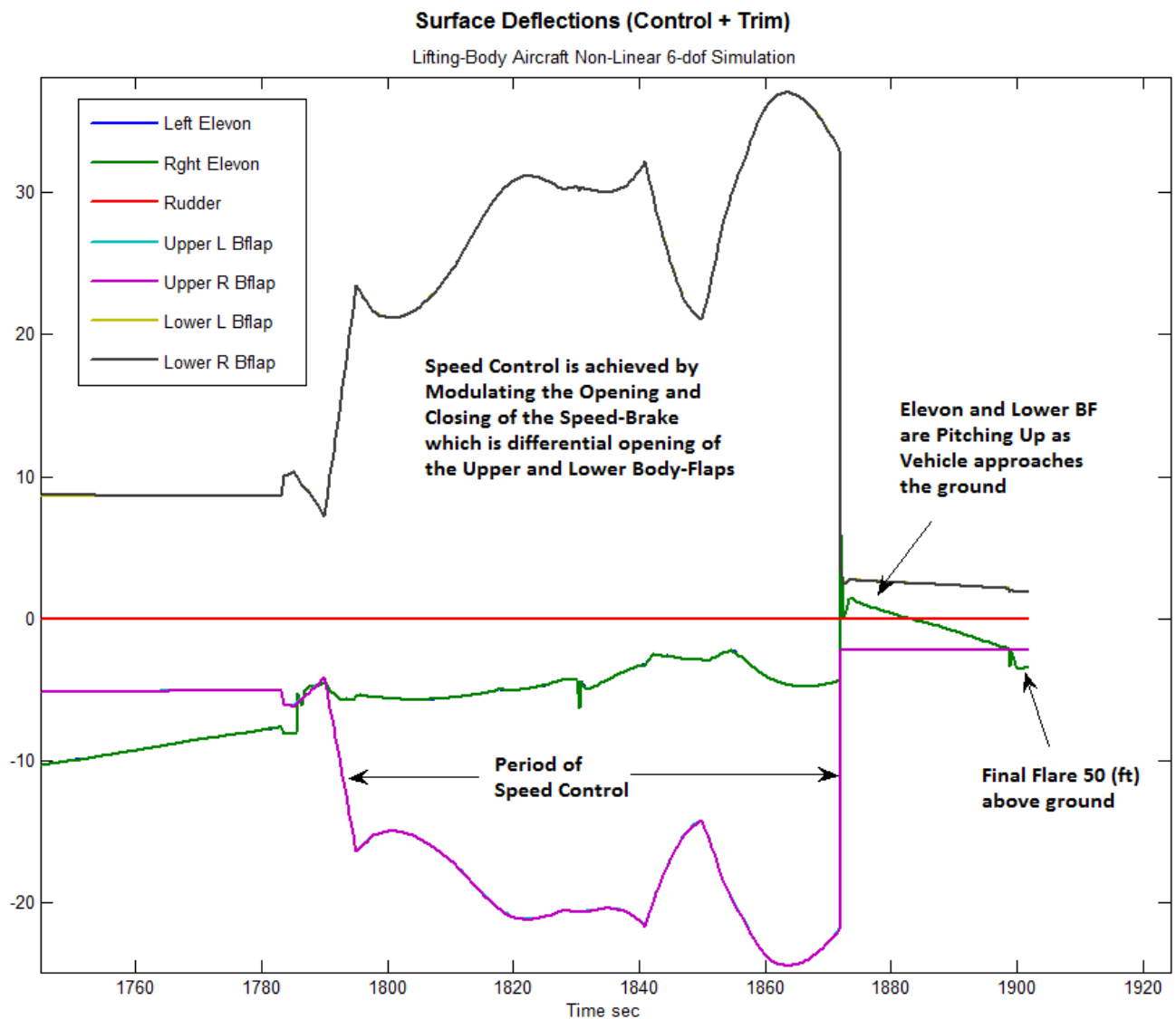
## Surface Deflections

This figure shows the aero-surface deflections as a function of time. It includes the control signals in addition to the trim deflections shown in Figure (1.5.15). It shows the rudder and differential elevon deflections performing the two roll maneuvers. The upper body-flaps are also used in the heading alignment roll maneuver. Notice that the body-flaps are not only used for trimming but they also assist the elevons and rudder in providing roll, pitch, and yaw control torques.



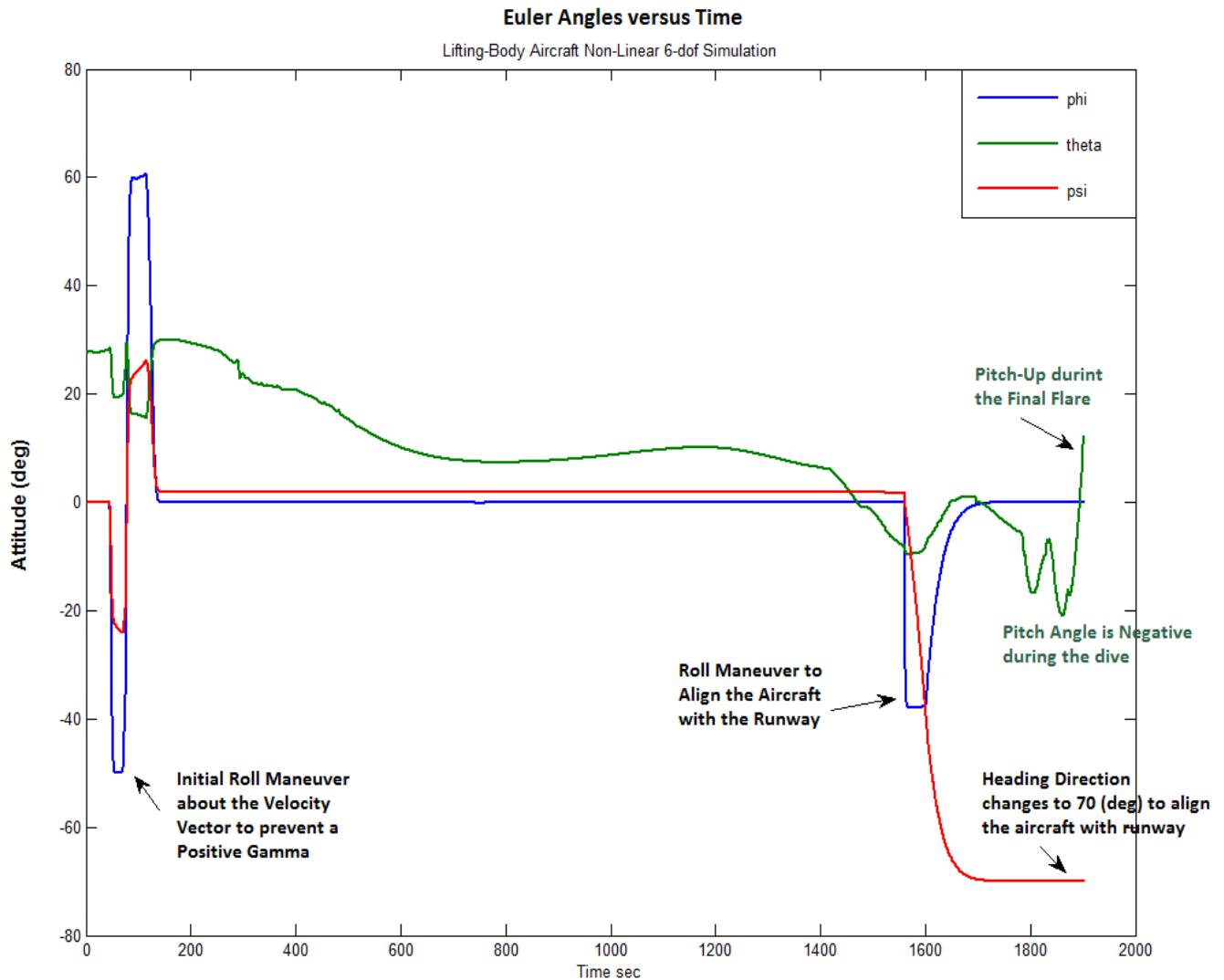
## Speed-Brake

This figure shows the velocity control operation by means of the speed-brake which occurs a couple of minutes before landing and lasts approximately 70 seconds. The speed-brake operates by differentially deflecting the upper and lower body-flaps. During this period the speed-brake is partially opened (trimmed) at approximately  $30^\circ$  for the lower flaps and  $25^\circ$  for the upper flaps. The further opening and closing is modulated by the velocity control system that attempts to control the slowing-down of the vehicle according to guidance commands. The ratio of upper to lower body-flap deflections are defined in the surface mixing-logic matrix. The velocity guidance in the simulation is represented by an open-loop command. The speed-brake is closed about a minute before landing to reduce drag and to maximize the accuracy and performance of the altitude control system.



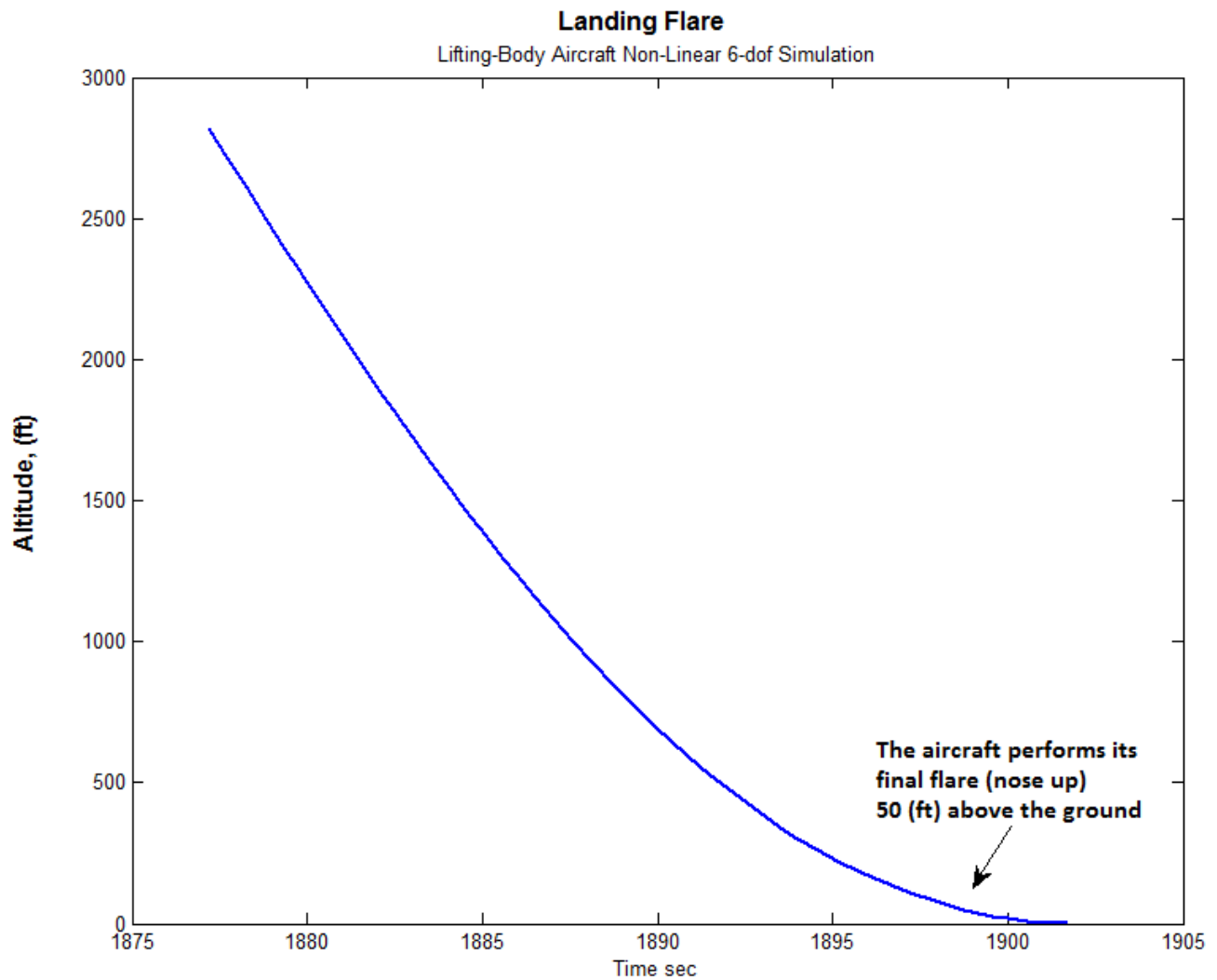
## Heading Alignment Maneuver

This figure shows the Euler angles as a function of time and mainly it demonstrates the second roll maneuver which aligns the vehicle direction with the runway. It is performed by the heading alignment control system, shown in Figure (1.5.12), which applies a roll command proportional to the alignment error. The red line is the heading angle which is approximately  $1.9^\circ$  after the first roll maneuver. It is modified to  $-70^\circ$  after the second roll maneuver which aligns the aircraft heading with the runway. The blue line shows the roll angle ( $\phi$ ) that reaches a peak value of  $-40^\circ$  during the maneuver. The green curve is the pitch angle ( $\theta$ ) that reaches  $-20^\circ$  during the steep dive. It is increased to  $13^\circ$  after the final pitch-up flare.



## Final Flare and Landing

This figure of altitude versus time shows the final 25 seconds of flight where the vehicle performs its final flare and lands on the runway with a  $\gamma=0^\circ$ . It shows how the velocity direction becomes horizontal after the final flare which occurs approximately 50 (ft) above the ground. The success of the final flare, however, depends on the landing speed which should be maintained above 350 (ft/sec) before it flares. Ground effects were not included in the simulation.



## 2.0 Vertical Launch

This vehicle is also capable of taking off vertically like a launch vehicle by using its two 18,000 (lb) TVC engines which are also capable of varying their thrusts and regulating the vehicle speed by a closed-loop throttle control system. During boosting all vehicle effectors, engines and aero-surfaces, are used for trimming as well as flight control. This is a good example for demonstrating how aero-surfaces, TVC, and throttling are combined together to control the vehicle in multiple directions. The trajectory used in this analysis is separated in two sections, the boost phase where the engines are active, and the descent phase where the unpowered vehicle glides back to land on the runway. Similar to the re-entry trajectory we will analyze both phases separately by trimming the effectors, analyzing static performance and controllability using contour plots and vector diagrams. We will also use Flixan to generate dynamic models at selected flight conditions, perform flight control designs, simulate and analyze stability in Matlab.



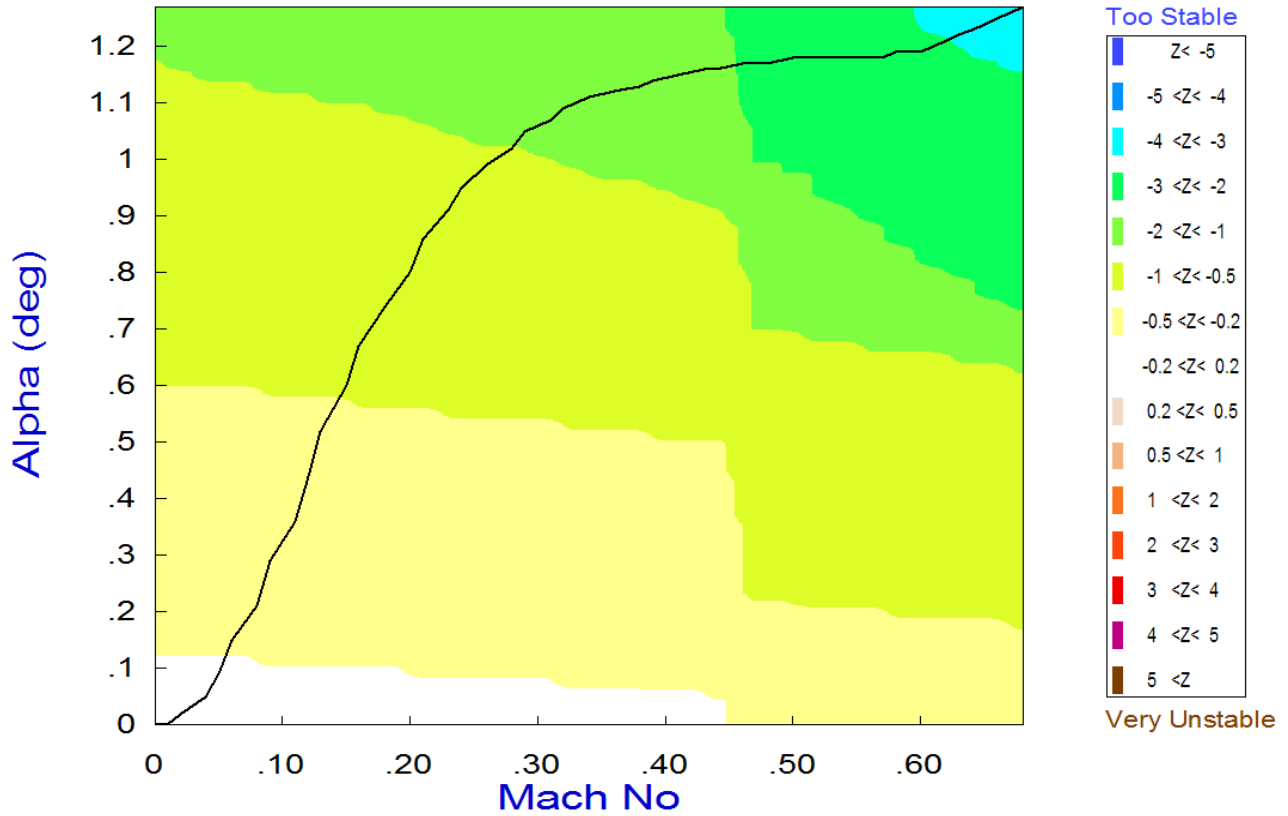
### 2.1 Ascent/ Boost Phase

The analysis during the boost phase is performed in folder "*C:\Flixan\Trim\Examples\Lifting-Body Aircraft\Vertical Launch\Boost Phase*". The first part of the trajectory which includes the engine thrust is in file "*LiftBo\_Ascent.Traj*". The thrust in the trajectory file is the total thrust from both engines. The engine information is included in the engines file "*Lift\_Body.Engn*" which specifies the number of engines, their nominal thrust, the gimbal locations, their mounting angles (relative to the vehicle -x direction), max deflections, and max throttling capability. The nominal thrust direction is along the vehicle x axis. The maximum deflections from mounting are  $\pm 5^\circ$  in pitch and yaw, and the max throttling capability is  $\pm 40\%$  relative nominal thrust. The engines mass, inertia, and the moment arms between the engine CG and gimbal are not used in this analysis.

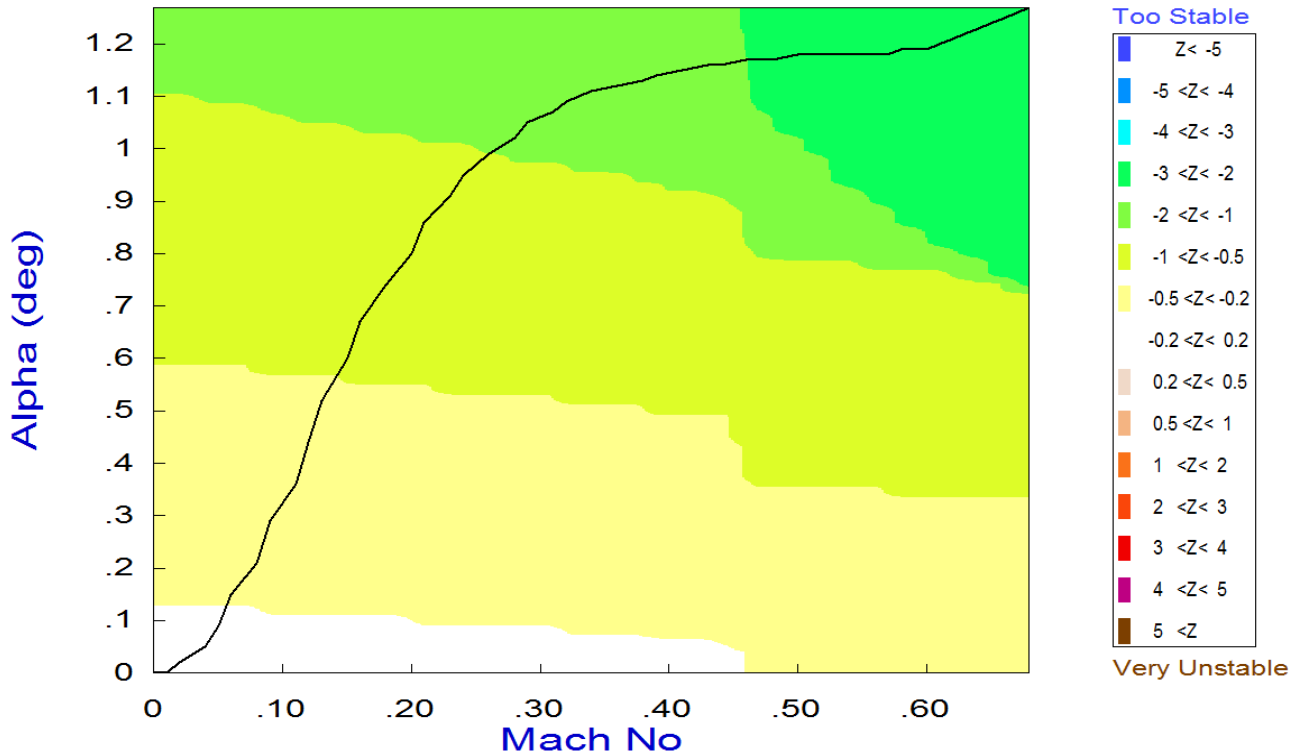
Lifting Body Aircraft Rocket Engines	Engine Description, Thrust (lb)	Mass (slug)	Ieng (slug-ft <sup>2</sup> )	Mom Arm (ft)	Location (x,y,z) (feet)	Mounting Angles (Dy, Dz) Elevat, Azimuth (degr)	Max Deflection Dym,Dzm (deg)	Max Thrott1 (0-1)
Left TVC Eng#1	18000.0	60.0	8.0	0.7	-33.5 -6.0 -2.2	0.0 0.0	5.0 5.0	0.4
Right TVC Eng#2	18000.0	60.0	8.0	0.7	-33.5 +6.0 -2.2	0.0 0.0	5.0 5.0	0.4

The vehicle mass properties are not constant during ascent but they vary as a function of mass. The mass properties file is the same as before "*Lift\_Body.Mass*", and it contains the vehicle moments of inertia and CG location as a function of its mass. The aero coefficients for the basic body and the aero-surfaces, files "*LiftBody\_Basic.Aero*" and "*LiftBody\_Surf.Delt*", are the same as during re-entry. The aero-surface bias positions and deflection range where modified, however, to better affect the trimming conditions. The hinge moment coefficient file, the damping derivatives, and the uncertainties file: "*LiftBody.HMco*", "*LiftBody.Damp*", and "*LiftBody.Unce*", are the same as before.

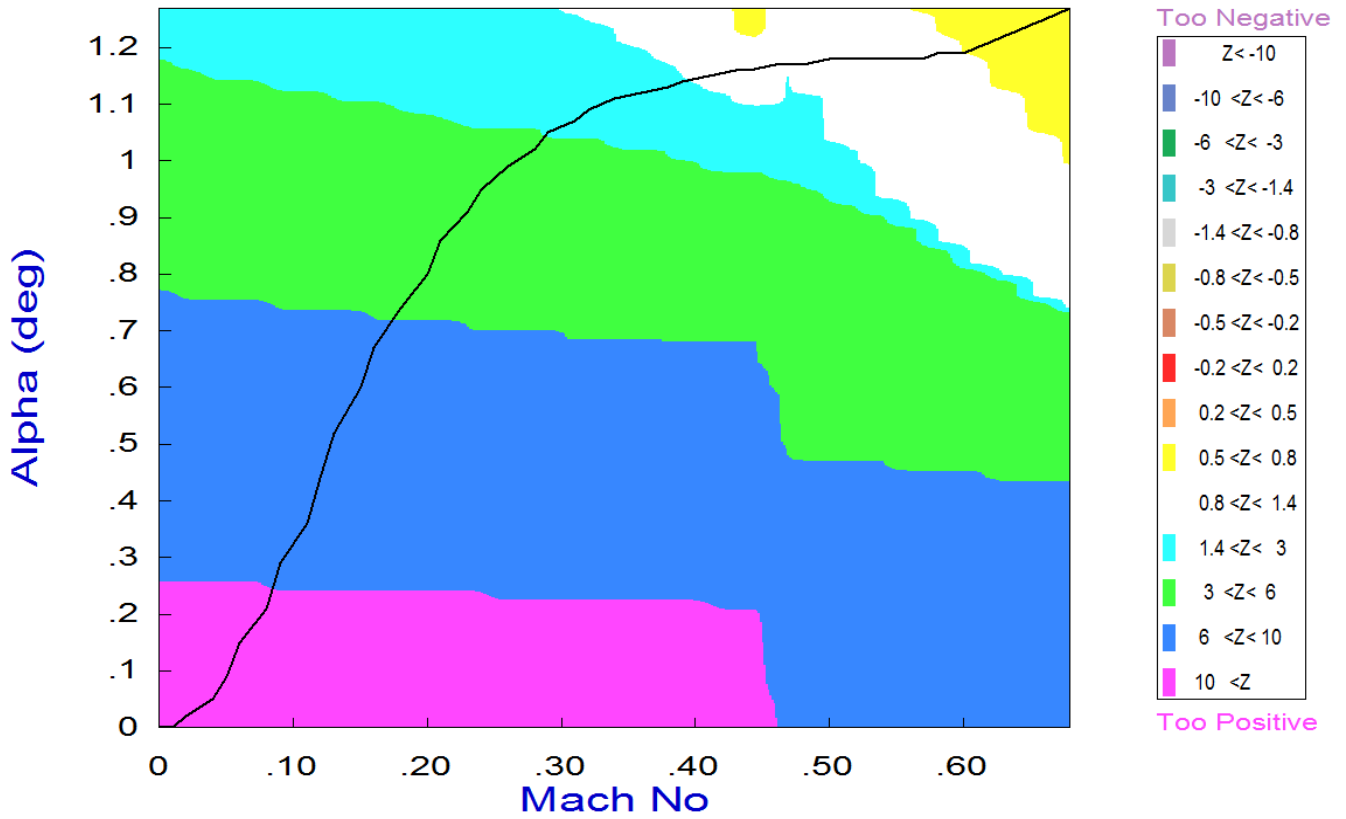
### Pitch Stability Contour Plot (Mach vs Alpha)



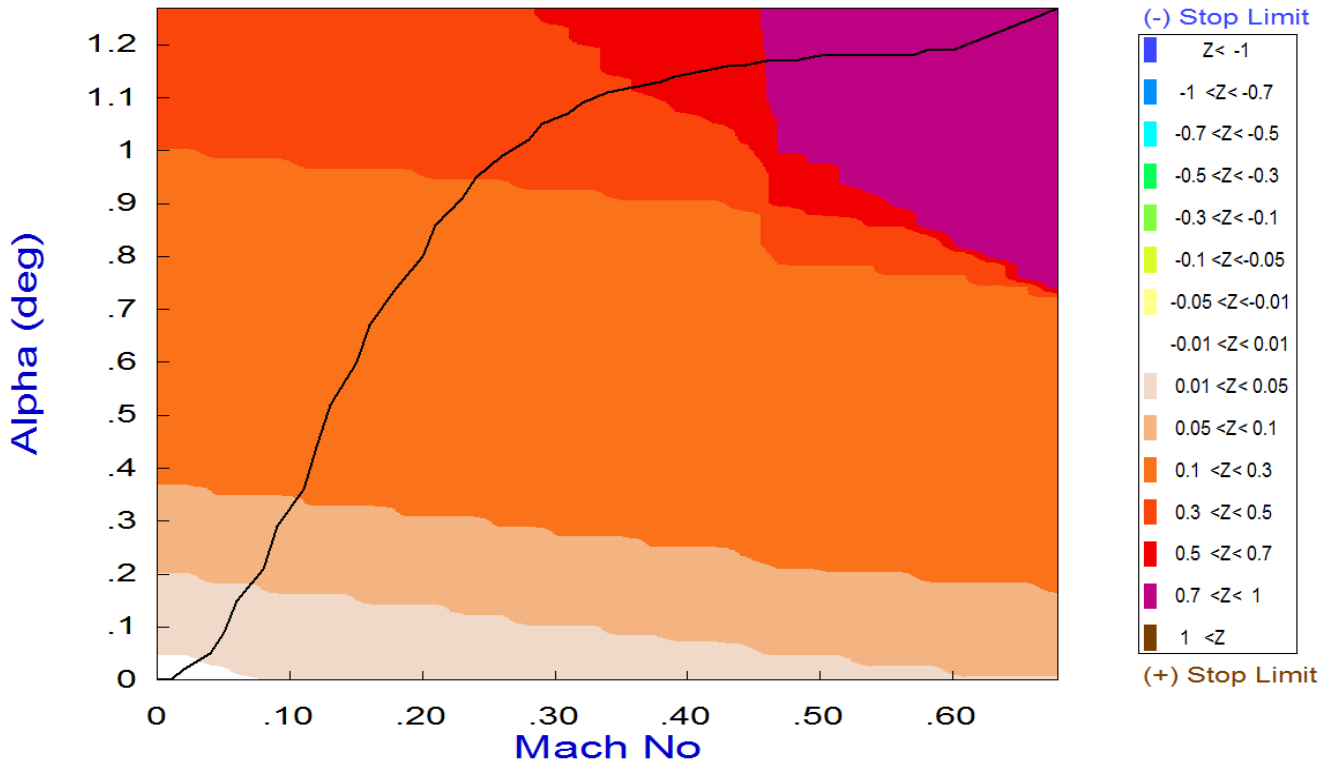
### Lateral Stability Contour Plot (Mach vs Alpha)



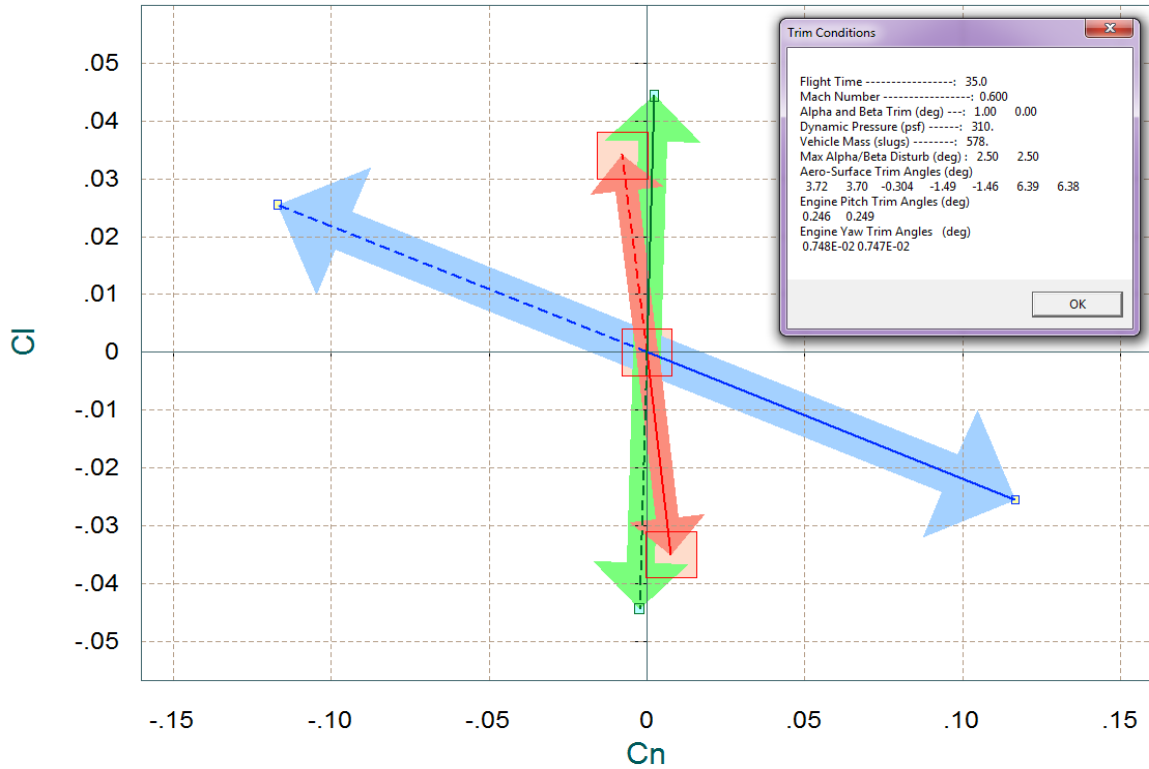
Roll Departure (LCDP) Contour Plot (Mach vs Alpha)



Roll Control Effort Contour Plot (Mach vs Alpha)



Comparison Between Maximum Control Moments Against Maximum Disturb Moments (red)  
Roll & Yaw Control Moments (non-dimension) vers Disturb Moment due to Max Beta/Alpha



Comparison Between Lateral Maxim Moment & Forces, Control Versus Beta Forces (red)  
Control Yaw Moment & Side-Force against Moment and Force due to Max Beta Variation

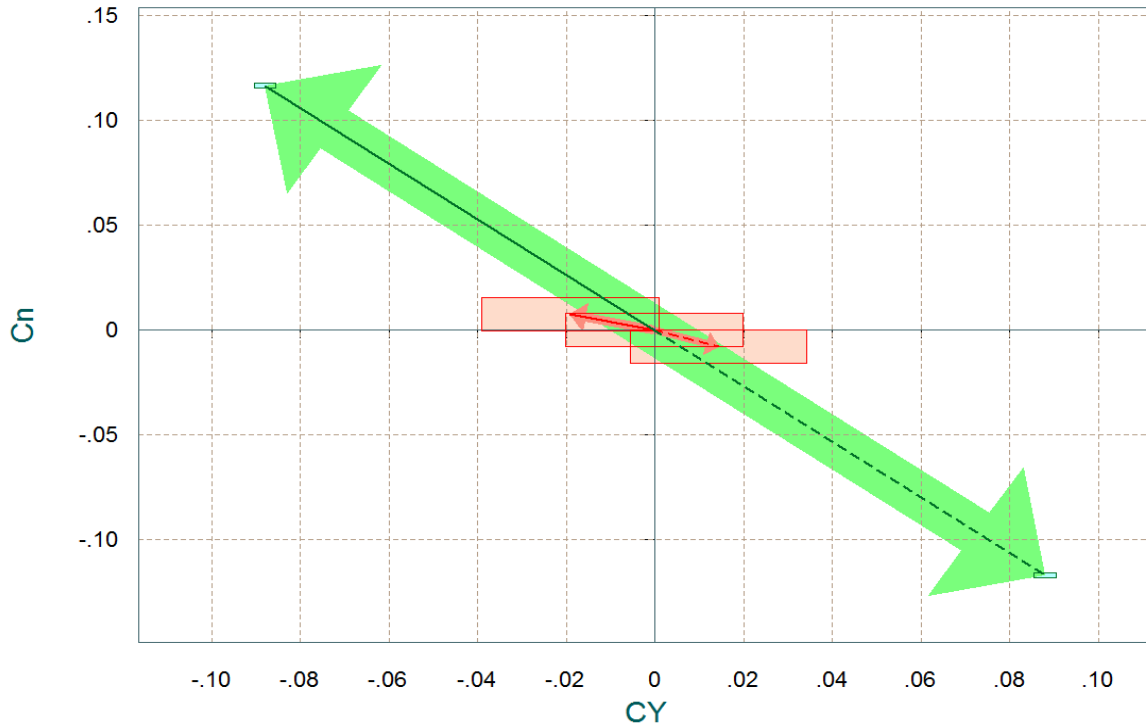


Figure 2.1.1 Maximum Roll and Yaw Moments and Side-Force produced due to  $\pm\beta_{max}$  and Controls

## 6-dof Linear Simulation 4 Control Loops

State-Feedback Loop  
(roll, pitch, yaw)

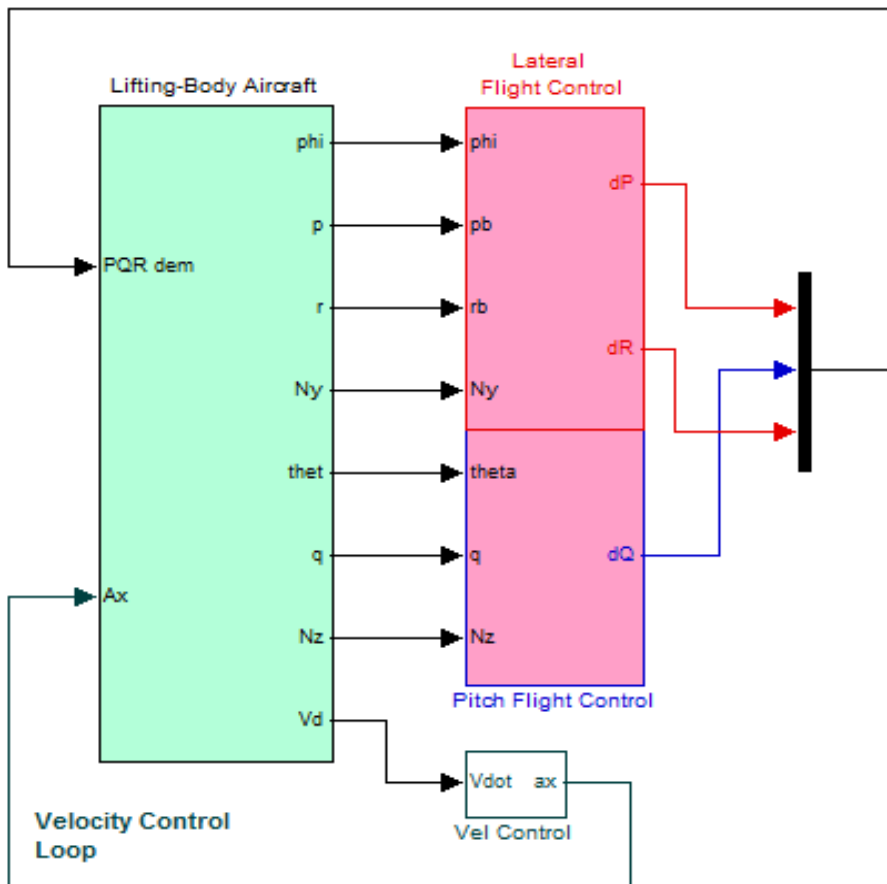
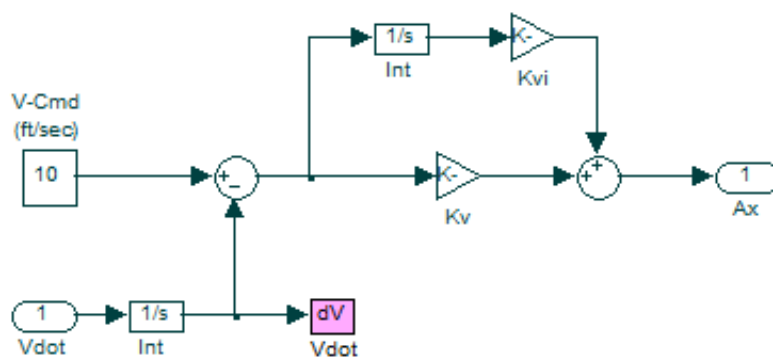


Figure 2.1.5 Ascent Simulation Model in File "Simul\_Ascent.Mdl"

## Velocity Control Loop

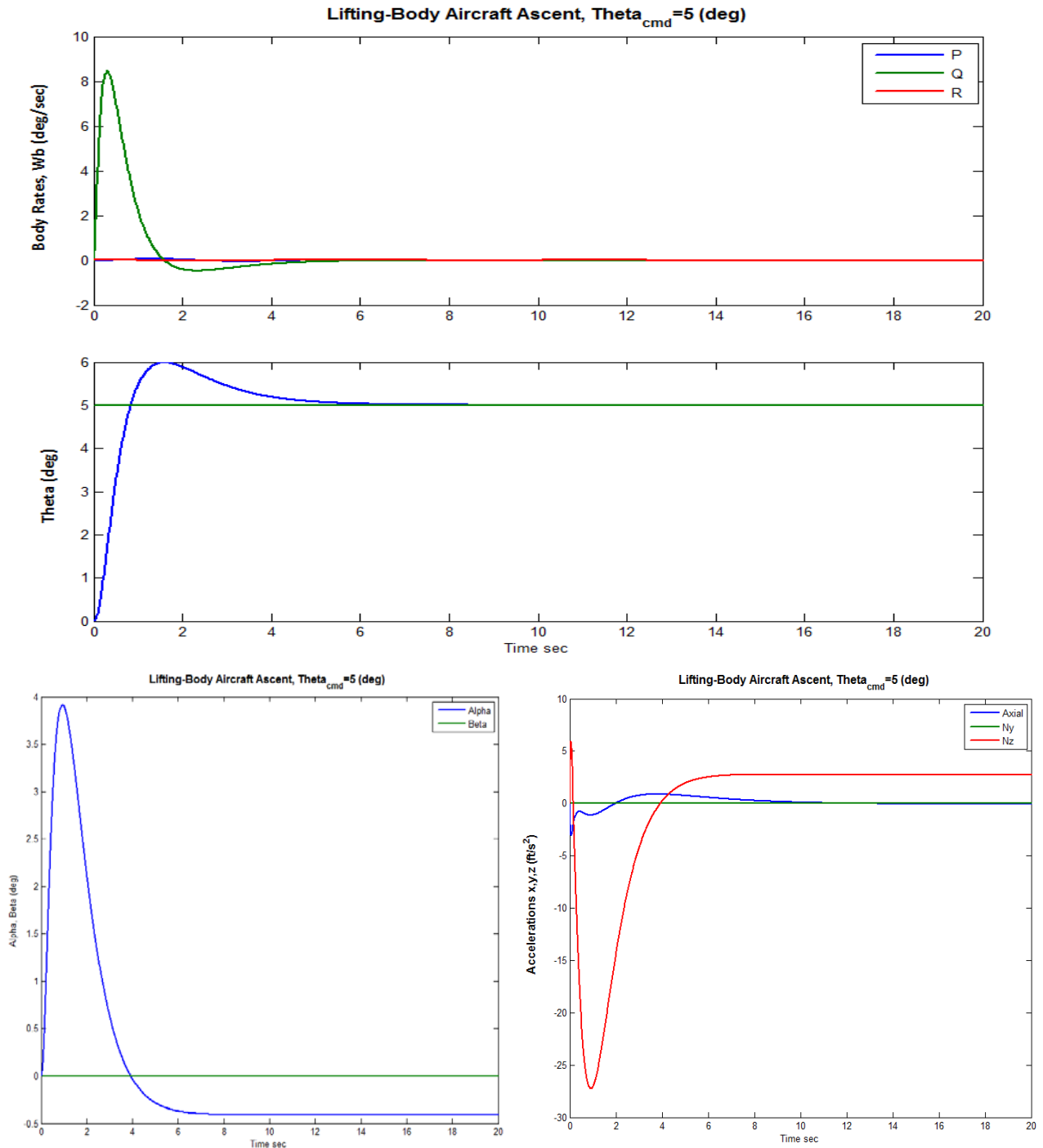




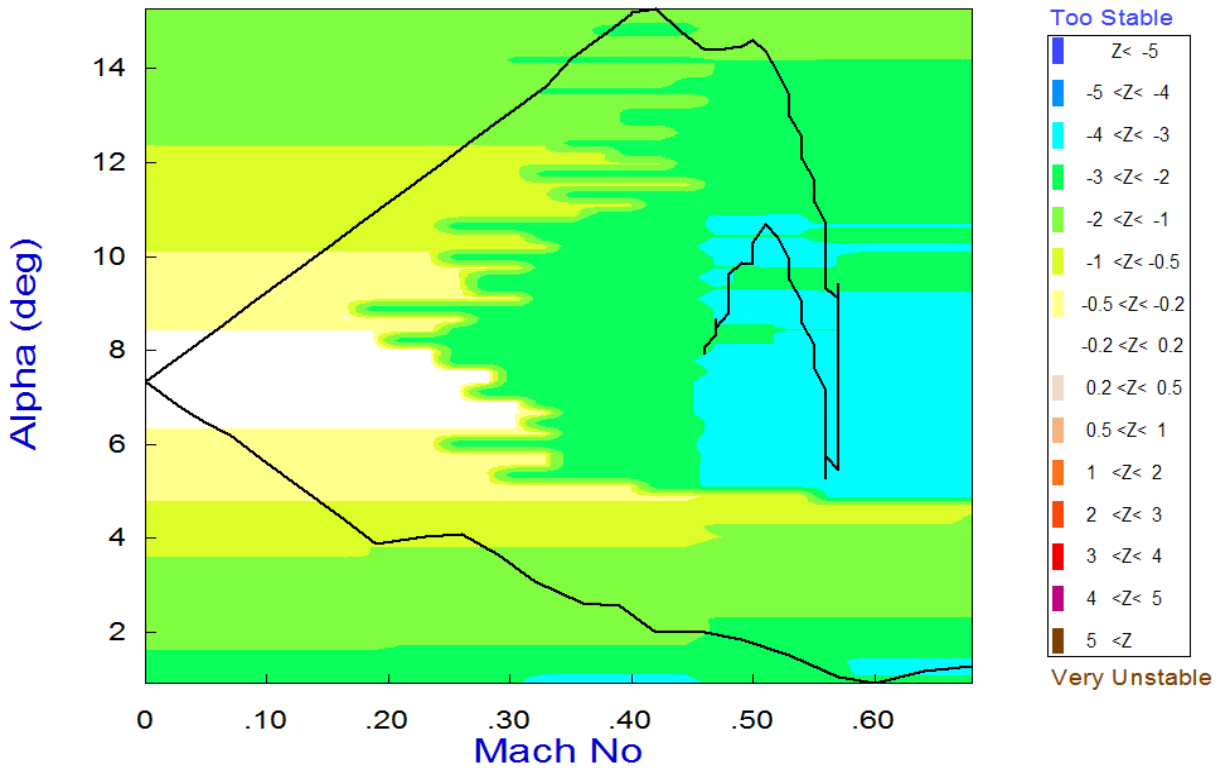
## Simulation Results

The simulation model "*Simul\_Ascent.Mdl*" will now be used to simulate the vehicle response to step commands in pitch and roll attitude and to a change in velocity.

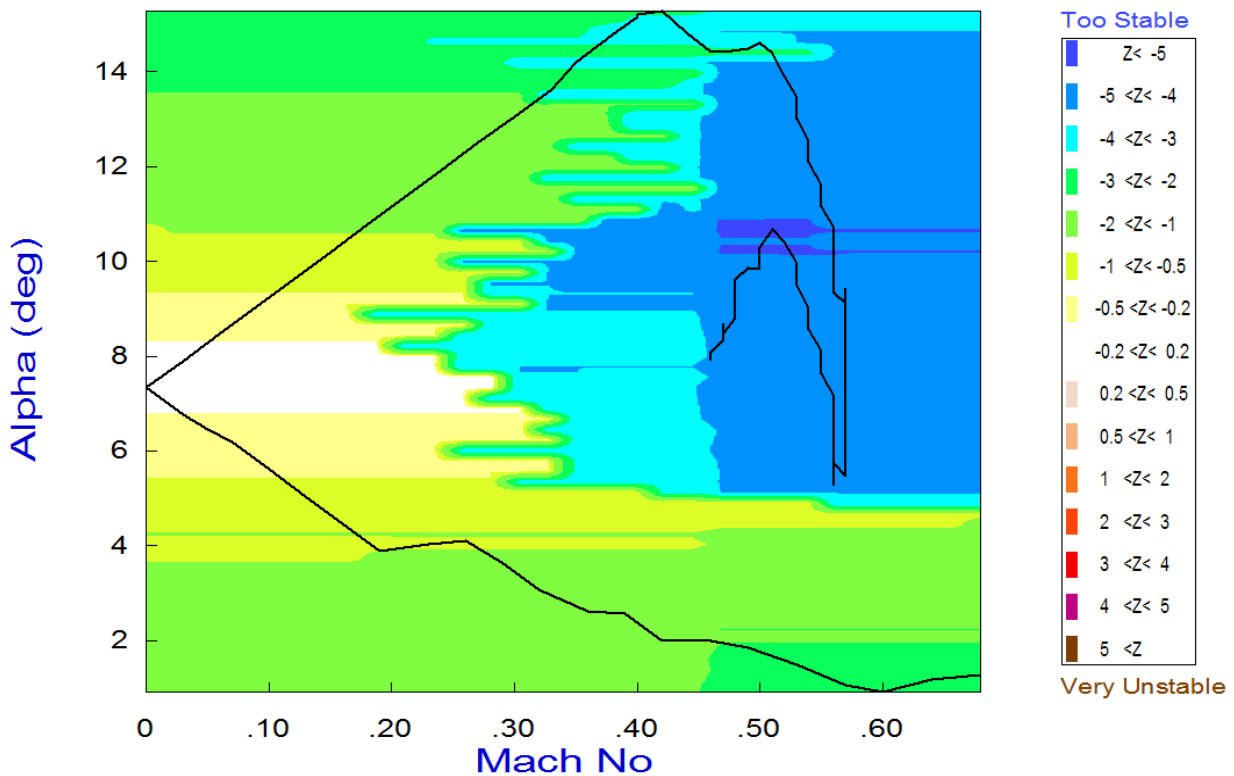
**Pitch Step Command:** Starting with a  $5^\circ$   $\theta_{cmd}$  step in pitch attitude. The plots show how the vehicle uses both: pitch TVC and elevon deflections to catch-up to the step attitude command. Notice the similarity between the angle of attack and the normal ( $N_z$ ) acceleration.



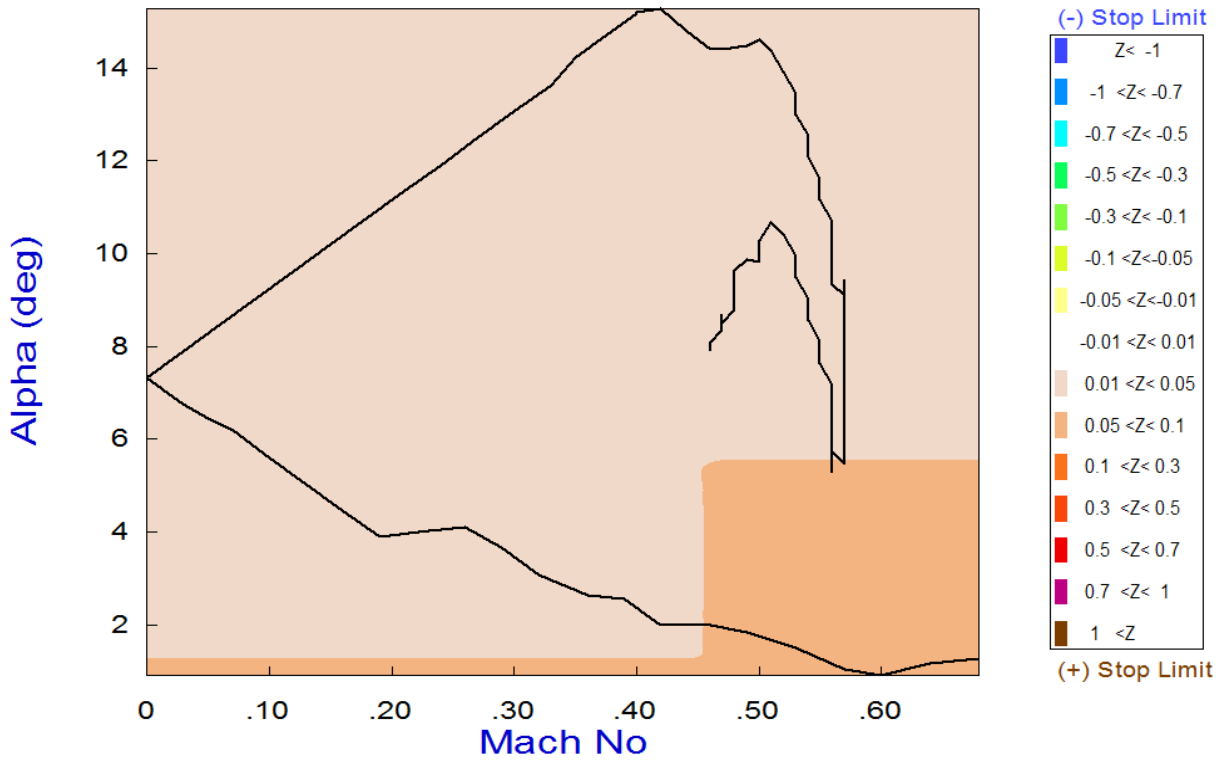
### Pitch Stability Contour Plot (Mach vs Alpha)



### Lateral Stability Contour Plot (Mach vs Alpha)



Pitch Control Effort Contour Plot (Mach vs Alpha)



Yaw Control Effort Contour Plot (Mach vs Alpha)

